

Pennsylvania State University

Annual Progress Report: 2006 Formula Grant

Reporting Period

July 1, 2009 – June 30, 2010

Formula Grant Overview

The Pennsylvania State University received \$7,201,999 in formula funds for the grant award period January 1, 2007 through December 31, 2010. Accomplishments for the reporting period are described below.

Research Project 1: Project Title and Purpose

Regulation of Gene Expression during Inflammation - Inflammation must be tightly controlled to prevent damage to host tissues; however, there is little known about the signals and molecular events that prevent excessive inflammation and tissue destruction. Furthermore, how these signals lead to the suppression of genes that mediate inflammatory responses and the activation of genes that promote wound repair has not been investigated. We propose to look at signals and mechanisms that regulate the macrophage receptor tyrosine kinase RON, which has been shown to temper the response of macrophages *in vitro* and *in vivo*. We will employ animal models and molecular approaches to gain insights into how macrophages balance activities associated with inflammation versus wound repair during a normal immune response.

Duration of Project

4/1/2007 – 6/30/2009

Summary of Research Completed

This project ended during a prior state fiscal year. For additional information, please refer to the Commonwealth Universal Research Enhancement Annual C.U.R.E. Reports on the Department's Tobacco Settlement/Act 77 web page at <http://www.health.state.pa.us/cure>.

Research Project 2: Project Title and Purpose

Meprins – Metalloproteinases of the Kidney and Intestine - Urinary tract infections are one of the most common bacterial infections in humans, and around 50% of women are affected at some point in their lifetimes. There are multiple factors involved in recurrent infections; however, there is a need to understand the mechanisms involved to develop more effective therapies and prevent renal scarring associated with infection. We have found that meprins are expressed by leukocytes and that meprins can cleave cytokines as substrates *in vitro* to an active form or to a non-active, degraded form. Use of unique meprin knock-out mice as models for inflammatory

diseases such as urinary tract infection and ischemia/reperfusion (I/R) induced acute renal failure show that: 1) mice lacking the meprin α subunit are more susceptible to kidney and bladder infections and 2) mice that lacked the meprin β subunit were more protected against I/R induced kidney injury. The cytokine cleavage data, the presence of meprin expression on leukocytes, and the data accumulated from the mouse models of disease indicate a role for meprins in modulating inflammatory responses.

Duration of Project

7/1/2007 – 6/30/2010

Project Overview

The overall, long-term objectives of this research are to elucidate mechanisms by which cell surface metalloproteases and their secreted counterparts are regulated, and to interact, activate and degrade peptides and proteins at the cell surface and extracellularly, as well as to define the roles of these proteases in health and diseases, such as a kidney and urinary tract disease.

Meprins are membrane-bound (heteromeric α/β and homomeric β) and secreted (homomeric α) mammalian metalloproteases that are abundantly expressed in the epithelial cells of the kidney, lower intestine and in certain leukocytes. Previous studies with meprin knockout mice revealed a role for these proteases in kidney damage in ischemia and in urinary tract infections.

Understanding the cellular and molecular mechanisms involved could result in prevention, diagnosis and/or treatment of these diseases. We propose that secreted isoforms of kidney meprins and leukocytic meprins protect against uropathic infections. The availability of meprin α , β and α/β knockout mice is a unique asset for the proposed experiments.

The specific aim of the studies is to determine whether or not meprin α secreted from the kidney, or leukocytic meprins, affect the establishment and severity of urinary tract disease. The hypothesis is that high levels of secreted meprins from the kidney and/or leukocytic meprins prevent or lessen the severity of urinary tract disease. Mice of the different meprin genotypes will be infected with uropathic bacteria in the bladder, and the susceptibility to bladder and kidney infections will be determined. The involvement of leukocytic meprins will be examined using chimeric mice. Bone marrow cells of wild-type and meprin β knockout mice will be destroyed by irradiation, and replaced by donor cells from wild-type or knockout mice. The donor cells will be from wild-type and knockout mice carrying a green fluorescent protein (GFP). Uropathic injection studies will determine whether or not the leukocytic meprins or kidney meprins are responsible for protection against infection. These mice also will be used to determine the cells responsible for changes in cytokine levels in the different genotypes. The activation of meprins at sites of infection, concentrations of active β -defensins, and ability of recombinant forms of meprins and brush border membranes from mice with different meprin genotypes to interact with bacteria and degrade bacterial pili will also be determined.

Principal Investigator

Judith S Bond, PhD
Pennsylvania State University

College of Medicine
500 University Dr., H171
Hershey, PA 17033

Other Participating Researchers

Renee Dusheck Yura (7/1/2007-12/31/2008), Timothy Keiffer (7/1/2009-present) - employed by Pennsylvania State University

Expected Research Outcomes and Benefits

The focus of the research project shifted when Renee Dusheck Yura left the project and Timothy Keiffer began work on the project. The revised research outcomes and benefits are as follows. While much is known about the substrates of meprin and its modulating role in several inflammatory diseases, very little is known about endogenous inhibitors of meprin. One group has identified mannose binding lectin (MBL) as an endogenous inhibitor of meprins. MBL was shown to interact with native mouse meprin A via glycan recognition and that MBL inhibited meprin cleavage of several extra-cellular matrix proteins. Many questions still remain about MBL-mediated meprin recognition and inhibition. For instance, it is not known if MBL recognizes only the hetero-tetramer form of mouse meprin A or if MBL recognizes most or all of the other meprin isoforms. MBL-mediated meprin inhibition of cytokine cleavage has not yet been evaluated. Furthermore, there is no data showing that MBL and meprin interact *in vivo*.

Deeper study of cytokine cleavage by different meprin isoforms is also warranted as the cytokine profiles between the wild-type and meprin knock-out mice show differences in cytokine levels, such as IL-6, during different inflammatory responses. This could be a very important mechanism of how meprins modulate the immune response by differential cytokine cleavage, depending on the balance of the different meprin isoforms expressed. The results of this project could be important in modulating the immune response.

Summary of Research Completed

The main focus of the work in this reporting period was to further characterize the meprin-mannose binding lectin (MBL) interaction and expand the pool of cytokine substrates for meprins using the mouse cytokine array data as a guide. Cell lines expressing the meprin A and B isoforms are readily available to use for testing MBL-mediated meprin inhibition and differential cytokine cleavage. These experiments aimed to determine if the MBL-mediated inhibition of meprin is isoform-specific. MBL was also used to determine if MBL-mediated meprin inhibition is effective against fluorogenic peptides and cytokines that are substrates for meprins. We aimed to determine whether MBL-mediated meprin inhibition is substrate size specific and show if MBL recognition affects meprin cytokine cleavage, which would also be another way of modulating inflammatory activity of the meprins. Meprin knock-out mice, unique and exclusive tools to the lab, are also available to determine if meprin and MBL interact *in vivo* by immunohistochemical and colocalization experiments. Elucidation of MBL-mediated meprin recognition and inhibition, and expanding the cytokine substrate pool for meprins, will further the understanding of how meprins modulate inflammatory diseases. There will also be a

side benefit for MBL research as more insight into how MBL, normally involved in recognizing exogenous pathogens, interacts with endogenous ligands such as meprins is found.

Methods:

- Human MBL was purified from human serum samples by mannose affinity chromatography and size exclusion chromatography. Recombinant MBL can also be generated by HEK293 cells.
- Recombinant meprin A and B isoforms were produced and isolated from HEK293 cells. Native mouse meprin A (heteromeric meprin A) was harvested and purified from C57BL6 mouse kidneys.
- Recognition of the different meprin A and B isoforms was analyzed via MBL lectin blotting. MBL inhibition of meprin hydrolysis of peptide substrates was analyzed using bradykinin analog (BK+) and orckinin (OCK+) fluorogenic peptide assays, which are specific for meprin A and B, respectively. Inhibition of meprin hydrolysis of protein substrates was analyzed by azocasein assay as well as densitometric SDS-PAGE gel fragmentation analysis.

Results:

- MBL was successfully purified from human serum. However, the estimated yield was approximately 30 µg/Liter (L) of serum – much lower than anticipated (approximately 0.5 - 1.0 mg per L of serum). A human MBL construct in pcDNA3.1 (-) vector has been shown to express MBL in HEK293 cells, but a stable cell line expressing large amounts of MBL has not been isolated yet. This hampered further analysis of the meprin/MBL interaction.
- MBL interacts with both the meprin A and B isoforms in a carbohydrate-dependent manner. This was demonstrated with lectin blotting and deglycosylases.
- No significant MBL-mediated inhibition was seen with the meprin A or meprin B isoforms against either the fluorogenic peptide substrates BK+ or OCK+ or the protein substrate, azocasein. In one assay, MBL showed partial inhibition (approximately 35-40%) of native meprin A hydrolysis of gelatin, via laser densitometry, but the lack of large quantities of MBL made it impossible to confirm this result.

Conclusions:

- The data amassed so far indicate that while MBL does interact with meprin A and B in a glycan-dependent manner, MBL is not a potent inhibitor of meprin hydrolysis of either protein or peptide substrates. It is possible that the Hirano *et al* data (J Immunol 175:3177-3185, 2005) is based on a sub-population of native heteromeric meprin A that is optimally glycosylated for recognition by MBL. Attempts to purify this hypothesized meprin sub-population using hMBL antibody conjugated protein A agarose, which would bind to hMBL covalently, but leave the hMBL able to bind to meprin were unsuccessful, as meprin A itself was found to also bind to protein A.

Overall, our studies demonstrate that meprins are critical factors in the immune response and support our contention that meprins influence the barrier function in epithelial tissues, cytokine profiles in inflammation, and can be damaging to cellular proteins as well as beneficial in enabling an initial immune response. In our attempts to establish the physiologically important mechanisms by which meprins affect the immune system and cell damage in urinary tract disease, we have found that MBL probably is not responsible for modulating the proteolytic action of meprins. However, because MBL physically interacts with meprins, it may be that this lectin affects the localization of meprin proteases and consequently its damaging actions. The understanding of the roles of meprin proteases in normal and pathological situations may enable us to interfere with damaging processes, such as occurs in urinary tract infections.

Research Project 3: Project Title and Purpose

Glucocorticoid/Stress Effects on Dendritic Cell Function - There is substantial evidence for psychological stress-induced, neuroendocrine-mediated modulation of the immune function. The long-range goal of this project is to define the mechanisms by which stress and its associated increase in corticosterone affect cytotoxic T lymphocyte (CTL) responses. An efficient and robust CTL lymphocyte response is necessary for the successful defense against many diseases that are immunologically resisted, in particular, virus infections and some tumors. The efficiency and robustness of this response is dependent upon the efficient functioning of dendritic cells. In this project, those components of crucial dendritic cell functions that are affected by stress and glucocorticoids and the resulting impact on the generation of CTL responses will be identified.

Duration of Project

9/1/2007 – 8/31/2008

Summary of Research Completed

This project ended during a prior state fiscal year. For additional information, please refer to the Commonwealth Universal Research Enhancement Annual C.U.R.E. Reports on the Department's Tobacco Settlement/Act 77 web page at <http://www.health.state.pa.us/cure>.

Research Project 4: Project Title and Purpose

Cellular Machinery in Cytomegalovirus-mediated MHC Class I HC Degradation - Human cytomegalovirus is a beta-herpesvirus that infects approximately 70% of our population. The genome of this virus encodes specific genes that, when expressed as proteins, interfere with the detection and destruction of infected cells by the human immune systems. In one mechanism of immune evasion, the virus expresses a protein known as US11 that causes the degradation of MHC class I heavy chain proteins, leading to the absence of these proteins in infected cells. MHC class I heavy chain proteins at the surface of infected cells normally signal to immune cells the presence of viral infection. Thus, the absence of this signaling protein enables infected cells

to escape detection. The purpose of this research is to identify the human machinery co-opted by the virus US11 protein for this evasion, with the long-term goal of designing therapeutic interventions.

Duration of Project

4/1/2007 – 12/31/2008

Summary of Research Completed

This project ended during a prior state fiscal year. For additional information, please refer to the Commonwealth Universal Research Enhancement Annual C.U.R.E. Reports on the Department's Tobacco Settlement/Act 77 web page at <http://www.health.state.pa.us/cure>.

Research Project 5: Project Title and Purpose

Cytosol-Vesicle-Vacuole Protein Degradation Pathway - Protein degradation is critical for cell cycle division, cell growth control, transcriptional regulation and metabolic control. The gluconeogenic enzyme fructose-1,6-bisphosphatase (FBPase) is degraded when yeast cells are shifted from poor carbon sources to fresh glucose, and this degradation prevents energy futile cycles that are harmful to cells. FBPase can be degraded either in the proteasome or in the vacuole depending on the duration of starvation. Our long-term goal is to understand the mechanisms underlying the vacuolar dependent pathway of FBPase degradation. The objective of this application is to understand why FBPase switches its degradation from the proteasome to the vacuole. We will test the hypothesis that the switch is controlled by multiple protein complexes that can be activated or inactivated depending upon the duration of starvation.

Duration of Project

1/1/2007 - 12/31/2010

Project Overview

Autophagy is a process whereby lysosomes degrade cytosolic proteins and organelles when cells are starved of nutrients. Defects or changes in autophagy have been linked to cancer development, neuromuscular dystrophies and aging. Multiple forms of autophagy exist, and a unique autophagy pathway has been identified in our lab. The gluconeogenic enzyme fructose-1,6-bisphosphatase (FBPase) is degraded when yeast cells are shifted from poor carbon sources to fresh glucose, and this degradation prevents energy futile cycles that are harmful to cells. FBPase can be degraded either in the proteasome or in the vacuole depending on the duration of starvation. For the vacuolar pathway, FBPase is first targeted to Vid vesicles and then to the vacuole. A number of *VID* genes function in both degradation pathways and they are evolutionarily conserved. The Vid pathway is utilized for multiple cargo proteins including isocitrate lysase, phosphoenopyruvate carboxykinase and malate dehydrogenase. The objective of this project is to understand the molecular mechanisms mediating the switch of degradation from the proteasome to the vacuolar pathway. *Our central hypothesis states that the site of*

FBPase degradation is controlled by multiple protein complexes that are activated or inactivated depending upon the duration of starvation. We plan to test this hypothesis by pursuing the following aims. 1. We will study why the Vid vesicle trafficking pathway is inactive in short termed starved cells. Is this because of an inactive cAMP signaling pathway, the absence of Vid vesicles, or incompetent Vid vesicles? 2. FBPase physically interacts with components of the Tor1 complex (TORC1). We will study how Tor1 regulates the vacuolar pathway. 3. Vid28p and Vid30p form a stable complex. We will study how this complex regulates both degradation pathways. The completion of the proposed experiments will enhance our understanding regarding how these two major proteolytic pathways are regulated. This may provide therapeutic advantages to eliminate abnormal proteins that accumulate in Parkinson's disease, Huntington's disease, or other pathological conditions. The proposed aims are expected to establish the roles of signaling molecules and the Vid28p/Vid30p complex in controlling the switch from the proteasome to the vacuolar pathway. Such results will have important implications, since knowing how the switch works may ultimately lead to the development of therapeutic strategies to eliminate abnormal proteins that accumulate under pathological conditions

Principal Investigator

Hui-Ling Chiang, Ph.D.
Pennsylvania State University
College of Medicine
Cellular and Molecular Physiology
500 University Drive
Hershey, PA 17033

Other Participating Researchers

C. Randell Brown, Ph.D. - employed by Pennsylvania State University, Abbase Alibhoy-Graduate Student, Genetics Program, Penn State College of Medicine

Expected Research Outcomes and Benefits

Our experiments will allow us to determine if the inability of 1d cells to degrade FBPase in the vacuole is due to the fact that Vid vesicles are not formed or if they are import incompetent. We expect that there is an overall decrease in proteasome function and an increase in vacuolar functions with prolonged starvation. We will also learn whether differential ubiquitination of FBPase or differential regulation of ubiquitin conjugating enzymes in 1d versus 3d cells accounts for the switch. Our experiments should reveal whether the cAMP pathway is inactive in cells starved for 1d. For Aim 2, we will test the working hypothesis that TORC1 regulates one or multiple steps of the early parts of the FBPase pathway. Although FBPase binds to both Tor1p and Tco89p, our results suggest that Tor1p is inhibitory, while Tco89p is stimulatory, and they may exert their functions at different steps of the pathway. We expect that Tco89p positively regulates early steps of the vacuolar FBPase degradation pathway, at the step of FBPase inactivation, phosphorylation or import into Vid vesicles. The experiments should also reveal whether TORC1 plays a role in the proteasome pathway. For Aim 3, we will study the functions of Vid28 and Vid30p in vacuolar dependent degradation of FBPase. Both proteins contain

protein-protein interaction domains. We have found that the ARM4 domain is required for the interaction of Vid28p with Vid30p during vacuolar degradation. We expect that the LisH domain of Vid30p is required for vacuole degradation, but not proteasome degradation. We expect that other sequences of Vid28p or Vid30p are also required, either for the proteasome pathway, for the vacuole pathway, or for both. If we understand the molecular mechanisms regulating the switch of protein degradation from the proteasome to the vacuolar pathway, we can utilize the information to activate the vacuole pathway when proteasomal function is compromised. Alternatively, we can inactivate the vacuole pathway when excessive vacuolar degradation produces harmful effects to cells.

Summary of Research Completed

We have received additional monies to expand our project by conducting studies directly related to Aim 2. In our earlier studies, we proposed to investigate how the Tor1 complex (TORC1) that consists of Tor1p and Tco89p regulates FBPase degradation in the vacuole in Aim 2. With our additional monies, we studied the role of Vps34p in the Vid pathway. Vps34p is the major PI3K in yeast and is a downstream regulator of TORC1.

We proposed to study the role that the PI3K plays in the Vid pathway. The yeast *VPS34* gene encodes the PI3K that phosphorylates PI3 to produce PI3P. This gene is involved in multiple protein targeting pathways to the vacuole. For the Vps pathway, Vps34p forms a complex with Vps15p. In cells lacking either *VPS34* or *VPS15*, FBPase degradation was blocked, suggesting that the PI3K complex is required for the degradation of FBPase. We also showed that the trafficking of TOR1C to the vacuole was affected in cells lacking the *VPS34* gene, suggesting that *VPS34* plays a role in the trafficking of TORC1 to the vacuole. Based on these preliminary results, we proposed to study the distribution of Vps34p in wild type cells and in various mutant strains in Aim 1. We also proposed to study the trafficking of PI3P using the FYVE-RFP and FYVE-GFP constructs that specifically bind to PI3P (Aim 2).

FBPase association with actin patches is prolonged in cells lacking the *VPS34* and the *VPS15* genes - In yeast, endocytic vesicles are formed at actin patches on the plasma membrane. In wild type cells, cargo proteins such as FBPase and MDH2 associated with actin patches transiently. Therefore, we examined whether or not the association of FBPase with actin patches was affected in cells lacking the *VPS34* gene. FBPase-GFP was expressed in the $\Delta vps34$ mutant strain that was glucose starved and then transferred to media containing fresh glucose. Cells were fixed, permeabilized and actin patches were stained with phalloidin conjugated with rhodamine (Fig. 1A). In the $\Delta vps34$ mutant, FBPase was associated with actin patches before and after glucose addition for up to 30 min. FBPase remained associated with actin patches at the 60 min time point in this strain. Thus, the absence of *VPS34* appears to prolong the association of FBPase with actin patches.

In the $\Delta vph1$ mutant that blocks a late step of endocytosis, FBPase was in the lumen of endocytic compartments that were labeled with the FM dye, suggesting that FBPase is targeted to these FM-containing compartments. The FM dye is internalized and travels to endosomes in 30-60 min and then to the vacuole in 60-120 min. We next determined whether FBPase trafficked to the FM endocytic compartments. For these studies, FBPase-GFP was expressed in the $\Delta vps34$

mutant that was starved for 3 days and shifted to glucose in the presence of the FM dye (Fig. 1B). In this strain, FBPase-GFP was diffuse during glucose starvation. This protein showed uneven distribution following glucose re-feeding. FM staining was also uneven in this strain. Some FBPase-GFP appeared to be in areas that co-localized with FM staining.

We repeated the same experiments with cells lacking the *VPS15* gene. FBPase-GFP was expressed in the $\Delta vps15$ strain and the distribution of FBPase with actin patches was examined (Fig. 2A). FBPase was associated with actin patches before and after the addition of glucose in this strain. Since FBPase remained associated with actin patches at the 60 min time point in cells lacking the *VPS15* gene, this gene may have a role in the dissociation of FBPase-GFP from actin patches.

The FBPase-GFP $\Delta vps15$ strain was also examined for FBPase distribution with FM containing compartments (Fig. 2B). FBPase-GFP and FM signals were uneven in this strain. Some FBPase appeared to co-localize with FM following the addition of glucose for 60-120 min. In cells lacking the *VPS34* or the *VPS15* genes, FBPase appears to traffick to FM containing endosomes, but the endosome to the vacuole step is affected.

Vid24p association with actin patches is prolonged in the $\Delta vps15$ mutant – We next determined whether the association of Vid vesicle protein Vid24p with actin patches was affected in cells lacking the *VPS34* or the *VPS15* gene. Vid24p is a peripheral protein on Vid vesicles and has been used to follow the trafficking of Vid vesicles. In wild type cells, Vid24p associates with actin patches at the 15 and 30 min time points. However, this protein dissociates from actin patches at the 60 min time point. GFP-Vid24p was expressed in the $\Delta vps15$ mutant that was starved and shifted to glucose for the indicated time points. In this strain, GFP-Vid24p associated with actin patches before and after the addition of glucose for up to 30 min (Fig. 3A). GFP-Vid24p remained associated with actin patches at the 60 min time point. Therefore, we suggest that *VPS15* has a role in the dissociation of Vid24p from actin patches.

Next, we examined whether GFP-Vid24p was targeted to FM containing compartments in cells lacking the *VPS15* gene. GFP-Vid24p was expressed in the $\Delta vps15$ mutant and shifted to glucose in the presence of the FM dye (Fig. 3B). In this strain, GFP was in punctate dots before glucose addition. Following the addition of glucose, a percentage of GFP-Vid24p was in areas that co-localized with FM. These results suggest that GFP-Vid24p trafficked to FM-containing endosomes, but failed to reach the vacuole in the absence of the *VPS15* gene. The results regarding GFP-Vid24p trafficking will be repeated once we obtain the $\Delta vps34$ strain that expresses GFP-Vid24p.

Vps34p is localized to actin patches – Our above results indicate that Vps34p/Vps15p has a role in the dissociation of FBPase, Vid24p and Tor1p from actin patches. Therefore, we next examined whether Vps34p is also localized to these patches. Vps34p-GFP was expressed in wild type cells that were starved and shifted to glucose for the indicated time points (Fig. 4A). In these cells, GFP showed punctate dots that co-localized with actin patches during glucose starvation and also following the shift of cells to glucose for 15 and 30 min. It is interesting that Vps34p-GFP remained associated with actin patches at the 60 min time point. Therefore, Vps34p-GFP associates with actin patches for a prolonged period of time. This feature is

different from that seen for FBPase, MDH2, and other proteins that participate in the Vid pathway in which they all dissociate from actin patches by the 60 min time point.

Vps34p is distributed in endosomes and in retrograde vesicles that form from the vacuole membrane - We next examined whether Vps34p-GFP trafficked to FM-containing compartments. For these studies, wild type cells expressing Vps34p-GFP were glucose starved and then shifted to glucose in the presence of the FM dye (Fig. 4B). Vps34p-GFP co-localized with FM containing endosomes at 30-60 min. This protein was on the vacuole membrane at the 120 min time point. Thus, this protein travels to FM-containing endosomes and to the vacuole in response to glucose refeeding.

We have shown recently that Sec28p, Tco89p and Tor1p are localized to retrograde vesicles that form from the vacuole membrane. Therefore, we determined whether Vps34p-GFP is also localized to retrograde vesicles. For these studies, we pre-labeled the vacuole membrane with the FM dye for 16 hours. Cells were then shifted to glucose in the absence of the FM dye (Fig. 4C). A percentage of Vps34-GFP was found as punctate dots that were adjacent to the vacuole membrane. Therefore, Vps34p appears to be distributed to retrograde vesicles in wild type cells.

FYVE-RFP is localized to the vacuole lumen - Vps34p produces PI3P which binds to target proteins that contain the FYVE domain. As such, the FYVE-GFP and the FYVE-RFP constructs have been used to follow the distribution of PI3P in wild type and mutant strains. We have obtained the FYVE-GFP and the FYVE-RFP constructs from Dr. Emr (Cornell University) and transformed them into our wild type and mutant strains. In wild type cells, the majority of FYVE-GFP or FYVE-RFP was in the vacuole lumen (Fig. 5).

Multiple protein trafficking pathways target proteins from various parts of the cells to the vacuole. To determine whether disruption of these vacuole pathways affects the distribution of FYVE-RFP or GFP in the vacuole lumen, we transformed FYVE-RFP or GFP into various mutant strains (Fig. 5). We used the *Arvs161* mutant that blocks the endocytosis pathway and the *Avps10* mutant that blocks the Vps pathway. FYVE-RFP was in the vacuole lumen in the *Arvs161* mutant and the *Avps10* mutant, suggesting that FYVE-RFP distribution is independent of these two pathways. Furthermore, FYVE-RFP was in the vacuole lumen in the *Avid24* mutant and also in the *Atg8* mutant that blocks the autophagy and the Cvt pathways. Therefore, vacuole localization of FYVE is independent of the endocytic pathway, the Vps, the Cvt and the Vid pathways.

FYVE-RFP does not co-localize with Sec28p in the *ret2-1* mutant – In addition to the distribution in the vacuole lumen, FYVE-RFP was also seen in dots that were adjacent to the vacuole membrane. Therefore, we next determined whether or not these dots localize to the Sec28p-containing retrograde vesicles. To investigate this, FYVE-RFP was transformed into the Sec28p-GFP *ret2-1* cell that contains a defective coatamer subunit (Fig. 6). We did not observe co-localization of Sec28p-GFP with FYVE-RFP in this strain, suggesting that most of FYVE-RFP does not target to the same vesicles that contain Sec28p, at least under our experimental conditions.

In summary, we have characterized the distribution of the Vps34p-GFP and FYVE-RFP. Vps34p-GFP is distributed in multiple locations along the endocytic pathway. FYVE-GFP and RFP are localized to the vacuole lumen. In the absence of the *VPS34* gene or the *VPS15* gene, FBPase, Vid24p and Tor1p failed to dissociate from actin patches at the 60 min time point, suggesting that these genes have a role in the dissociation of these proteins from actin patches. We propose that Vps34p is a component of actin patches and is required for protein dissociation from actin patches.

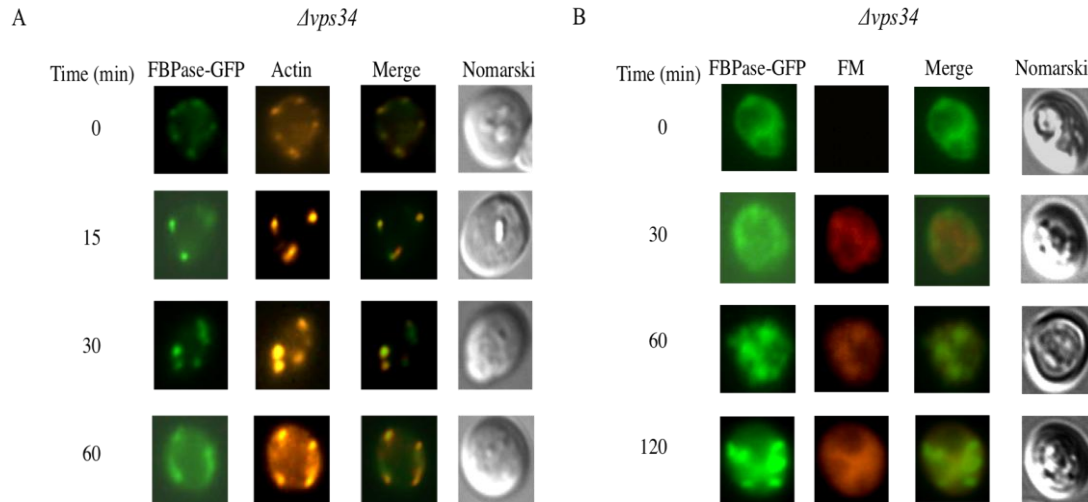


Fig. 1. The association of FBPase with actin patches is prolonged in the $\Delta vps34$ mutant. A, FBPase-GFP was expressed in the $\Delta vps34$ mutant that was starved of glucose and then shifted to glucose for the indicated time points. The association of FBPase with actin patches was examined. B, FBPase-GFP $\Delta vps34$ strain was glucose starved and shifted to glucose for the indicated time points. The distribution of FBPase and FM containing compartments was examined.

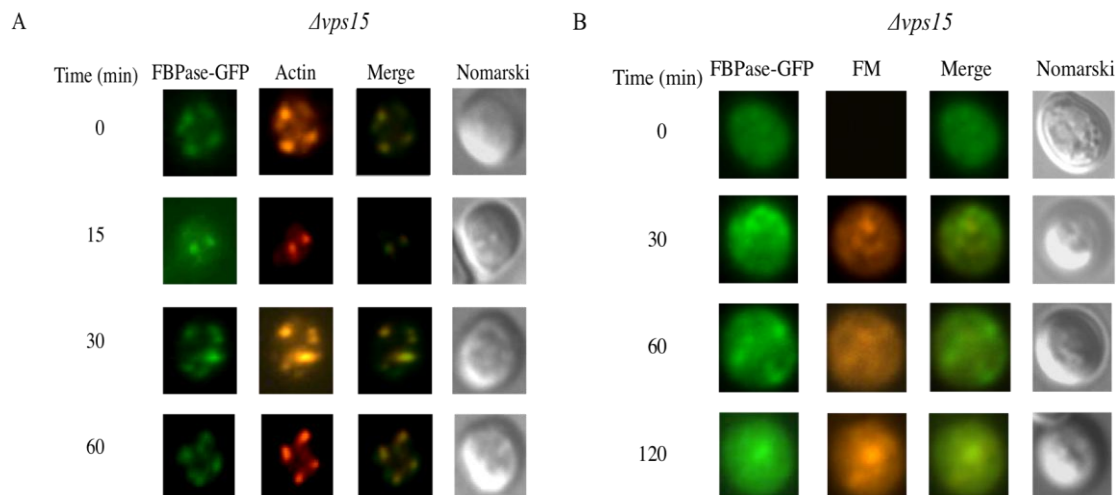


Fig. 2. The association of FBPase with actin patches is prolonged in the $\Delta vps15$ mutant. FBPase-GFP was expressed in the $\Delta vps15$ mutant that was starved and replenished with fresh glucose. A, the association of FBPase with actin patches was determined. B, the distribution of FBPase and FM was examined.

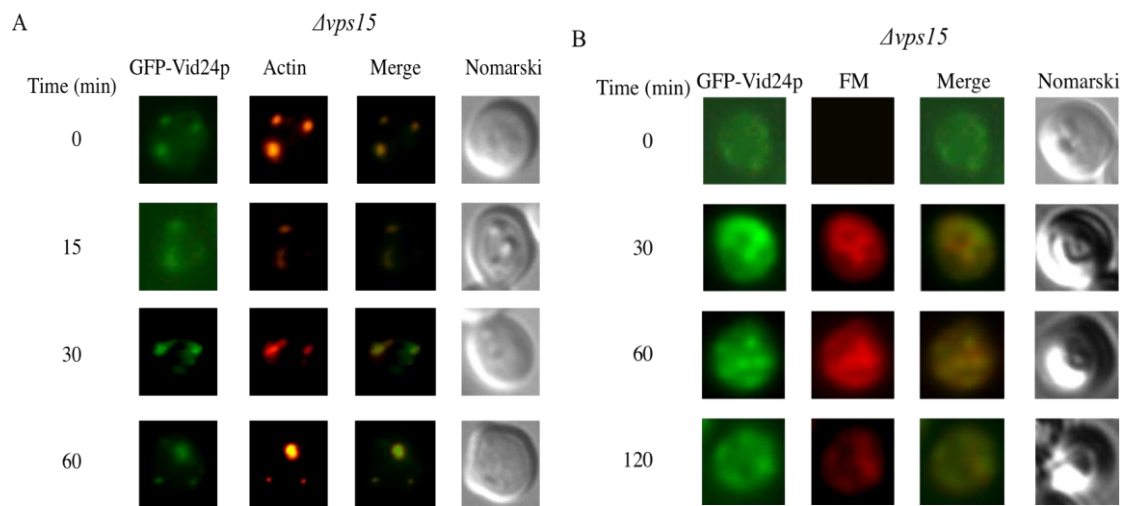


Fig. 3. Vid24p is associated with actin patches in the *Δvps15* mutant. GFP-Vid24p was expressed in the *Δvps15* mutant that was starved and re-fed with glucose. The distribution of GFP-Vid24p with actin patches (A) and FM (B) was visualized.

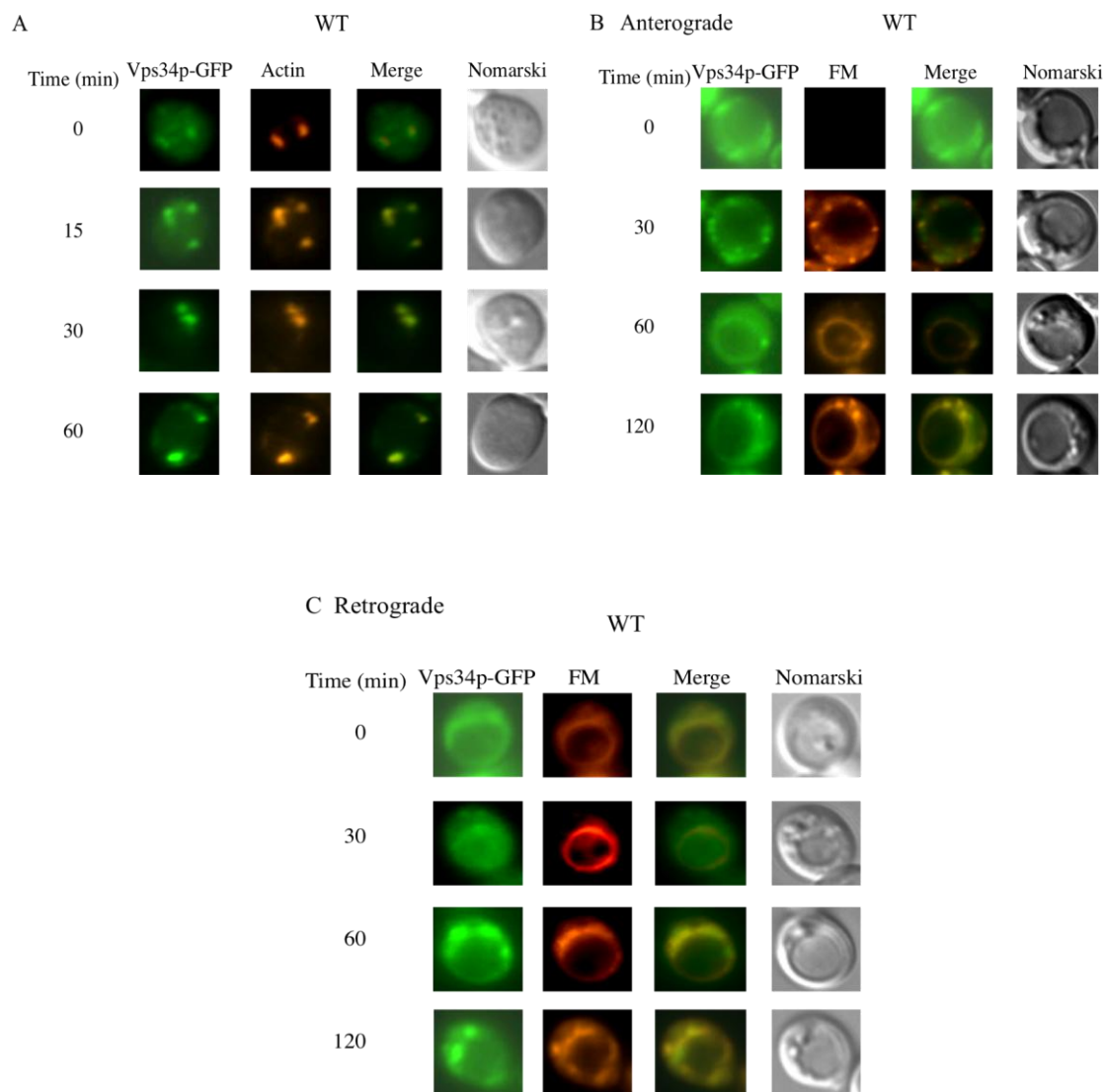


Fig. 4. Vps34p is distributed to multiple locations. Vps34p-GFP was expressed in wild type cells that were starved and re-fed with glucose. Cells were examined for the distribution of Vps34p-GFP with actin patches (A) and FM (B).

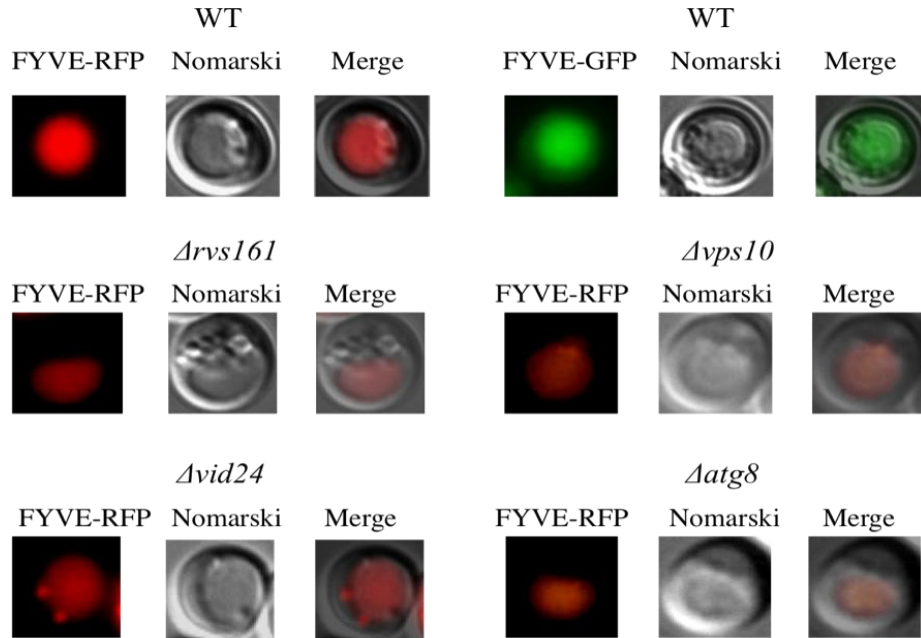


Fig. 5. FYVE is in vacuole lumen and punctate structures on the vacuole membrane. FYVE-RFP and FYVE-GFP was expressed in wild type cells and the distribution was examined. FYVE-RFP was expressed in *Δrvs161*, *Δvps10*, *Δvid24*, and *Δatg8* mutant strains. The distribution of FYVE-RFP was determined.

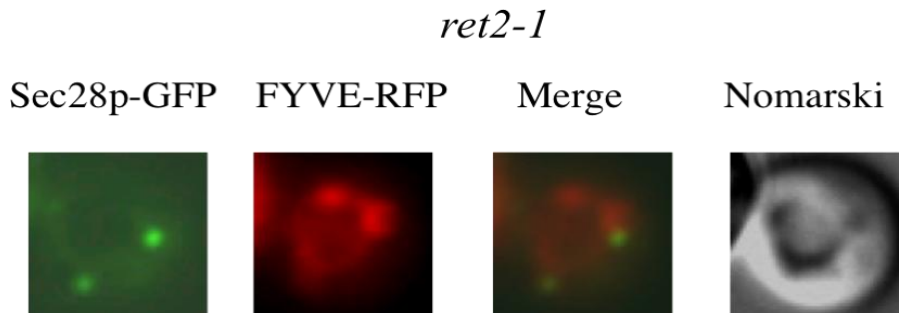


Fig. 6. FYVE-RFP does not co-localize with Sec28p-GFP in the *ret2-1* mutant. The *ret2-1* mutant expressing Sec28p-GFP and FYVE-RFP was glucose starved and shifted to glucose for 60 min and the distribution of FYVE-RFP with Sec28p-GFP was examined.

Research Project 6: Project Title and Purpose

Innate Immune Responses to the Malaria Parasite - Malaria is a major public health crisis around the world, affecting ~40% of the population and killing 2–3 million people annually. Currently, malaria is spreading rapidly due to drug resistance. A significant number of people from non-malaria regions (military and business personnel, diplomats and visitors) are also at increased risk and are particularly vulnerable to severe or even fatal forms of the disease because of their non-immune status. Therefore, novel drugs/therapeutics and/or vaccines are needed urgently. We propose to study cell signaling mechanisms in the innate immune responses produced by the host in response to malaria parasite infection and the regulation of innate immune responses. The knowledge gained by the proposed studies should prove to be valuable in developing novel immunotherapeutics and/or vaccines for combating malaria.

Duration of Project

1/1/2007 - 6/30/2010

Project Overview

The broad objective of this research project is to understand the mechanisms of cell signaling, the regulation of innate immune responses during malaria infection, and the role of innate immune responses in modulating adaptive immunity, and to use the information gained for developing immunotherapeutics and/or vaccines for malaria.

The following are the specific aims of this project:

- (1) *To study the expression of TLR2 in macrophages and dendritic cells stimulated with GPIs.* We will study the changes in expression of TLR2 in wild-type and TLR4-deficient macrophages in response to malarial Glycosylphosphatidylinositols (GPIs) by analyzing mRNA by RT-PCR, and of proteins on the cell surface by immunofluorescence and flow cytometry analyses using anti-TLR2 monoclonal antibodies. We will also study the changes in expression of TLR2 in TLR4^{-/-} and MyD88^{-/-}, and in wild-type dendritic cells.
- (2) *To understand the regulation of TNF- α and IL-12 production by MK2 and TPL2 knockout macrophages.* We will: (i) determine the expression of TNF- α and IL-12 in MK2- and TPL2-deficient macrophages stimulated with malarial antigens; (ii) study the production of TNF- α and IL-12 by macrophages pretreated with ERK and p38 MAPK inhibitors upon stimulation of cells with malarial antigens; (iii) analyze the expression of I κ B ζ , a newly discovered nuclear factor that is specifically involved in the transcription of a subset of cytokine genes, particularly *IL-12*, but not *TNF- α* ; and (iv) study the role of transcription inhibitory factors, such as c-Maf and GAP-12, in the transcription of *IL-12* in macrophages stimulated with malarial antigens.
- (3) *To identify the receptors on cells of the innate immune system involved in the recognition of malaria parasite factors that interact with the host.* The malarial factors that interact with the host during blood stage infection include parasite membranes, digestive vacuoles, and hemozoin that are released during the schizont burst. We will determine the receptor involved in the

recognition of malaria parasite membranes and digestive vacuoles, and hemozoin using bone marrow-derived macrophages and dendritic cells obtained from wild-type and various TLRs- and MyD88-knockout mice.

Principal Investigator

Channe D. Gowda, PhD
Penn State University
College of Medicine
Dept. of Biochemistry and Molecular Biology
Room C5710, Mail Code H171
500 University Drive
Hershey, PA 17033

Other Participating Researchers

None

Expected Research Outcomes and Benefits

Inappropriate regulation of proinflammatory responses by the host during the blood stage of *Plasmodium* species parasites is thought to play a key role in malaria pathogenesis. Many of the malaria symptoms, including periodic fever, chills, malaise, and cerebral and other organ-related dysfunctions are associated with the excessive and prolonged production of inflammatory cytokines such as TNF- α , IFN- γ and IL-1. Recovery without adverse sequel from malaria infection is associated with significant levels of anti-inflammatory responses produced soon after the acute phase infection. Therefore, it is essential that the innate immune responses that are induced early during malaria infections for parasite killing should be appropriately controlled to avoid pathogenic processing. However, very little is known about the cell signaling mechanisms involved in initiating proinflammatory responses to malaria, the malarial factors that contribute to the initiation of innate immune responses, and the regulation of these immune responses. A clear and comprehensive knowledge of the initiation and regulation of innate immune responses will help further the understanding of malaria pathogenesis with significant implications for malaria control strategies. The studies proposed should identify the host receptors involved in recognizing the malaria antigens that induce innate immune responses, determine whether or not the expression of host receptors is altered during infection, and identify key signaling pathways and their regulation, thereby establishing a platform for further studies on the regulation of innate immune responses. Knowledge gained by these studies will be valuable in developing novel immunotherapeutics and/or vaccines for malaria.

Summary of Research Completed

I κ B ζ is a nuclear factor that is related to the I κ B family of proteins. It is readily and strongly induced upon stimulation of macrophages with TLR ligands. Generally, the I κ B family of proteins binds NF- κ B proteins and inhibits their activity. In contrast, I κ B ζ complexes with p50 homodimer and binds to promoters of cytokines, such as IL-12 and IL-6, and growth factors and

induces their expression. Thus, we hypothesize that I κ B ζ plays critical roles in the TLR ligand-induced, high level expression of IL-12, IL-6, and other cytokines. During the current grant period, we studied the role I κ B ζ in the IFN γ -induced production of IL-12 in response to malarial glycosylphosphatidylinositols (GPIs), the ligand that activates macrophages through the recognition of TLR2, leading to the production of various cytokines, including IL-12. During malaria infection, IL-12 is produced at very high levels. IL-12 plays an important role in the control of infection by modulating adaptive immune responses. Thus, understanding of how the expression of IL-12 is regulated may provide targets for therapeutic interventions for malaria.

Our working hypothesis is that while classical NF- κ B family proteins such as NF- κ B/p65 and NF- κ B/c-Rel are involved in the moderate expression of IL-12 in response to TLR ligands, I κ B ζ is required for the high level production of IL-12 IFN γ -primed macrophages stimulated with TLR ligands. It is possible that I κ B ζ collaborates with the IFN γ -induced transcription factors to produce high levels of IL-12. To test this hypothesis and to investigate the role of I κ B ζ in the malaria parasite ligand-induced IL-12 expression, we used gene knockdown procedures using siRNA corresponding to the 617-637 and 824-844 bp of I κ B ζ gene open reading frame. We used GPIs purified from cultured malaria parasite *Plasmodium falciparum* and macrophages derived from the differentiation of mouse bone marrow cells by macrophage colony-stimulating factor. A CpG oligodeoxynucleotide (TLR9 ligand) and Pam₃CSK₄ (TLR2 ligand) were used as controls.

The kinetics of I κ B ζ induction by macrophages stimulated with malarial GPIs is shown in Fig. 1. Transfection of IFN γ -primed macrophages with I κ B ζ siRNA resulted in the knockdown of I κ B ζ mRNA expression to substantial levels (Fig. 2). siRNA used for the gene knockdown correspond to the 617-637 and 824-844 nucleotide base regions of the I κ B ζ gene open reading frame and their sequences are depicted below.

While both siRNA could knockdown the I κ B ζ gene considerably (Fig. 2, lanes 6 and 8), control siRNA had no noticeable effect (Fig. 2, lane 4), demonstrating the observed lower level of I κ B ζ induction is due to specific knockdown of the gene. Of the two siRNA tested, the 824-844 siRNA showed considerably higher capacity to knockdown I κ B ζ mRNA level than 617-137 siRNA (Fig. 2; compare lane 8 with lane 6).

Knockdown of I κ B ζ gene expression by transfection with siRNA caused ~50% decrease in the production of IL-12 by IFN γ -primed macrophages stimulated with GPIs, CpG oligodeoxynucleotide or Pam₃CSK₄ compared to the cells transfected with control siRNA. These results strongly suggest that I κ B ζ plays an important role in the expression of IL-12 by macrophages activated with malarial and other pathogenic ligands.

824-844 sense - GCGUCAAUGUACCAGUAUU
 antisense - AAUACUGGUACAUUGACGC

Control sense - GCCGUAACCAUUGACUAUUTT
 antisense - AAUAGUCA AUGGUUACCGCTT

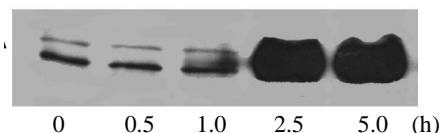


Fig. 1. Time course of I κ B ζ induction of by macrophages stimulated with GPIs.

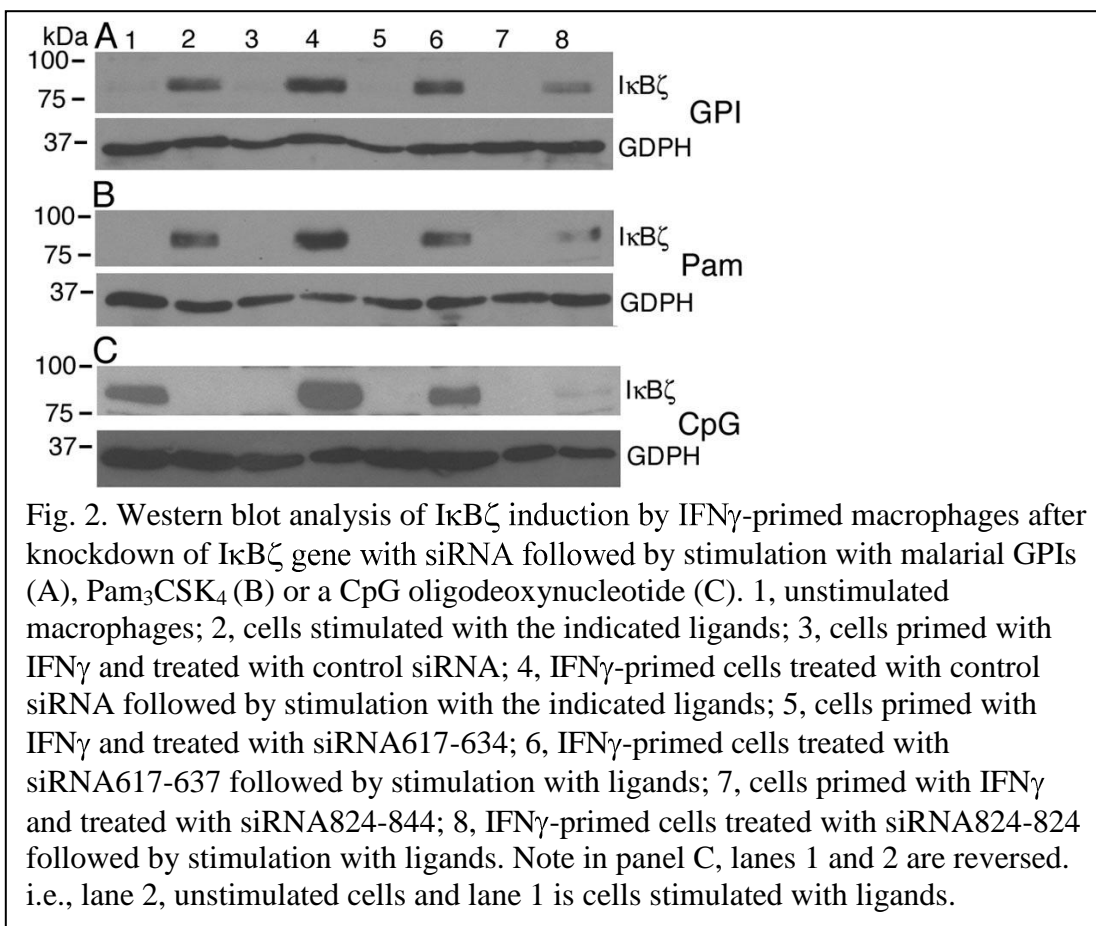


Fig. 2. Western blot analysis of IκBζ induction by IFNγ-primed macrophages after knockdown of IκBζ gene with siRNA followed by stimulation with malarial GPIs (A), Pam₃CSK₄ (B) or a CpG oligodeoxynucleotide (C). 1, unstimulated macrophages; 2, cells stimulated with the indicated ligands; 3, cells primed with IFNγ and treated with control siRNA; 4, IFNγ-primed cells treated with control siRNA followed by stimulation with the indicated ligands; 5, cells primed with IFNγ and treated with siRNA617-634; 6, IFNγ-primed cells treated with siRNA617-637 followed by stimulation with ligands; 7, cells primed with IFNγ and treated with siRNA824-844; 8, IFNγ-primed cells treated with siRNA824-824 followed by stimulation with ligands. Note in panel C, lanes 1 and 2 are reversed. i.e., lane 2, unstimulated cells and lane 1 is cells stimulated with ligands.

Research Project 7: Project Title and Purpose

Chromatin Structure in Silent and Active URA3 Gene In Vivo - We have developed a novel technique: EM-assisted nucleosome interaction capture (EMANIC) for studying nucleosome interactions in condensed chromatin in vitro. The purpose of this work is to extend this technique to study chromatin organization of a single gene (URA3) *in vivo*. URA3 is one of the most widely used genetic models. This gene has been placed in a yeast *S.cerevisiae* plasmid under control of silencing (HML) and activation (STAR) genetic regulators and functionally tested.

Duration of Project

4/1/2007 -12/31/2008

Summary of Research Completed

This project ended during a prior state fiscal year. For additional information, please refer to the Commonwealth Universal Research Enhancement Annual C.U.R.E. Reports on the Department's Tobacco Settlement/Act 77 web page at <http://www.health.state.pa.us/cure>.

Research Project 8: Project Title and Purpose

The Effects of Sleep Deprivation on Addiction and Relapse - The proposed studies will evaluate whether chronic sleep deprivation (SD), akin to levels commonly experienced by humans, facilitates addiction and relapse to cocaine in rats, and the underlying neural mechanisms by which those effects are mediated.

Duration of Project

4/1/2007 – 12/31/2007

Summary of Research Completed

This project ended during a prior state fiscal year. For additional information, please refer to the Commonwealth Universal Research Enhancement Annual C.U.R.E. Reports on the Department's Tobacco Settlement/Act 77 web page at <http://www.health.state.pa.us/cure>.

Research Infrastructure Project 9: Project Title and Purpose

Research Infrastructure: Renovations to Chandlee and Wartik Laboratories - The demand for campus-wide core facilities has increased significantly in the last five years, particularly the Nucleic Acid Sequencing facility, the DNA Microarray facility, and the Biotechnology teaching labs. These facilities are currently housed in the 2nd floor of the Wartik laboratory and will be moved to the 4th floor of Chandlee. The renovation of Chandlee will allow researchers easy access to the new facilities. The 2nd floor of Wartik will then be renovated and become a state-of-the-art facility to house new faculty in Genomics and Proteomics, and will cater to the structural biology research needs of more than fifty investigators from five different colleges.

Anticipated Duration of Project

7/1/2007 - 6/30/2009

Summary of Research Completed

This project ended during a prior state fiscal year. For additional information, please refer to the Commonwealth Universal Research Enhancement C.U.R.E. Annual Reports on the Department's Tobacco Settlement/Act 77 web page at <http://www.health.state.pa.us/cure>.

Research Project 10: Project Title and Purpose

Analyzing Hepatitis B Virus Pathogenesis - The goal of this project is to investigate and characterize the effect of a novel anti-Hepatitis B virus (HBV) agent (shRNA-458) on HBV replication, specifically focusing on its effect on nuclear HBV covalently closed circular DNA (cccDNA) pools, which are responsible for HBV transcription and persistent HBV infections and the recycling of HBV nucleocapsids back into the nucleus. The efficacy of shRNA-458 will be compared to those of nucleoside and nucleotide analogues currently used to treat chronic HBV infections and other shRNA sequences targeting a different region of the HBV genome (HBV 2/20) other than that targeted by shRNA-458. The efficacy of shRNA-458, when administered at multiple doses and in conjunction with nucleoside and nucleotide analogues or HBV 2/20, will also be investigated.

Duration of Project

1/1/2007 – 6/30/2010

Project Overview

The broad objective is to evaluate novel agents for intervention in chronic HBV infection. The specific aims are:

1. The time course and magnitude of (1) the effect of shRNA-458 on HBV transcription, and (2) the expression levels of shRNA-458 will be determined by transducing HepG2 cells at a multiplicity of infection (MOI) of 100, with shRNA-458 expressing recombinant baculovirus 24 hrs prior to initiation of a HBV infection. Total RNA will be harvested at various time points post-HBV infection and visualized by Northern blotting using specific probes for HBV and shRNA-458.
2. The efficacy of shRNA-458 will be compared to that of nucleoside and nucleotide analogues currently used to treat HBV-infected patients and to other shRNAs (HBV 2/20) targeting different HBV sequences using a novel HBV-infected HepG2 subculture system where an HBV infection is initiated in HepG2 cells using HBV expressing recombinant baculovirus (MOI 100) 10 days prior to the cells being subcultured 1:4. In this aim, the HBV infected cells will be transduced with shRNA-458 expressing recombinant baculovirus (MOI 100), HBV 2/20

expressing recombinant baculovirus, or nucleoside/nucleotide analogues 24 hrs post subculture, and their effect on the various HBV DNA species will be visualized by Southern blotting and compared to each other and control treated cells.

3. The subculture system will be utilized to investigate and maximize the antiviral effects on HBV cccDNA levels. HBV-infected subcultured HepG2 cells will be transduced with recombinant baculovirus expressing shRNA-458 alone, at multiple doses, and in conjunction with nucleoside analogues, nucleotide analogues, novel anti-HBV agents, or HBV 2/20, and their effect on HBV replication, specifically focusing on HBV cccDNA levels, will be investigated.

4. The HBV infected HepG2 cell subculture system will be used to measure the effect of shRN-458 on HBV nucleocapsid recycling back to the nucleus to amplify cccDNA pools. HBV infected subcultured HepG2 cells will be transduced with shRNA-458 (MOI 100) and the levels of HBV cccDNA and HBV nucleocapsids will be measured by Southern blotting and Western blotting respectively. Nucleocapsid localization will be analyzed using confocal microscopy.

Principal Investigators

Harriet C. Isom, PhD
Pennsylvania State University
College of Medicine, H107
500 University Dr.
Hershey, PA 17033

Other Participating Researchers

None

Expected Research Outcomes and Benefits

HBV cccDNA is the source of HBV transcripts and replication as well as the causative agent of persistent HBV infections. It is critical to investigate and determine whether or not novel anti-HBV agents, such as shRNA-458, are capable of affecting HBV cccDNA levels and the mechanism by which this may occur. By measuring the effect of shRNA-458 on HBV transcript levels and the levels of shRNA-458 during this time, it is possible to confirm shRNA-458's mechanism of action and determine appropriate dosing regimes. We expect that shRNA-458 is capable of inhibiting HBV replication by significantly degrading the major HBV transcripts, and that its expression levels will remain elevated through day 6 post-treatment based on previous data concerning baculovirus persistence.

In order to maximize the antiviral effect on HBV cccDNA, multiple aspects of the viral life cycle must be targeted. This project will focus on combining various anti-HBV agents, each specifically targeting a different aspect of the viral lifecycle, with the ultimate goal of reducing HBV cccDNA pools during a persistent infection. We project that by significantly inhibiting HBV replication through the combination of various anti-HBV agents, HBV cccDNA amplification will be adversely affected. Affecting HBV cccDNA levels is an extremely

important step in curing a persistent HBV infection, since cccDNA is the primary source of HBV transcripts and HBV rebound after treatment withdrawal.

Newly generated HBV nucleocapsids recycle back to the nucleus in order to amplify HBV cccDNA levels. It is vital to the generation of successful anti-HBV agents that this process is investigated during a persistent infection. This project will focus on the effect of shRNA-458 on HBV nucleocapsid recycling. We hypothesize that shRNA-458 will adversely affect HBV nucleocapsid formation, and therefore, the recycling of nucleocapsids back to the nucleus.

Summary of Research Completed

Delivery of cationic nanoliposome-encapsulated siRNA to HepG2 cells. Different cationic nanoliposome formulations were evaluated for their ability to fuse with and to deliver functional siRNA to HepG2 cells. Several rhodamine (Rh)-labeled cationic nanoliposomes formulations bound to HepG2 cells. GAPDH siRNA in the proprietary STEALTH background and the matched scrambled control were purchased (Invitrogen) and 80nM GAPDH siRNA was encapsulated in each formulation. Each formulation protected siRNA from RNase. However, when HepG2 cells were treated with each encapsulated siGAPDH, marked inhibition of GAPDH mRNA was only observed using the LiP9 formulation. In addition, only a slight reduction in GAPDH mRNA levels was observed when HepG2 cells were treated with Lipofectamine 2000 siGAPDH. Experiments described below were pursued with LiP9 cationic nanoliposomes. The LiP9 cationic nanoliposomes were prepared as follows. The lipids, N-[1-(2,3-Dioleoyloxy)propyl]-N,N,N-trimethylammonium methylsulfate (DOTAP), 1,2-distearoyl-sn-glycero-3-phosphoethanolamine-N-[methoxy(polyethylene glycol)-2000] (ammonium salt), and 1,2-distearoyl-sn-glycero-3-phosphocholine, dissolved in chloroform, were combined. The lipid mixture was then dried under a stream of nitrogen above lipid transition temperatures and hydrated with sterile PBS. The resulting solution was sonicated for 10 min followed by extrusion through 100-nm polycarbonate membranes for 11 times. The final concentration of LiP9 is 45.4% DOTAP, 11.0% PEG(2000)-DSPE, and 43.6% DOPE. To prepare loaded liposomes, 20 µM siRNA stock was diluted into RNase-free water. 6.5 µl liposomes were added to diluted siRNA, mixed gently and incubated 16h at room temperature. Culture media was added to the passively loaded liposomes. Media from the cells in a 6-well plate was removed and the 0.5 ml solution was added drop wise. Culture plates were incubated at 37C for one hour with rocking every fifteen minutes at which time 1.5 ml of media was added to each well of cells for a final volume of 2 mls.

The effect of HBV-specific U6S siRNA or GAPDH siRNA, each encapsulated in LiP9 on HBV and GAPDH transcripts using the subculture HBV bac system. The U6S siRNA molecule used in these experiments was designed to mimic the final processed siRNA product generated from the U6S shRNA sequences. For U6S (starting at nt 456 in the Eco R1 site-based numbering system): UAUCAAGGUAUGUUGCCCGUUUGUC and GACAAACGGGCAACAUACCUUGAUA, and for U6C: UAUGAUGUAUGGUCCGCUUUAC.GUC and GACGUAAAGCGGACCAUACAUCAUA. Since the HBV bac system produces very high levels of HBV replication and in the subculture system, the high level of CCC DNA continuously replenishes the HepG2 cells with HBV transcripts, it was also important in the same *in vitro* subculture HBV system to use an additional

target to address the general question of efficacy of the LiP9 nanoliposomes to successfully deliver a functional siRNA to HepG2 cells. The cellular GAPDH mRNA was selected as the target. The first study carried out was a concentration curve (Fig. 1). HepG2 cells, at day 10 p.t. with HBV bac (100pfu/cell), were subcultured 1:7 into 6 well plates. 24h post subculture, cells were mock treated, treated with empty LiP9 nanoliposomes; 80nM, 160nM, and 240nM U6C siRNA (scrambled control) encapsulated in LiP9 nanoliposomes; 80nM, 160nM, and 240nM U6S siRNA (HBV specific) encapsulated in LiP9 nanoliposomes; 3TC (0.2uM); and 80nM, 160nM, and 240nM GAPDH siRNA encapsulated in LiP9 nanoliposomes (Fig. 2). For all treatments, the LiP9 concentration was 97.5mg/1.5x10⁶ cells. The U6S and U6C siRNAs both act as siRNA controls for the GAPDH siRNA. Similarly, both the scrambled U6C siRNA and the GAPDH siRNAs act as siRNA controls for the HBV-specific U6S siRNA. Treatment with 3TC at a concentration that inhibits HBV replication was included as a control since it acts downstream of the HBV transcripts and should have no effect on HBV RNA levels. Total RNA was harvested from subcultured HBV-HepG2 cells at 48h post nanoliposome or mock treatment and analyzed by Northern blotting. Probes were generated from full-length double-stranded HBV genome and GAPDH double-stranded DNA radiolabeled with [α -³²P]dCTP using a Random Prime Labeling kit (Roche Diagnostics). The membranes were hybridized with a mixture of HBV and GAPDH-specific [α -³²P]dCTP probes. The positions of the major HBV transcripts (3.5, 2.4 and 2.1kb) and the GAPDH RNA are indicated (Fig. 2A). The marked down regulation of GAPDH RNA (82%) reduction strongly suggests that delivery was highly efficient. In addition the finding that GAPDH siRNA had essentially no effect on the HBV transcripts indicates the specificity of the siRNA approach. The 3.5, 2.4 and 2.1kb transcripts were all down regulated as predicted because of the overlapping nature of the three HBV transcripts. 3TC had no effect on the HBV and GAPDH transcripts as expected. Quantification of the data for the 3.5 kb transcript is shown (Fig. 2B). The data were normalized for loading to the GAPDH band and the imager units for treatment with each concentration of the matched encapsulated scrambled control siRNA was set to 100%. Treatment with 80 nM U6S siRNA encapsulated in LiP9 nanoliposomes resulted in 36.1% reduction in the HBV 3.5kb RNA transcript compared to treatment with 80nM U6C siRNA. Increasing the amount of U6S siRNA encapsulated caused reductions in the 3.5 kb transcript of 25.6% for 160nM and 42% for 240nM). The previous study was limited to evaluating the effects of a single treatment with siRNA and a single endpoint of 48h after treatment. The next goal was to increase the number of treatments. Two separate approaches were taken; two treatments with a total exposure time to therapy of 72h and three treatments with a total exposure time of therapy of 120h (Fig. 3).

The amount of siRNA delivered at each treatment was 80nM. HepG2 cells at day 10 p.t. with HBV bac (100pfu/cell), were subcultured. 24h post subculture, therapy was initiated. Two treatments (with harvest at 72h after the first treatment) with U6S siRNA (80nM) encapsulated in LiP9 nanoliposomes resulted in 39.2% reduction in the level of the HBV 3.5kb RNA transcript compared to treatment with U6C siRNA (control scrambled) and had no effect on the level of the GAPDH transcript (Fig. 3A). Three treatments (with harvest at 120 h after the first treatment) with U6S siRNA (80nM) encapsulated in LiP9 nanoliposomes resulted in 47% reduction in the level of the HBV 3.5kb RNA transcript compared to treatment with U6C siRNA (control scrambled) and had no effect on the level of the GAPDH transcript (Fig. 3B). Two treatments with GAPDH siRNA (80nM) encapsulated in LiP9 resulted in an average of 86% reduction in

GAPDH RNA level and had no effect on the HBV transcripts and three treatments resulted in an average of 89% reduction in GAPDH RNA with no effect on the HBV transcripts.

Summary: (1) The LiP9 is highly efficient for delivering functional siRNA to HepG2 cells. (2) STEALTH GAPDH siRNA is highly effective at down regulation of human GAPDH RNA in cells of hepatic origin. (3) The combination of multiple treatments and prolonged time course has a greater effect on down regulation of the HBV targeted transcripts than a single delivery followed by analysis at 48h after treatment.

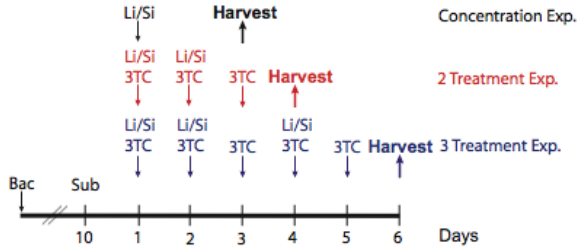


Fig. 1. Experimental protocols

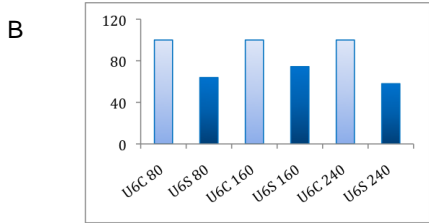
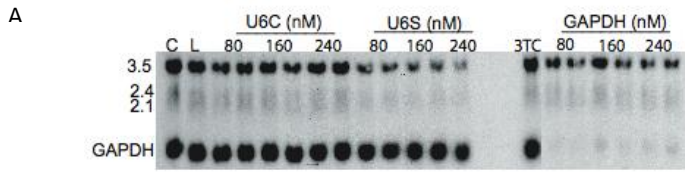


Fig. 2. Effect of siRNA concentration on GAPDH and HBV mRNAs. (A) Northern (B) Quantitative evaluation of U6S

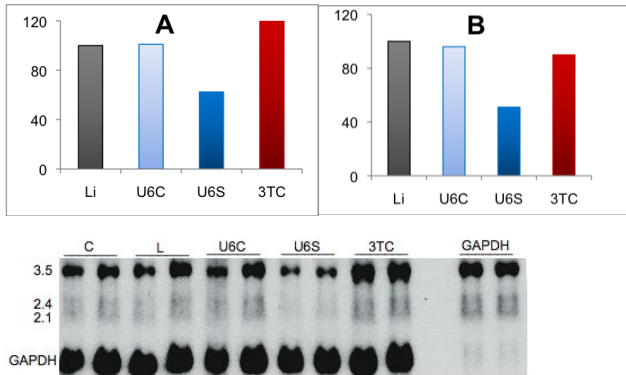


Fig 3. Effect of multiple siRNA treatments on GAPDH and HBV mRNAs. Quantification of 2 (A) and (B) 3 treatments. Y axis: imager units normalized to GAPDH for loading (C) Northern blot for three treatments

Research Project 11: Project Title and Purpose

Dopamine Mediated Calcium Dynamics in Schizophrenia - Schizophrenia is a devastating neuropsychiatric disorder, the etiology of which is unknown. Dysfunction in dopamine neurotransmitter signaling has been implicated as an important component of the disease. However, no defects in the cellular receptors, which transduce the dopamine signal, have been found. This project will identify components of the dopamine signaling system that may be altered in schizophrenia. We have recently identified a novel dopamine receptor interacting protein called TRPC (transient receptor potential channel) that connects dopamine and calcium signaling pathways in cells. This channel has been shown to be required for nicotine dependent behaviors in *C. elegans*, a model genetic system. In this project, we seek to validate the dopamine receptor-TRPC interaction and to understand the significance of this interaction for cellular function.

Duration of Project

4/1/2007 - 6/30/2009

Summary of Research Completed

This project ended during a prior state fiscal year. For additional information, please refer to the Commonwealth Universal Research Enhancement Annual C.U.R.E. Reports on the Department's Tobacco Settlement/Act 77 web page at <http://www.health.state.pa.us/cure>.

Research Infrastructure Project 12: Project Title and Purpose

Research Infrastructure: Center for the Treatment, Prevention, and Cure of Cancer - To design and construct a new building for the Penn State Cancer Institute that will bring together patient care, and basic and translational research under one roof to enhance our ability to provide comprehensive, coordinated cancer care. The new facility will allow top researchers to work together to create new therapies and to bring them quickly into state-of-the-art clinical care for the patients of central Pennsylvania. The funds requested are in addition to tobacco settlement Year 2005 funds allocated, since the entire project cost is estimated to be ~\$100 million.

Duration of Project

7/1/2007 - 12/31/2010

Project Overview

The long-range goal of this project is to continue to work towards developing the Penn State Cancer Institute (PSCI) as a world-class center for the treatment, prevention, and cure of cancer in Central Pennsylvania, and achieving designation by the National Cancer Institute as a Comprehensive Cancer Center. Cancer has been designated as the primary priority area for growth by the Pennsylvania State College of Medicine/Hershey Medical Center, and a new 165,000 square foot cancer center building is proposed that will combine clinical cancer care

with basic and translational research. It is estimated that the costs for this entire project are ~\$100 million. The aims of this project continue our intention to: (1) integrate cancer patient services at the Hershey Medical Center into one building designed specifically for cancer care; (2) develop the research infrastructure to bring together patient care, and basic, and translational research under one roof to enhance the ability of PSCI to provide comprehensive, coordinated cancer care to Central Pennsylvania; and (3) develop the resources, infrastructure and leadership to apply for designation from NCI as a Comprehensive Cancer Center. Centralizing patient care and basic and translational research in one location will greatly enhance the ability of PSCI to provide comprehensive, coordinated care. However, the greatest impact of the new building will be on the lives of cancer patients in Central Pennsylvania and their families, who will benefit from the increased efficiency in translating advanced medical research into increased survival and a better quality of life. The funds requested for this project will bring us closer to achieving our goals.

Principal Investigators

Thomas Loughran, Jr., MD
Dept. Medicine, H069
Pennsylvania State University
Hershey, PA 17033

Other Participating Researchers

Philip Lazarus, PhD, Karam El-Bayoumy, PhD, Harriet Isom, PhD, Witold Rybka, MD -
employed by Pennsylvania State University

Expected Research Outcomes and Benefits

There is a need for academic health centers, in the nation, state, and Central Pennsylvania, to increase the knowledge base related to cancer, and to aggressively prevent, treat and cure the many forms of this disease in diverse populations. The construction of a new facility at Penn State Cancer Institute (PSCI) combining clinical care and basic science research under one roof will allow for the recruitment and retention of outstanding cancer researchers in Central Pennsylvania, enable State funds to be leveraged for federal and industrial funds to enhance innovative research discoveries and effective treatments, and increase interactions between basic and clinical scientists, thus translating promising scientific discoveries into new and better options for the prevention, diagnosis, and treatment of cancer. The benefits will be improved care for cancer patients, and, through interactive community education programs, improved knowledge about all aspects of cancer, including prevention and control, by diverse individuals in the communities in Central Pennsylvania. Recognition of the PSCI as a Cancer Center by the National Cancer Institute will increase the recognition and competitiveness of Penn State researchers and colleagues for national funding. It will also allow PSCI to recruit the best trainees and new scientists and clinicians, and encourage the establishment of new high technology “spinoffs” as an economic engine for Central Pennsylvania. Meanwhile, cancer patients in Central Pennsylvania and their families will benefit from the increased efficiency in translating advanced medical research into increased survival and better quality of life.

Summary of Research Completed

Aim (1) Construction progress:

The construction of the Penn State Hershey Cancer Institute is complete. The Certificate of Occupancy was awarded on June 8, 2009 and Clinical operations opened to the public on July 13, 2009. The total cost of the PSHCI building is projected to be \$125.2 million. Note that this is research infrastructure project and funds from this grant for this project are being used to pay for construction costs, not for staffing of the Institute.

Aim (2) Development of Research Infrastructure:

The PSHCI continued to focus on improving the infrastructure of the organization. A new shared resource, Community Sciences and Health Outcomes, was created in 2010 with the staff located within the building. In addition, new staff members of the PSHCI Biostatistics Core and CTO are housed in the building. In March of 2010 we also successfully recruited a new Chief of the Division of Hematology Oncology who will also serve as the Associate Director for Translational Research. Dr. El-Deiry has institutional resources to support the recruiting of new investigators to strengthen the clinical trials and the translational research programs.

Aim (3) Progress towards NCI designation:

With the encouragement of the PSHCI External Advisory Board, in May of 2010 we submitted our first P30 CCSG application. The site visit for this application will take place in September of 2010.

Research Project 13: Project Title and Purpose

Role of Leucine Metabolism in Leucine Signaling - Recent evidence has suggested that increasing protein in the diet or some high protein diets promote weight loss through unexplained mechanisms. A component of protein called Leucine appears to be responsible. To examine the effect of elevating leucine, we knocked out an enzyme (BCATm) that begins leucine metabolism. The resulting mice had high plasma leucine concentrations in most tissues except their brain. More importantly, they were lean (about 60% less adipose tissue) and robustly resistant to obesity with improved glucose tolerance and insulin sensitivity. They actually eat more food. Our research is now focused on the molecular mechanisms explaining how knockout of this gene and increasing leucine brings about this phenotype. It should be possible to make blockers for this enzyme to bring about the same effects in humans.

Duration of Project

4/1/2007 - 6/30/2008

Summary of Research Completed

This project ended during a prior state fiscal year. For additional information, please refer to the Commonwealth Universal Research Enhancement Annual C.U.R.E. Reports on the Department's Tobacco Settlement/Act 77 web page at <http://www.health.state.pa.us/cure>.

Research Project 14: Project Title and Purpose

Mechanisms of TGF-beta Production in Human Cancer Cells - Tumor cells that are resistant to the growth inhibitory effects of TGF β can still secrete TGF β , which enhances tumorigenesis. It is advantageous to block this secreted TGF β in late-stage tumors. These studies will investigate the role of a novel component (km23) in controlling TGF β 1 production using a novel, multidimensional approach. The results of the studies should reveal significant differences between human colon carcinoma cells (HCCCs) and untransformed epithelial cells (UECs) in the altered compartmentalization of signaling complexes, as well as in the differential utilization of signaling components. The goal of this project is to reduce production of a growth factor that enhances the spread of colon cancer. The results should lead to the development of novel approaches to treat colon cancer. The tobacco funds for this project will be used as bridge funding to enable a Senior Research Associate and a Postdoctoral scholar gather additional data in response to reviewer's comments for the renewal of our NIH grant # NIH 2 RO1 CA 090765.

Duration of Project

1/1/2007 - 6/30/2008

Summary of Research Completed

This project ended during a prior state fiscal year. For additional information, please refer to the Commonwealth Universal Research Enhancement Annual C.U.R.E. Reports on the Department's Tobacco Settlement/Act 77 web page at <http://www.health.state.pa.us/cure>.

Research Project 15: Project Title and Purpose

Mechanisms of Cross Priming In Vivo - CD8+ T cells can protect against many pathologies, including viral, bacterial and fungal infections, as well as against many different kinds of tumors. These cells are only triggered after recognition of pathogen- or tumor-derived peptides in complex with MHC Class I molecules. The processes by which these peptide-MHC complexes are generated have been investigated in vitro, but the contribution of different pathways has not been investigated in vivo. Information about the mechanisms involved in peptide-MHC complex generation is essential for inclusion of the most efficient and effective formulation of antigen in vaccine preparations. In this project, those critical components of one antigen processing pathway, the cross priming pathway, will be identified.

Duration of Project

1/1/2007 - 6/30/2008

Summary of Research Completed

This project ended during a prior state fiscal year. For additional information, please refer to the Commonwealth Universal Research Enhancement Annual C.U.R.E. Reports on the Department's Tobacco Settlement/Act 77 web page at <http://www.health.state.pa.us/cure>.

Research Project 16: Project Title and Purpose

Proteomics of Substance Abuse - Ethanol abuse and alcoholism remain very serious societal problems producing a tremendous toll in terms of loss-of-life, adverse health effects, and lost productivity. A significant problem is the lack of a sensitive and specific clinical test to diagnose alcohol abuse either in the general population or within selected groups of individuals such as recovering/relapsing alcoholics. The goal of this project is to screen for signature biomarkers in a well-controlled and extensively documented non-human primate model of self-administration in order to develop diagnostic markers of excessive alcohol consumption.

Duration of Project

4/1/2007 - 6/30/2007

Summary of Research Completed

This project was dropped prior to the expenditure of any grant funds.

Research Project 17: Project Title and Purpose

Positive Selection-dependent Skin-homing of Fetal Thymic $\gamma\delta$ T Cells - To fight efficiently against cancers, infection and other diseases, immune cells reside in specific tissues where they function uniquely to protect the local tissues. Disruptive localization of the immune cells in proper tissues renders a body susceptible to diseases. Therefore, understanding molecular mechanisms of development and localization of these immune cells in specific tissues is important for our effort to improve our health. The purpose of this project is to determine molecular and cellular events regulating the developmental process of skin-specific $\gamma\delta$ T cells, an important class of immune cells.

Duration of Project

1/1/2007 - 6/30/2010

Project Overview

$\gamma\delta$ T cells are a unique class of immune cells that plays important roles in tumor surveillance, microbial immunity and others. Many $\gamma\delta$ T cells preferentially reside in epithelial layers of various tissues underlying external and internal surfaces of the body, such as skin, lung and intestines, where they function as the first line of defense. The murine skin-specific intraepithelial $\gamma\delta$ T cells (sIELs) are some of the most representative tissue-specific $\gamma\delta$ T cells, which play important roles in the prevention of cutaneous tumors, regulation of skin-allergic responses and others. Nearly all sIELs express identical V γ 3/V δ 1 g δ T cell receptors (TCR) and originate from the fetal thymus. Recently, it was discovered that the skin-specific $\gamma\delta$ T cell precursors generated in the fetal thymus underwent a unique selection process that renders them unique homing properties, which may determine their specific migration and localization into the

skin. These findings suggest that central selection in the thymus determines their peripheral tissue distribution, a novel conceptual advance in understanding the development of the tissue-specific lymphocytes. To test and define this hypothesis, the project proposed here will include two specific aims to study molecular and cellular events that link fetal thymic selection of $\gamma\delta$ T cells with their skin-specific tissue distribution.

Specific Aim 1: To dissect TCR/ligand interaction-mediated fetal thymic $\gamma\delta$ T cell selection, in relationship with its unique homing properties and skin-specific tissue distribution. $\gamma\delta$ TCR transgenic mice with known ligands will be employed to investigate how TCR/ligand engagement mediates selection of fetal thymic $\gamma\delta$ T cells and determines their homing properties and unique peripheral tissue distribution in the skin.

Specific Aim 2: To determine the roles of CCR10 in sIEL development using CCR10-knockout/EGFP-knockin mice. Chemokine receptor CCR10 is upregulated in the positively selected fetal thymic sIEL precursors. Constitutive expression of its ligand CCL27 in the skin suggests a potential role of CCR10 as a skin-homing receptor for the sIEL precursors. CCR10-knockout/EGFP-knockin mice will be generated and used to determine the role of CCR10 in sIEL development.

Principal Investigators

Na Xiong, PhD
Pennsylvania State University
221 ASI
Dept. of Veterinary and Biomedical Sciences
115 Henning Building
University Park, PA 16802

Other Participating Researchers

Anthony P. Schmitt, PhD - employed by Pennsylvania State University

Expected Research Outcomes and Benefits

This project will improve the fundamental understanding of genesis of the skin-specific $\gamma\delta$ T cells. Furthermore, as the first approach to investigate differential homing processes of various immune cell populations, this project will serve as a paradigm for understanding specific migration and localization of other tissue-specific immune cells. By identifying molecules that regulate migration and localization of $\gamma\delta$ T cells in the skin, we might be able to design a better strategy to target these important immune cells to specific tissues to fight against diseases.

Summary of Research Completed

Murine skin-specific intraepithelial T cells (sIELs) are prototypic tissue specific “innate lymphocytes” that play important roles in maintaining skin integrity, through processes such as tumor surveillance and wound healing. Nearly all the sIELs express canonical $V\gamma 3^+$ $\gamma\delta$ T cell

receptors (TCR) and are derivatives of thymic $V\gamma 3^+ \gamma\delta$ T cells that are generated only at the fetal stage of ontogeny. We hypothesized that central selection of the fetal thymic $V\gamma 3^+ \gamma\delta$ T cells determines their peripheral tissue distribution in the skin and proposed two specific aims to study molecular and cellular events that link fetal thymic selection of $\gamma\delta$ T cells with their skin-specific tissue distribution: 1) To determine the roles of CCR10 in sIEL development using CCR10-knockout/EGFP-knockin mice and 2) To dissect TCR/ligand interaction-mediated fetal thymic $\gamma\delta$ T cell selection in relationship with its unique homing properties and skin-specific tissue distribution.

In previous report period, we successfully generated CCR10 knockout mice and used them to analyze the development of sIEL as proposed in the Specific Aim 1. In this report period (July 1, 2009-June 30, 2010), we focused on the Specific Aim 2 to dissect mechanisms of TCR/ligand interaction mediated selection of fetal thymic sIEL precursors for their development into skin-specific T cells and found that a TCR signaling molecule Itk is a critical signaling molecule regulating the acquirement of the skin-homing property by the fetal thymic sIEL precursors. In ITK-knockout mice, the sIEL precursors could not undergo the positive selection-associated upregulation of thymus-exiting and skin-homing molecules S1PR1 and CCR10 and accumulated in the thymus. On the other hand, the survival and expansion of sIELs in the skin did not require the ITK-transduced TCR-signaling while its persistent activation impaired the sIEL development by inducing apoptosis. These findings provide insights into molecular mechanisms underlying differential requirements of the TCR signaling in peripheral localization and maintenance of the tissue specific T cells. Following are details of the results.

Defective development of epidermal $\gamma\delta$ T cells in ITK-knockout mice

To evaluate the role of ITK-mediated signaling in the sIEL development, we first assessed the sIEL populations in ITK^{-/-} and wild-type mice by flow cytometry (Fig. 1A). Compared to the wild type controls of same ages, 6-8 week old ITK^{-/-} mice had reduced percentages of $V\gamma 3^+$ sIEL (14.73±0.41% vs. 3.56±0.32%, p<0.0001). In situ examination of sIELs on skin epidermal sheets by immunofluorescent microscopy confirmed the impaired development of sIELs in ITK^{-/-} mice [181.8±19.5 (WT) vs. 66.3±4.3 (ITK^{-/-}) cells/field, p<0.05] (Fig. 1B and C). The defective development of ITK^{-/-} sIELs could be observed in the early fetal thymic stage. Compared to the wild type controls, transcripts of rearranged $V\gamma 3$ TCR in the fetal skin were dramatically decreased in ITK-knockout mice (> 10 fold reduction) (Fig. 1D), suggesting that the defective sIEL development originates at the fetal stage, likely due to impaired generation and/or selection of the fetal thymic sIEL precursors.

sIEL precursors undergo a seemingly normal positive selection process but accumulate in the fetal thymus of ITK^{-/-} mice

We then determined whether ITK deficiency affects their positive selection and maturation, which are associated with upregulation of CD122 and downregulation of CD24 in wild type mice. Surprisingly, this was also the case in fetal thymic $V\gamma 3^+$ cells of ITK^{-/-} mice (Fig. 2A), indicating that ITK-deficiency does not affect their general selection and maturation processes.

Generation of the fetal thymic $V\gamma 3^+$ sIEL precursors was not impaired significantly in ITK^{-/-} mice either. Although there was a slight delay in the appearance of $V\gamma 3^+ \gamma\delta$ T cells in E15 fetal thymi of ITK^{-/-} mice, this was no longer the case by E16 (Fig. 2B). In fact, as the fetuses aged,

there was gradual accumulation of $V\gamma 3^+$ cells in the $ITK^{-/-}$ fetal thymi. By E18 when the number of $V\gamma 3^+$ cells was decreased in wild type fetal thymi due to the egress of mature $V\gamma 3^+ \gamma\delta$ T cells and the reduced generation of new $V\gamma 3^+$ cells, the number of $V\gamma 3^+$ cells continued to increase in the $ITK^{-/-}$ fetal thymi, resulting in significantly more of these cells in $ITK^{-/-}$ than in wild type mice (Fig. 2B). These findings raise a possibility that the ITK deficiency might affect the proper migration of the sIEL precursors.

ITK-deficient fetal thymic sIEL precursors cannot undergo a proper switch in the expression of thymus-exiting and skin-homing molecules

To determine whether different migration molecules are properly expressed in ITK-knockout sIEL precursors. As shown in Fig. 3A, compared to the wild type controls, the upregulation of homing molecules CCR10 and S1PR1 expression in the $ITK^{-/-}$ fetal thymic $CD122^+ V\gamma 3^+ \gamma\delta$ T cells was significantly impaired (Fig. 3A). The mature fetal thymic $CD122^+ V\gamma 3^+$ T cells of $ITK^{-/-}$ mice also expressed a lower level of KLF2 (Fig. 3A), a transcription factor critical in the regulation of chemokine receptor expression in positively selected $\alpha\beta$ T cells, suggesting that KLF2 might be involved in the ITK-mediated chemokine receptor expression.

To further confirm that the ITK deficiency impaired the CCR10 upregulation in the positively selected sIEL precursors, we crossed $ITK^{-/-}$ mice with CCR10 knockout/GFP knockin mice that use the EGFP as a reporter for the CCR10 expression. The resultant $ITK^{-/-} CCR10^{+/EGFP}$ mice had a significantly reduced percentage of $CCR10(EGFP)^+ V\gamma 3^+ \gamma\delta$ T cells in the early fetal thymus (Fig. 3B, top group). However, as the fetus aged, this reduction disappeared (Fig. 3B, bottom group). Considering that the $ITK^{-/-}$ mature $V\gamma 3^+ \gamma\delta$ T cells are defective in the upregulation of S1PR1, a molecule important for their thymic egress, one plausible explanation for this is that although the $ITK^{-/-} V\gamma 3^+$ T cells have the impaired upregulation of CCR10 after the positive selection, the smaller number of $CCR10^+ V\gamma 3^+$ cells are unable to emigrate and accumulate in the thymus. Consistent with this, $ITK^{-/-}$ fetal thymic $V\gamma 3^+ \gamma\delta$ T cells migrated much less efficiently than wild type controls towards its ligand S1P in an in vitro migration assay (Fig. 3C). The $ITK^{-/-} V\gamma 3^+ \gamma\delta$ T cells also had defects in migration towards CCL27 and culture media of the fetal skin (Fig. 3C), suggesting that they have impaired ability in the CCL27-mediated skin homing. Together, these results demonstrate that ITK-mediated signaling is important for the positive selection associated acquisition of the unique homing property in the fetal thymic $V\gamma 3^+$ sIEL precursors for their egress from the thymus and localization in the skin.

ITK-regulated TCR signals are not required for the expansion of sIELs in the skin

Even though the $ITK^{-/-}$ fetal thymic sIEL precursors exhibited severe defects in the skin-seeding at the fetal stage, the reduction in the number of sIELs in adult $ITK^{-/-}$ mice is not as much severe (Fig. 1). This suggests that there might be a homeostatic compensation by which the few ITK-deficient sIEL precursors that make it to the skin are capable of the extensive expansion. Supporting this, the ITK-deficient sIELs incorporated BrdU at the level similar as, if not higher than, wild type sIELs in vivo (Fig. 4A). In addition, there was no significant difference in the in vitro proliferation of the $ITK^{-/-}$ and wild-type fetal thymic sIEL precursors in response to the anti- $\gamma\delta$ TCR antibody stimulation (Fig. 4B). These results support a notion that the TCR-mediated signaling is not required for the peripheral expansion of sIELs. Likely, the expansion of

sIELs in the skin is driven by the IL-15/receptor signaling. Consistent with this, $ITK^{-/-}$ fetal thymic $\gamma\delta$ T cells proliferated normally in response to IL-15 (Fig. 4C).

Continuous ITK-transduced, TCR/ligand initiated signals in sIELs impairs their maintenance in the skin due to activation-induced apoptosis

To directly characterize the role of ITK-regulated TCR signaling in the development of sIELs, we crossed $ITK^{-/-}$ mice with KN6 $\gamma\delta$ TCR transgenic (Tg) mice. The $V\gamma 2^+$ KN6 $\gamma\delta$ TCR recognizes ligands T10/T22, two non-classical MHC class I molecules whose expression is high in C57BL/6 (B6). As observed in $ITK^{-/-}$ $V\gamma 3^+$ sIEL precursors, the fetal thymic transgenic $V\gamma 2^+$ T cells of wild type and $ITK^{-/-}$ KN6 mice on the B6 background could be positively selected to undergo the $V\gamma 3$ -like maturation process but the $ITK^{-/-}$ transgenic $V\gamma 2^+$ cells had defects in seeding the fetal skin (Last year's report and data not shown). Surprisingly, the absence of ITK had opposite effects on development of the transgenic $V\gamma 2^+$ and natural $V\gamma 3^+$ sIELs in adult mice. Compared to the ITK-sufficient KN6 mice, $ITK^{-/-}$ KN6 mice had significantly increased numbers of transgenic $V\gamma 2^+$ sIELs (Fig. 5A-C), while ITK-deficiency impaired the $V\gamma 3^+$ sIEL development (Fig. 1A-C).

Unlike those for the natural sIEL-specific $V\gamma 3^+$ $\gamma\delta$ TCR, ligands for KN6 $\gamma\delta$ TCR are reported to express in the skin of B6 mice, raising a possibility that the continuous TCR/ligand mediated signaling in transgenic sIELs, transduced via ITK, may lead to their reduction, likely due to the persistent activation-induced apoptosis. Reduction of such signaling in the absence of ITK reverses the effect. Supporting this idea, the in situ TUNEL analysis of epidermal sheets found significantly lower percentages of apoptotic transgenic sIELs in $ITK^{-/-}$ KN6 than in ITK-sufficient KN6 mice (Fig. 5D). In addition, after adoptively transferred into ligand-negative $\beta 2m^{-/-}$ TCR $\delta^{-/-}$ recipients, the $ITK^{-/-}$ fetal thymic KN6Tg $\gamma\delta$ T cells gave rise to fewer sIELs than the $ITK^{+/+}$ donor cells (Fig. 5E), a difference that is a reversal from that seen in the $ITK^{-/-}$ KN6 mice. Together, these results demonstrate that the continuous peripheral TCR/ligand interaction, signaling through ITK, impairs the maintenance of transgenic sIELs by promoting their apoptosis, which could be corrected by removing ITK-mediated signals.

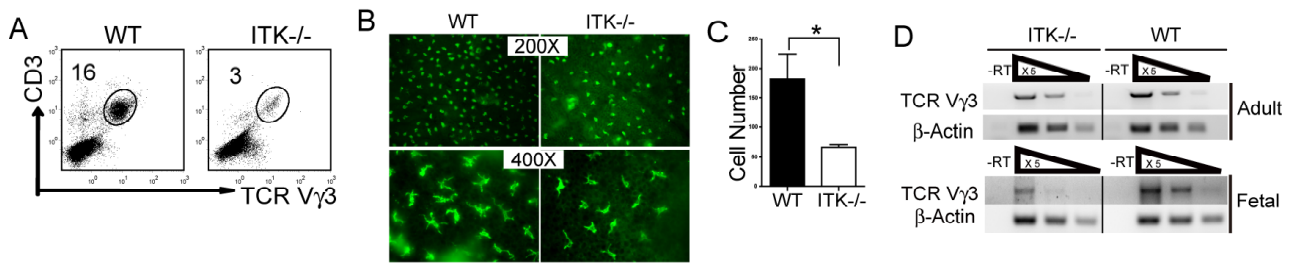


Figure 1. Impaired development of sIELs in $ITK^{-/-}$ but not $Vav1^{-/-}$ mice. A. Skin cell preparations from 6-8 week old $ITK^{-/-}$ and wild type mice were stained with anti-CD3 and $V\gamma 3$ antibodies, and analyzed for percentages of the $CD3^{+}V\gamma 3^{+}$ population by flow cytometry. One representative of three independent experiments is shown. B and C. Ear epidermal sheets from wild type and $ITK^{-/-}$ mice were stained with fluorescent anti- $V\gamma 3$ antibody and observed under a fluorescent microscope (Olympus BX61) for the $V\gamma 3^{+}$ sIELs (B), average numbers of which per field at the 200X amplification were plotted (C). Data were obtained from three independent experiments. * $P < 0.05$. D. Total RNA from fetal and adult mouse skin was reverse transcribed to cDNA. Serially 5 fold-diluted cDNA were subject to semi-quantitative PCR to determine expression levels of rearranged $TCR\gamma 3$ gene. β -actin was used as a control. Data shown were obtained from three independent experiments.

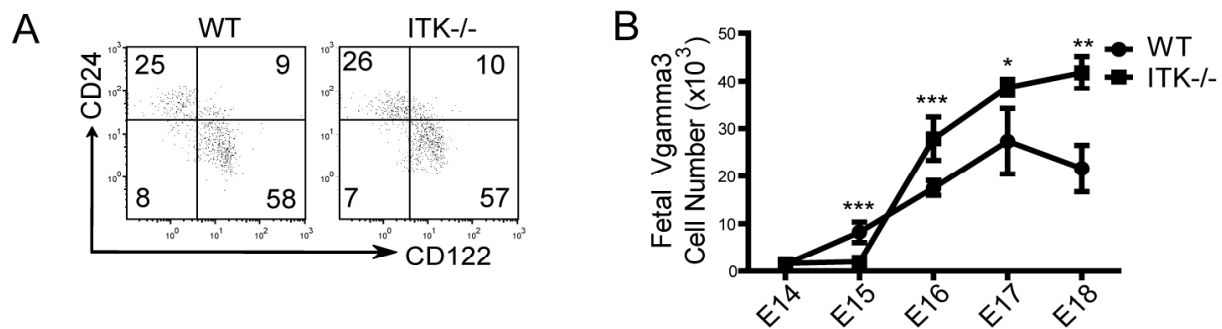


Figure 2. $V\gamma 3^{+}$ sIEL precursors undergo a normal maturation process but accumulate in the fetal thymus of $ITK^{-/-}$ mice. A. Flow cytometric analysis of CD122 and CD24 expression on gated E16-17 fetal thymic $V\gamma 3^{+}\gamma\delta$ cells. One representative of three independent experiments is shown. B. Numbers of $V\gamma 3^{+}\gamma\delta$ T cells in wild type and $ITK^{-/-}$ fetal thymi of different gestation ages. The numbers were calculated based on total numbers of thymocytes and percentages of $V\gamma 3^{+}$ cells per thymus. Data presented were means and standard deviations from three to five experiments. * $P < 0.05$, ** $P < 0.01$, *** $P < 0.001$.

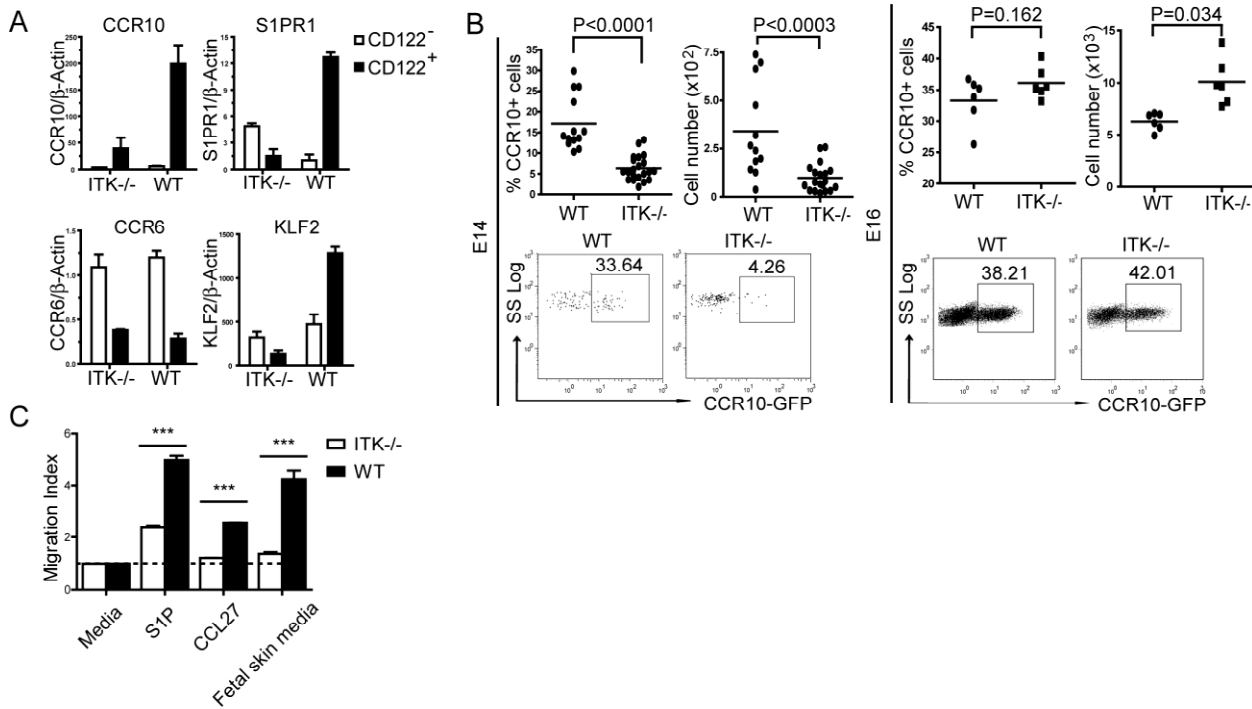


Figure 3. $ITK^{-/-}$ fetal thymic sIEL precursors exhibit the altered migration molecule expression and defective migration capability. A. Real-time RT-PCR analysis of the expression of indicated molecules in purified $CD122^{-/-}$ and $CD122^{+} CD3^{+} V\gamma3^{+}$ cells of E16 wild type and $ITK^{-/-}$ fetal thymi. Data shown were obtained from three independent experiments, presented as mean and deviation. B. E14 or E16 fetal thymocytes of $ITK^{-/-} CCR10^{+/EGFP}$ and $ITK^{+/+} CCR10^{+/EGFP}$ mice were analyzed for CCR10 (EGFP) expression on $V\gamma3^{+}$ cells. Percentages and numbers of CCR10 (EGFP)⁺ $V\gamma3^{+}$ cells were shown. Data presented is one representative from at least 6 mice of each genotype. C. In vitro migration of wild type and $ITK^{-/-}$ E16 fetal thymic $V\gamma3^{+} \gamma\delta$ T cells to S1P, CCL27 and conditioned medium of fetal skin cultures. The migration index was calculated as a ratio of numbers of $V\gamma3^{+}$ cells migrating into the bottom chamber in presence of attractants vs. medium only. Data shown were obtained from two independent experiments, presented as mean and deviation. *** $P < 0.001$.

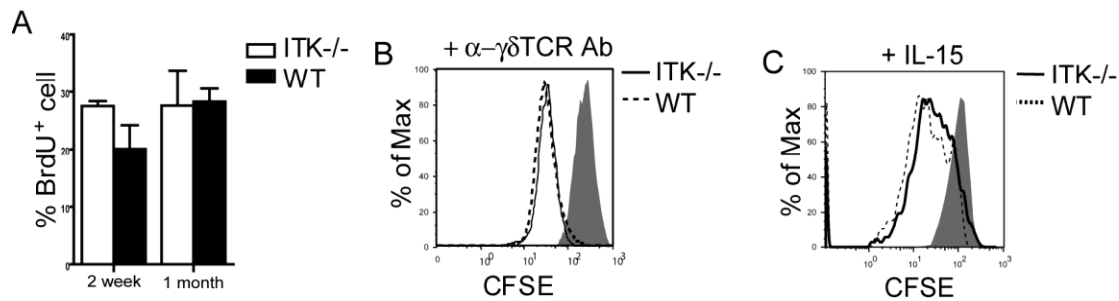


Figure 4. ITK^{-/-} sIELs and their fetal thymic precursors have normal proliferation capacities. A. Similar in vivo proliferation rates of wild type and ITK^{-/-} sIELs. Two week or one-month old mice were treated with BrdU for 9 days and then sIELs were isolated and analyzed for BrdU incorporation by flow cytometry. B and C. CFSE-labeled E16 fetal thymocytes from ITK^{-/-} or wild type mice were stimulated with anti- $\gamma\delta$ TCR antibody (1 μ g/ml) or IL-15 (50 ng/ml) for 3 days, and analyzed by flow cytometry for the proliferation of CD3⁺ $\gamma\delta$ T cells.

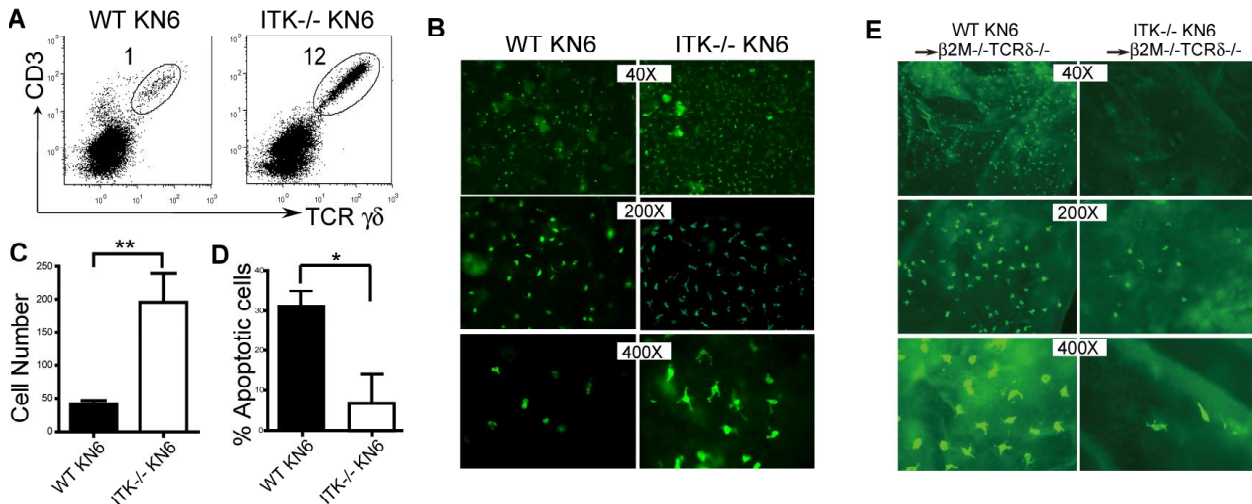


Figure 5. ITK-mediated TCR/ligand induced signaling in the skin impairs the development of sIELs by promoting their apoptosis. A. Skin cell preparations of KN6 transgenic mice of wild type and ITK^{-/-} backgrounds were analyzed for transgenic V γ 2⁺ sIELs by flow cytometry. Percentages of the transgenic sIELs were indicated. B and C. Ear epidermal sheets of ITK-sufficient and knockout KN6 mice were stained and observed under a fluorescent microscope for transgenic V γ 2⁺ sIELs (B), average numbers of which per field at the 200x amplification were plotted (C). Data were obtained from three experiments. ** P < 0.01. D. Lower percentages of apoptotic KN6 transgenic sIELs on ITK^{-/-} than wild type background. The percentages of apoptotic sIELs were calculated based on ratios of numbers of apoptotic vs. total sIELs from in situ TUNEL analyses of ear epidermal sheets. Data shown were obtained from at least four mice of each genotype in two independent experiments. * P < 0.05. E. The development of KN6 transgenic sIELs in β 2m^{-/-} TCR δ ^{-/-} recipients from adoptively transferred fetal thymic ITK-sufficient or knockout fetal thymic KN6 transgenic $\gamma\delta$ T cells. Ear epidermal sheets of the recipients were analyzed for donor-derived sIELs by in situ immunofluorescent staining.

Research Project 18: Project Title and Purpose

In Vivo Brain Tissue Iron Measurement with R2 Mapping in Alzheimer's Disease* - To develop quantitative *in vivo* MRI methods to evaluate brain iron associated with early Alzheimer's disease (AD) pathology.

Duration of Project

4/1/2007 - 6/30/2008

Summary of Research Completed

This project ended during a prior state fiscal year. For additional information, please refer to the Commonwealth Universal Research Enhancement Annual C.U.R.E. Reports on the Department's Tobacco Settlement/Act 77 web page at <http://www.health.state.pa.us/cure>.

Research Project 19: Project Title and Purpose

Combined Effects of a Hypoxia Selective Prodrug and Herceptin to Breast Cancer - Clinical studies suggest that the addition of Herceptin to anthracycline-based chemotherapy, such as doxorubicin, increases its clinical benefit and reduces the recurrence rate by approximately 50%. Although doxorubicin is very effective against breast cancer, the development of heart toxicity and drug resistance by doxorubicin leads to a need in finding safe alternatives. A recently developed novel anticancer agent, acridiol-sulfoxide, may selectively kill solid tumor cells by being converted into its active form in the oxygen deficient environment of a tumor. Therefore, the goal of current study is to establish the use of acridiol-sulfoxide as an alternative to doxorubicin, in combination with Herceptin to treat breast cancer in *in vitro* cell culture models.

Duration of Project

8/9/2007 – 12/31/2009

Project Overview

The combination therapy of doxorubicin with new drugs, such as Herceptin, in the treatment of metastatic breast cancer has yielded impressive results but also unexpected cardiotoxicity. Therefore, novel therapies are needed including alternatives to anthracyclines and combination strategies against breast cancer. A novel anticancer agent, acridiol-sulfoxide, has recently been developed as a potential bioreductive prodrug against solid tumors. Acridiol-sulfoxide was found to be bioreduced to its ultimate drug form, acridiol-sulfide, under anaerobic conditions. The acridiol-sulfide is an intercalating agent, and is highly active *in vivo* against p388 leukemia bearing mice. Based on the above evidence, we *hypothesize* that the combination of acridiol-sulfoxide and herceptin is an effective alternative to the combination of doxorubicin and Herceptin against breast cancer. The *goal* of the current study is to evaluate the potential use of a solid tumor prodrug, acridiol-sulfoxide, as an alternative to doxorubicin in breast cancer treatment in an *in vitro* HER-2/neu overexpressed cell culture model. Therefore, the following

aims are formulated.

Aim 1. Investigate the in vitro metabolic activation of acridiol-sulfoxide by BT474 and SKBR3 breast cancer cell lines under hypoxia condition. To be qualified as a bioreductive prodrug against breast cancer, acridiol-sulfoxide has to be converted into its more cytotoxic metabolite under hypoxia condition. We will examine the ability of human BT474, SKBR3 breast carcinoma cell lines to convert acridiol-sulfoxide to its active metabolite, acridiol-sulfide, under hypoxia condition.

Aim 2. Investigate the cytotoxic effects of acridiol-sulfide alone or combined with Herceptin to the HER-2/neu overexpressed cell line. Continued from aim 1, both acridiol-sulfide, the active form, and acridiol-sulfoxide, the prodrug, alone or in combination with Herceptin will be examined in MDA-MB-231 cells that lack HER-2 expression and two HER-2-positive cell lines (BT474, SKBR3) using MTT assay.

Aim 3. Proteomics-based identification of biomarkers for predicting chemosensitivity to acridiol-sulfoxide in BT474, SKBR3 cells. Global proteomic profiles will be compared in BT474 and SKBR3 cells treated with acridiol-sulfide versus vehicle control to identify specific protein clusters, which might correlate with the drug efficacy and could become biomarkers for acridiol-sulfide treatment. Our long term goal in aim 3 is to use the identified biomarkers as a measurement of chemosensitivity to acridiol-sulfoxide in breast cancer treatment.

Principal Investigator

Kun-Ming Chen, PhD
H171, Department of Biochemistry and Molecular Biology
College of Medicine
Penn State University
500 University Drive
Hershey, PA 17033

Other Participating Researchers

Allan Lipton, MD – employed by Penn State University

Expected Research Outcomes and Benefits

We expect that a substantial amount of prodrug will be reduced to an active drug by breast cancer under oxygen deficient conditions. The cancer killing under oxygen deficient conditions is contributed by both the reduced prodrug and the remaining unchanged prodrug. We also expect that the combination of prodrug or active drug with Herceptin will result in a synergistic cytotoxic effect, which means the combinational treatment at the same dose will be more cytotoxic than the addition of the cytotoxicities of each individual treatment.

In addition, we expect to identify how the protein markers respond to the active drug, and how these treatment-responsive proteins can be used as markers to monitor the anticancer effects or

toxicities of the prodrug or the active drug. The successful completion of this project will provide better and broader insights into the mechanisms of its anticancer activity before entering an *in vivo* study. The results of our studies will be highly useful for future competitive applications that can be submitted to various funding agencies.

Summary of Research Completed

In *aim 3*, the levels of a number of proteins were previously found changed by the treatment of acridiol-sulfide. During the reporting period 7/1/09-12/31/2009 we found that the level of a calcium binding protein, S100 A7, in MCF-7 cells was changed after being treated with acridiol-sulfide. S100 proteins are a group of multigenic, non-ubiquitous cytoplasmic Ca²⁺-binding proteins that are linked to several human diseases, and differentially expressed in a wide variety of cell types. At least 16 of these genes cluster to chromosome 1q21, known as the epidermal differentiation complex. Characteristically, these proteins have high homology, low molecular weight, two EF-hands, and they are tissue-specifically expressed. Although a number of distinct functions have been attributed to the S100 proteins, their biological functions still remain unclear. However, it is acknowledged that the specific expression patterns of these proteins are a valuable diagnostic tool. Many of the S100 protein family members have a role in modulating cytoskeletal dynamics. They can direct interaction with tubulins, intermediate filaments, actin, myosin and tropomyosin. Some of these processes have been implicated in mediating metastasis. S100A7 is highly expressed in high-grade comedo ductal carcinoma in situ (DCIS), with a higher risk of local recurrence. Alteration of psoriasin (S100A7) expression has previously been identified in association with the transition from preinvasive to invasive breast cancer, metastasis, poorer prognosis and reduced survival, but expression of S100A7 results in enhanced sensitivity to etoposide.

In figure 1, we showed that the S100 protein expression in MCF-7 cells was enhanced by the treatment of acridiol-sulfide dose and time dependently. To avoid side effects and unnecessary treatments to insensitive patients, it is desirable to use identified biomarkers as a clinical indicator for acridiol-sulfide or acridiol-sulfoxide treatment in breast cancer patients. Our results suggest that the induced expression of S100A7 may be a potential indicator (therapeutic responder) among others for cancer patients who are treated with acridiol-sulfide.

The levels of protein S100 A7 induced by acridiol-sulfide in MCF-7 cells were analyzed by western blotting. MCF-7 cells were obtained from American Type Culture Collection (Manassas, VA) and grown in a petri dish at 37 °C in a humidified atmosphere with 5% CO₂ in air. MCF-7 cells were maintained in IMDM/F12 (1:1 mixture) supplemented with 10% FBS and penicillin/streptomycin (50 µg/mL). MCF-7 cells were treated with Acridiol-sulfide (0, 1 and 5 µmol/L) for 24 hrs or 72 hrs. Total cellular protein was homogenized in lysis buffer containing 20 mM Tris buffer, pH 7.4, 150 mM NaCl, 1mM EDTA, 1mM EGTA, 1% Triton X-100, 2.5 mM sodium pyrophosphate, 1 mM β-glycerol phosphate, 1 mM Na₃VO₄, 1 mM NaF, 10 µg/ml leupeptin, 1 mM PMSF, 10 µg/ml aprotinin and 10 µg/ml pepstatin A. Cell debris and particulate fractions were removed by centrifugation at 13,000 x g for 10 min at 4 °C. Protein concentration was measured using a Bio-Rad DC protein assay kit. Equal amounts of protein (approximately 35 µg) were diluted with 3 × sample buffer containing β-mercaptoethanol and bromophenol blue and then heated at 100 °C for 5 min. Proteins were separated by 10% SDS-

PAGE, transferred onto PVDF membranes (Bio-Rad, Hercules, CA), and subjected to immunoblot analysis using the respective antibody against: S100A7, and β -actin. Immunoreactive proteins were subsequently detected with appropriate secondary antibodies conjugated with HRP and enhanced chemiluminescence kits and exposed in the SynGene Gene Gnome.

Research Project 20: Project Title and Purpose

Nitroaromatics and Breast Cancer - The cause of most breast cancers remains unknown. In addition to genetic predisposition, exposure to chemical carcinogens in the diet, tobacco, and polluted air has been implicated as a factor in the development of breast cancer. A representative example is the environmental pollutant 6-nitrochrysene (6-NC) which is normally produced from incomplete combustion of organic compounds such as diesel, gas, kerosene and liquid petroleum; 6-NC is a powerful carcinogen in breast tissues of rodents. Studies have shown that 6-NC can be detected in human blood measured as hemoglobin adducts and can damage DNA in breast tissue of animals. The goal of this study is to use state of the art technology, liquid chromatography-tandem mass spectrometry (LC-MS-MS), to identify and quantify the levels of DNA damage induced by this environmental pollutant initially in animals, and eventually in humans.

Duration of Project

8/9/2007 – 6/30/2010

Project Overview

The broad objective of this project is to assess the contribution of a representative environmental pollutant in the development of human breast cancer. However, using bridge funding we will focus on a specific task that was requested by the review committee of the original grant that was submitted to the National Cancer Institute. Therefore, the goal of this study is to develop and validate a method using high performance liquid chromatography (HPLC)-MS/MS for the detection and quantification of DNA adducts derived from 6-NC, a potent rat mammary carcinogen. The *specific aims* are (1) preparation of isotope and non-isotope 6-NC-DNA adduct standards for HPLC-MS/MS detection; the stable isotope labeled DNA adducts will be used as internal standards for the detection and quantitation by MS; and (2) analysis of the above DNA adducts isolated from rat mammary glands.

Research Design and Methods.

(1) Preparation of major DNA adducts derived from 6-NC.

(a) *Reaction of calf thymus DNA with freshly prepared N-hydroxy-6-aminochrysene or 1, 2-dihydro-1, 2-dihydroxy-6-N-hydroxylaminochrysene (1,2-DHD-6-NHOH-C).* Resolution of racemic 1, 2-DHD-6-NC by chiral column (Welko-01, Regis Inc.) will be prepared to obtain pure (R,R)- and (S,S)-1,2-DHD-6NC followed by nitroreduction to form 1, 2-DHD-6-NHOH-C; levels of DNA adducts derived from each enantiomer will be quantified.

(b) *Synthesis of stable isotope-DNA adduct internal standards.*

(c) *Determination of DNA adducts using LC-MS/MS.* The adducted calf thymus DNA will be added to the corresponding stable isotope internal standard and then hydrolyzed followed by purification with HPLC. The mass spectrometer will be tuned by using dG standard solution and the sample will then be analyzed in positive ESI MS/MS SRM mode for the $[M+H]^+$ ion to adducted base $[B+H_2]^+$ transition of both non-isotope and isotope adducts.

(2) Analysis of DNA adducts isolated from rat mammary glands.

Mammary glands will be isolated from female rats that had been treated with 6-NC and will be homogenized and digested enzymatically to obtain DNA. The purity of DNA will be determined by measuring its UV absorption at 230, 160, and 280 nm. DNA will be then hydrolyzed to nucleosides as described previously and assayed for adducts using HPLC and ES-MS/MS.

Principal Investigator

Karam El-Bayoumy, PhD
H171, Department of Biochemistry and Molecular Biology
College of Medicine
Penn State University
500 University Drive
Hershey, PA 17033

Other Participating Researchers

Telih Boyiri, PhD – employed by Penn State University
Cesar Aliaga, MS (Research Animal Biologist) - employed by Penn State University from 7/1/09-6/30/10

Expected Research Outcomes and Benefits

There is evidence that exposure to carcinogens can lead to DNA damage. Furthermore, there is clear mechanistic evidence that carcinogen-DNA adduct formation is a key step in chemical carcinogenesis. However, due to several factors such as diverse etiologies, short half-lives of DNA adducts and multiple exposures, studies that sought to determine whether increased DNA adduct levels are associated with breast cancer incidence have been inconsistent and limited. An existing limitation is the methodological approaches described in the literature. Carcinogen-DNA adduct analysis by ^{32}P -postlabeling and by immunoassays are the most widely used methods to detect DNA damage in human breast tissues. Despite being highly sensitive, these methods do not provide structural characterization, which is pre-requisite for understanding the stability and biological activity of DNA adducts. In the last decade, mass (MS) spectrometry has become highly sophisticated, and the techniques currently employed permit the identification of specific DNA adducts in smaller quantities (10-100 μg) of human DNA and produce comparable detection sensitivity to that of other methods. Our previous studies have identified five DNA adducts in breast tissues of laboratory animals treated with 6-NC. However, DNA adducts detected in these mammary gland were identified and quantified based on ^{32}P -postlabelling analysis. LC-MS/MS approach requires the appropriate instrumentation as well as the expertise to synthesize the requisite isotope-labeled adduct standards (Nitrogen-15 or

deuterium labeled). Using LC-MS-MS approach will provide more precise quantification and structure information of 6-NC-DNA adducts in *in vivo* systems. Results of this study will provide the requisite technology to detect and quantify adducts in human breast tissue. The outcome is important in assessing human risk following exposure to this environmental carcinogen.

Summary of Research Completed

Originally, this project was planned to be completed in one year. It was extended by a year to provide support for a graduate student to continue work on the project.

Calibration Curve. In our previous annual progress report, we reported the synthesis and LC/MS/MS detection and quantification of 6-aminochrysene-C8-deoxyguanosine adduct (N-(dG-C8-yl)-6-AC) and its corresponding deuterated adduct (N-(dG-C8-yl)-6-AC-d10). We have now established the LC-MS/MS calibration curve for N-(dG-C8-yl)-6-AC; one of the DNA adducts that has been detected in the mammary gland of rats treated with 6-NC (Boyiri *et al.* Carcinogenesis, 2004; 25:637-43) (Fig. 1). The standard curve for N-(dG-C8-yl)-6-AC was constructed by mixing various amounts of N-(dG-C8-yl)-6-AC with a constant amount of the deuterated analog, N-(dG-C8-yl)-6-AC-d10, as the internal standard. Samples were analyzed by LC-MS/MS by monitoring ions at m/z 509 for N-(dG-C8-yl)-6-AC, and m/z 519 for the internal standard N-(dG-C8-yl)-6-AC-d10. Fig. 1 shows good reproducibility and a linear relationship between peak area ratio m/z 509 to m/z 519 at concentrations of N-(dG-C8-yl)-6-AC ranging from 0 to 100 pg/injection ($r^2 = 0.99$). The detection limit for N-(dG-C8-yl)-6-AC adduct is 5 pg/injection.

Detection of the N-(dG-C8-yl)-6-AC adduct from DNA isolated from the liver and mammary gland of female CD rats treated with 6-NC for 24 h.

We treated orally 6 female CD rats, at 30 days of age, with 6-NC (50 μ mol/rat) in 500 μ l of trioctanoin (3 rats/group) or with trioctanoin alone as vehicle control (3 rats/group) (2). The rats were killed 24 h, after carcinogen or trioctanoin treatment and the liver and mammary tissue were excised and stored at -80 °C. Although the liver is not the target organ for 6-NC carcinogenesis, we wanted to compare the levels of N-(dG-C8-yl)-6-AC in the liver to those in the mammary gland (target). We first isolated and hydrolyzed DNA from the liver, and the N-(dG-C8-yl)-6-AC adduct level was analyzed by LC/MS/MS (Fig. 2a and 2b). The adduct level in the liver was found to be below the detection limit (5 pg/injection); the results, although preliminary, demonstrating lack of 6-NC-DNA adducts in the liver may explain the lack of carcinogenicity of 6-NC in this organ. We are currently analyzing DNA from the target organ (mammary tissue) of rats treated with 6-NC by the LC-MS/MS method.

Insertion of N-(dG-C8-yl)-6-AC and 5-(dG-N2-yl)-6-AC lesions into 135-mer DNA duplex and incubation with NER-competent nuclear extracts from human HeLa cells.

Since our previous studies have identified five DNA adducts in breast tissues of laboratory animals treated with 6-NC by on 32 P-postlabelling analysis, we will eventually synthesize the requisite isotope-labeled adduct standards (deuterium labeled) for the remaining 4 adducts and,

using LC-MS-MS approach will provide more precise quantification and structure information of 6-NC-DNA adducts in *in vivo* systems. Ubiquitous environmental agents [e.g. polynuclear aromatic hydrocarbons (PAH), and their nitrated derivatives (NO₂-PAH) as well as the food derived heterocyclic aromatic amines (HAA)] that are known to induce mammary cancer in rodents must be regarded as potential human risk factors for inducing analogous human cancers. Although 6-nitrochrysene (6-NC) is less abundant than other NO₂-PAH in the environment, it is the most potent mammary carcinogen in the rat; its carcinogenic potency is not only higher than the carcinogenic PAH, benzo[a]pyrene but also of the well-known carcinogenic HAA, 2-amino-1-methyl-6-phenylimidazo[4,5-*b*]pyridine (PhIP). The presence of bulky DNA adducts in human breast tissues and blood, supports the notion that environmental carcinogens play an important role in the etiology of breast cancer. Studies in rats and *in vitro* assays have indicated that 6-NC can be activated by simple nitroreduction leading to the formation of the corresponding 6-hydroxylaminochrysene (6-NHOH-C); this metabolite yielded three major DNA adducts: N-(dG-8-yl)-6-AC, 5-(dG-N²-yl)-6-AC, N-(dI-8-yl)-6-AC. The second (major) pathway proceeds via a combination of oxidation and nitroreduction leading to the formation of 1,2-dihydroxy-1,2-dihydro-6-hydroxylaminochrysene (1,2-DHD-6-NHOH-C); this metabolite yielded 5-(dG-N²-yl)-1,2-DHD-6-AC and N-(dI-8-yl)-1,2-DHD-6-AC. These DNA lesions are likely to cause mutations if they are not removed by cellular defense mechanisms before DNA replication occurs. However nothing is known about the susceptibility of these adducts to nucleotide excision repair (NER), the major cellular repair system that removes bulky DNA lesions. In order to address this issue, we initially synthesized the N-(dG-C8-yl)-6-AC and 5-(dG-N²-yl)-6-AC lesions and inserted them individually into 135-mer DNA duplexes. These constructs were incubated with NER-competent nuclear extracts from human HeLa cells. The efficiencies of repair of these 6-NC-derived lesions were compared to the repair of the dG-C8 adduct derived from PhIP. The PhIP-dG-C8 adduct was readily removed by the NER system with efficiencies approaching those of the well-known pyrimidine (6-4) pyrimidone T-T dimer UV photoproduct. In contrast, the N-(dG-8-yl)-6-AC lesion in the identical sequence context was significantly more resistant to repair with 5 – 6 times lower NER efficiencies. These results suggest that the N-(dG-8-yl)-6-AC and 5-(dG-N²-yl)-6-AC lesions derived from the metabolic activation of 6-NC may be more persistent in mammalian tissues than the PhIP lesion which may account for the high tumorigenic activity of 6-NC. The efficiency of NER repair of these lesions is in the order N-(dG-C8-yl)-PhIP < 5-(dG-N²-yl)-6-AC < N-(dG-8-yl)-6-AC. The two 6-NC – derived DNA adducts are significantly more resistant to NER than the cisplatin, PhIP, and benzo[a]pyrene-derived DNA adducts (Fig. 3).

Calibration Curve

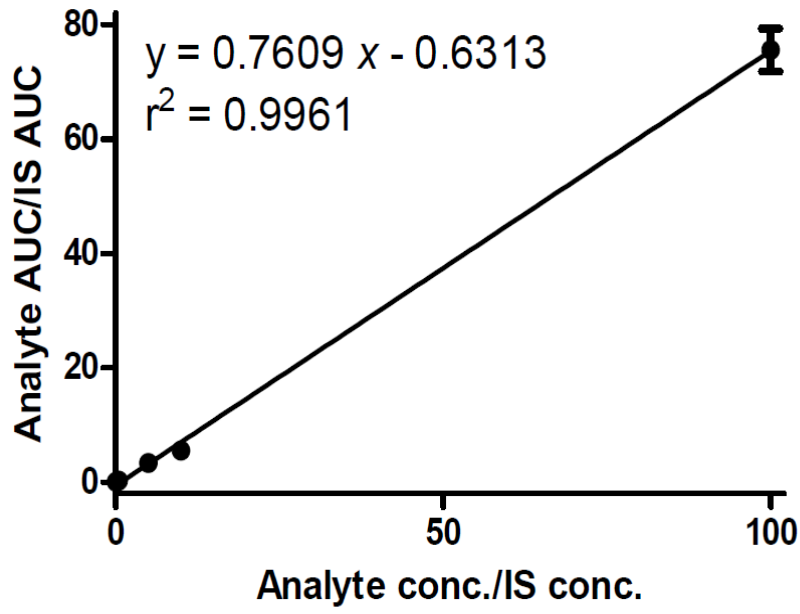


Fig. 1. Calibration curve for N-(dG-C8-yl)-6-AC

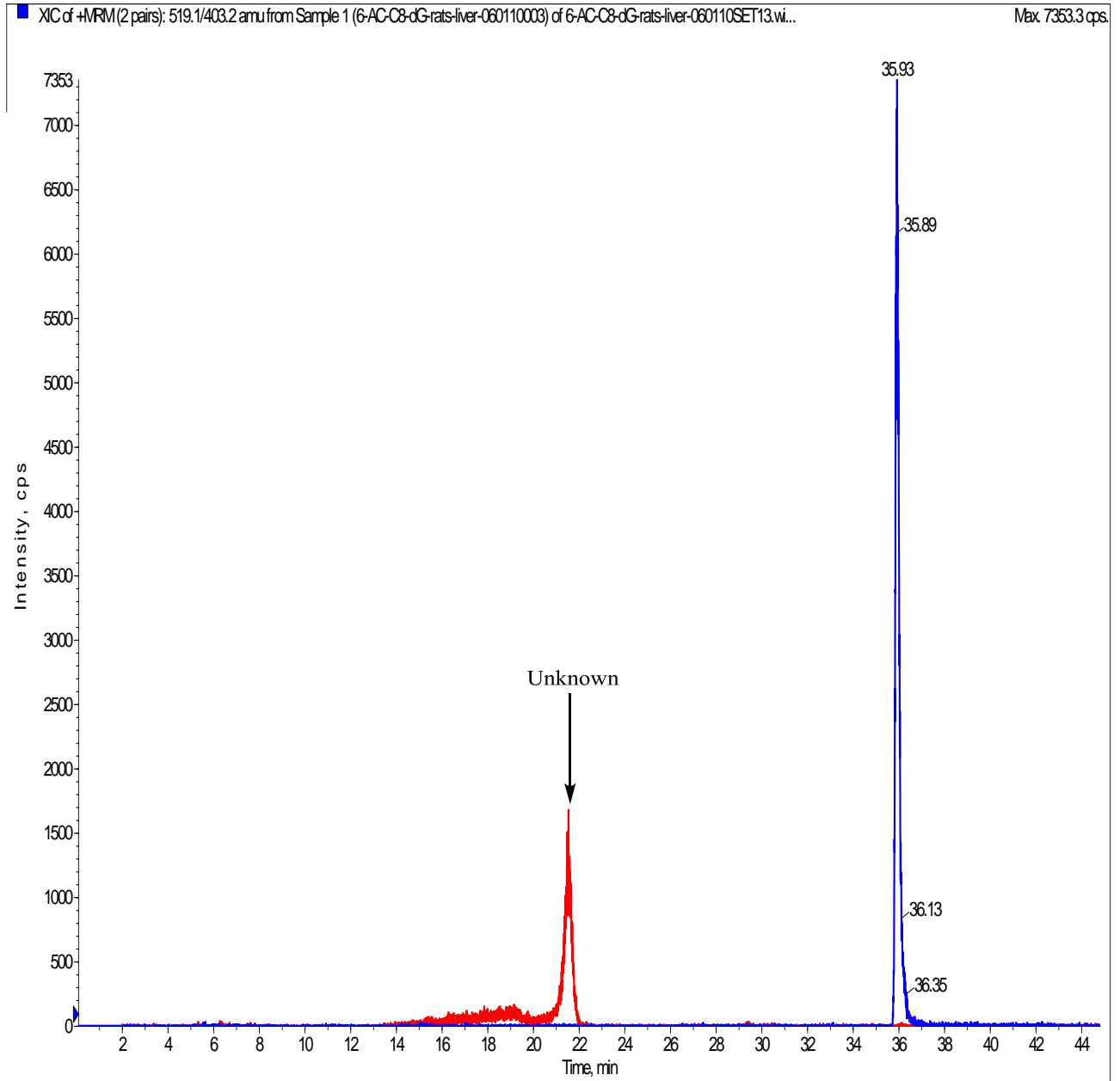


Fig. 2a. Level of N-(6-AC-C8-dG) adduct in rat liver (red) compared with the internal standard of N-(6-AC-C8-dG-d10) (blue)

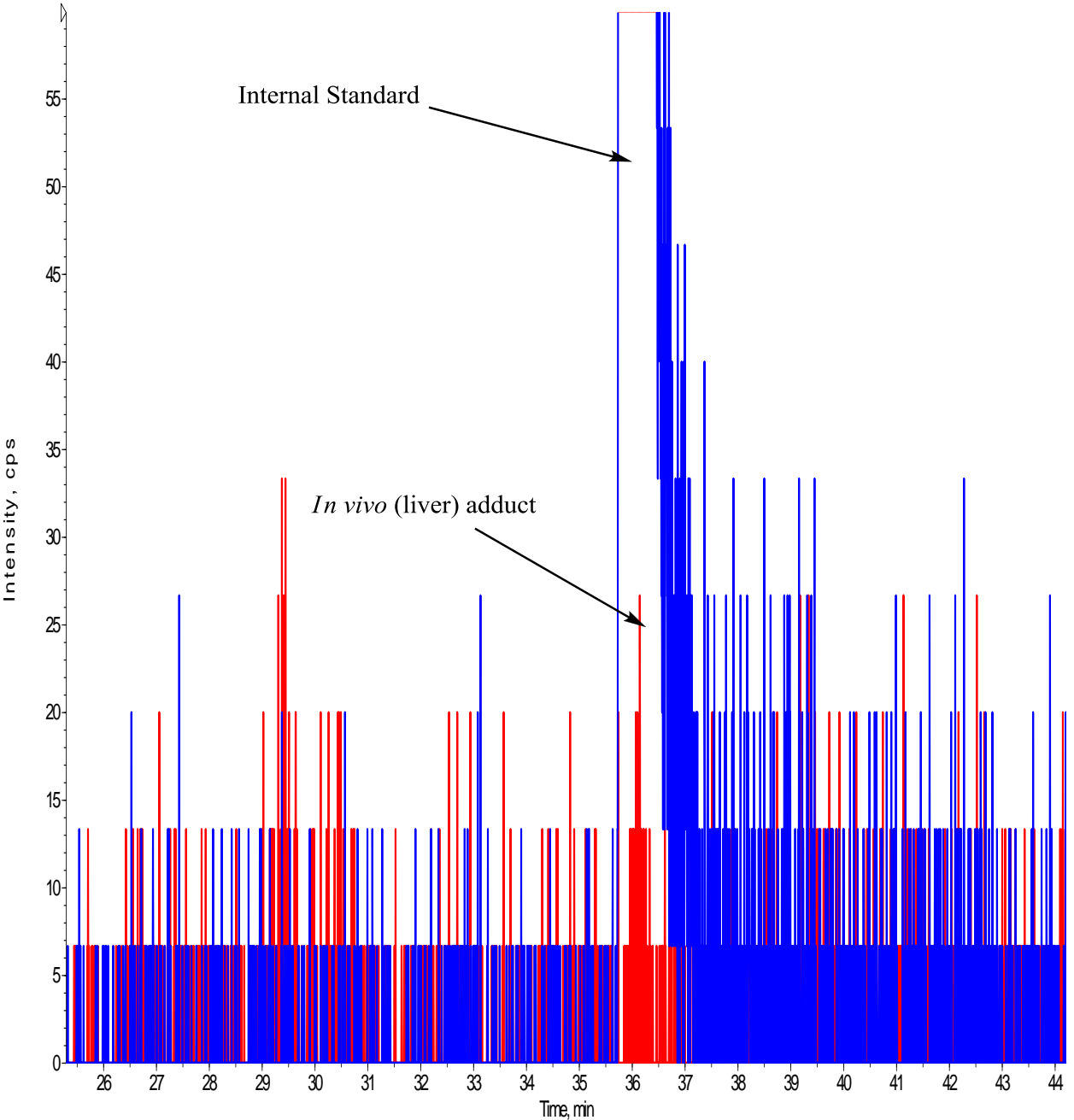


Fig. 2B. Expanded HPLC outline of level of N-(6-AC-C8-dG) adduct in rat liver (red) compared with the internal standard N-(6-AC-C8-dG-d10) (blue)

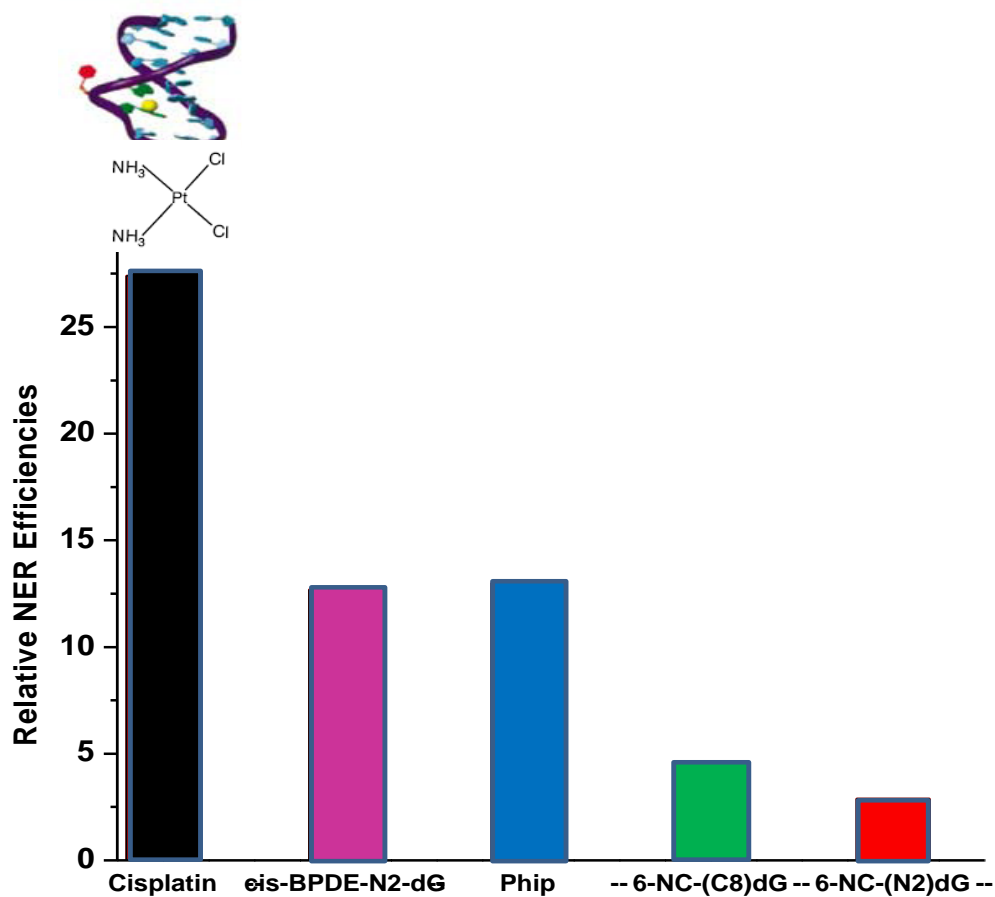


Fig. 3. Relative NER efficiencies of various carcinogen-DNA adducts

References:

1. Sun Y-W, Guttenplan JB, Krzeminski J, Boyiri T, Amin S and El-Bayoumy K. Stereoselective Metabolism of the Environmental Mammary Carcinogen 6-Nitrochrysene to trans-1, 2-Dihydroxy-1, 2-Dihydro-6-Nitrochrysene by Rat Liver Microsomes and Their Comparative Mutation Profiles in a lacI Mammary Epithelial Cell Line. *Chem Res Toxicol.* 22: 1992 -1997, 2009 (PMID: 19886636)

2. Krzeminski, J, Kropachev, K, Reeves, D, Kolbanovskiy, A, Geacintov, NE, Amin, S, and El-Bayoumy, K. Inefficient nucleotide excision repair of the N-(dG-8-yl)-6-AC adduct derived from 6-nitrochrysene, an environmental mammary carcinogen, in human cell extracts. *Proc. Am. Assoc. Cancer Res.* 51:3945, 2010

Research Project 21: Project Title and Purpose

Modeling Rapid Osteoblastic Bone Metastases - The effects of intermittent parathyroid hormone (PTH) on the establishment of *osteoblastic* bone metastases are unknown. The work to be completed with the requested funds is to establish that increased bone formation as a

consequence of intermittent PTH treatment, will facilitate colonization of human prostate cancer (PCa) cells in bone. Specifically, we plan to test two hypotheses: 1) that intermittent PTH treatment will facilitate the establishment and colonization of human osteoblastic PCa cells in bones of mice; and 2) that human osteoblastic PCa colonization of murine bone requires a bone environment that favors bone-formation.

Duration of Project

8/9/2007 – 12/31/2009

Project Overview

Our *long-term* goal is to identify mechanisms that regulate the establishment of cancer metastases in bone, and to employ this knowledge in the treatment and prevention of bone metastases. The *objective* in this project is to refine a model under development to fill the current gap in PCa models of bone metastasis. Our *central hypothesis* is that osteoblastic PCa cells will spontaneously colonize mouse bones whose microenvironment is in a state of active remodeling. This research is predicated upon our strong preliminary data demonstrating: 1. that bones of immune compromised mice remodel in response to changes in mechanical load and parathyroid hormone (PTH) treatment; and 2. that mouse bones in an active state of remodeling support the colonization of osteoblastic human PCa cells. Our *rationale* for this project is the potential to reduce spontaneous colonization of osteoblastic PCa to bone from 6.7 months (27 weeks) to 2.5 months (10 weeks). This also represents the first effort for osteoblastic PCa cells in a spontaneous colonization model. This model would allow for more rapid, cost effective testing of compounds that would interfere with or block PCa colonization of bone via a vascular mechanism. It also allows for the direct analysis of bone-derived factors required for successful colonization of bone by PCa. In addition to supportive preliminary findings, the principle investigator is well prepared to engage and complete this project since he collaborates with a PCa biologist (R. Sikes) who has worked in the field of PCa metastasis to bone for many years and has been instrumental in the development of many of the most widely used cellular models of this condition. To test our central hypothesis and attain the overall objective of this project, we propose the following Specific Aim: *Identify the requirement for osteoclastic activity in the successful establishment and colonization of human osteoblastic PCa cells in murine bone.* In this aim, we will determine the requirement of an osteoclastic phase for the successful colonization of PCa cells by combining bisphosphonate treatment with intermittent PTH treatment.

Principal Investigator

Ronald R. Gomes, Jr., PhD
Penn State College of Medicine
Department of Orthopaedics and Rehabilitation
Division of Musculoskeletal Sciences, H089
500 University Dr., PO Box 850
Hershey, PA 17033-0850

Other Participating Researchers

Arivalagan Muthusamy, PhD, Sarah Sheehan, Erin Gunderson, MD, Patricia Buttke, MD, employed by Penn State College of Medicine , Dyanna Gonzáles, SciTech High School –

Expected Research Outcomes and Benefits

In this project, we will refine a model system that shows great potential for studying the colonization of circulating human prostate cancer cells in the mouse skeleton. These studies will provide the cancer research community with a model system that will allow for the design and testing of novel therapeutic compounds that suppress, interfere, or reverse the early stages of prostate cancer cell:bone interaction. The ultimate goal is to be able to rapidly model suppression of early bone metastasis by osteoblastic prostate cancer. This model system is an exciting adjunct to models that test for the eradication of established PCa in bone. Nothing like this model currently exists for osteoblastic prostate cancer using human osteoblastic PCa cells in mice, in vivo, and within a timeframe for testing that does not exceed 10-12 weeks. Without good model systems to study this process of colonization, we will continue to examine the interaction between established tumor cells and the bone microenvironment via direct injection into bone and NOT the interaction of tumor cells with an un-manipulated, intact bone microenvironment. Knowledge of how prostate cancer cells spontaneously establish themselves in bone is essential for dissecting the components of the metastatic process that targets prostate and perhaps other cancer cells to bone.

Summary of Research Completed

During this reporting period the following manuscript was revised for publication:

“*Short-term Intermittent PTH 1-34 Administration Enhances Bone Formation in SCID/Beige Mice*”. Sarah Sheehan, Arivalagan Muthusamy, Emmanuel Paul, Robert A. Sikes, and Ronald R. Gomes, Jr. *Endocr J.* 2010;57(5):373-82. Epub 2010 Feb 6.

Abstract:

The anabolic effect of intermittent PTH on bone is variable depending on the species studied, duration/mode of administration, and location of skeletal response investigated. We tested the hypothesis low dose, short term, intermittent PTH 1-34 administration is sufficient to enhance bone formation without altering bone resorption. To test our hypothesis, mice were treated intermittently with one of three concentrations of PTH 1-34 (1 µg/kg; low, 10 µg/kg, or 20 µg/kg; high) for three weeks. The skeletal response was identified by quantifying: serum markers of bone turnover, cancellous bone parameters in distal femur, proximal tibia, and lumbar vertebrae by µCT, and number of osteoblasts and osteoclasts in distal femur. Mice receiving 20 µg/kg of PTH 1-34 demonstrated a 30% increase in serum osteocalcin, but no differences in serum calcium, type I collagen teleopeptides, or TRACP 5b. For all bones, µCT analysis suggested mice receiving 20 µg/kg of PTH 1-34 had increased cancellous bone mineral density, trabecular thickness and spacing, but decreased trabecular number. A 60% increase in the number of alkaline phosphatase positive osteoblasts in the distal femur was also observed in tissue sections; however, the number of TRAP positive osteoclasts was not different between test and control groups. While animals administered 10 µg/kg demonstrated similar trends for all

bone turnover indices, such alterations were not observed in animals administered PTH 1-34 at 1 µg/kg per day. Thus, PTH 1-34, administered intermittently for three weeks at 20 µg/kg is sufficient to enhance bone formation without enhancing resorption.

Research Project 22: Project Title and Purpose

Molecular Functional Studies of Neurog3 Gene Variants - The goals of the present study are 1) to establish in vitro the impact of NEUROG3 rare and common variants on NEUROG3 transcription regulation and downstream target gene modulation; and 2) to establish the potential role in the pathogenesis of T2D of NEUROG3 promoter and regulatory variants, NEUROG3 haplotypes and diplotypes.

Duration of Project

8/9/2007 – 6/30/2009

Summary of Research Completed

This project ended during a prior state fiscal year. For additional information, please refer to the Commonwealth Universal Research Enhancement Annual C.U.R.E. Reports on the Department's Tobacco Settlement/Act 77 web page at <http://www.health.state.pa.us/cure>.

Research Project 23: Project Title and Purpose

Role of Excess Nutrients in Diabetic Retinopathy - Interactions between dysregulated glucose and amino acid metabolism caused by Type 1 diabetes lead to inflammation followed by retinal cell death. Our goal is to evaluate these toxic processes and find out why they occur. Therefore, the study will facilitate development of drugs needed for reversal of toxicity. For example, interfering with the inflammatory response using the anti-inflammatory agent, minocycline, lowers neuronal cell death in diabetic rat retinas. Lowering formation of reactive oxygen species may also be therapeutic. These interventions will be studied for their potential in treating patients.

Duration of Project

8/9/2007 – 6/30/2008

Summary of Research Completed

This project ended during a prior state fiscal year. For additional information, please refer to the Commonwealth Universal Research Enhancement Annual C.U.R.E. Reports on the Department's Tobacco Settlement/Act 77 web page at <http://www.health.state.pa.us/cure>.

Research Project 24: Project Title and Purpose

HFE Polymorphisms on the Chemotherapy and Patient's Outcome of the Brain Tumors - This project will demonstrate that individuals with brain tumors that carry an HFE polymorphism have a worse outcome than those with wild type HFE, and provide a cell culture model in which to identify the mechanisms by which HFE polymorphisms affect cell behavior and provide a first line in which to test intervention strategies.

Duration of Project

8/9/2007 – 6/30/2008

Summary of Research Completed

This project ended during a prior state fiscal year. For additional information, please refer to the Commonwealth Universal Research Enhancement Annual C.U.R.E. Reports on the Department's Tobacco Settlement/Act 77 web page at <http://www.health.state.pa.us/cure>.

Research Project 25: Project Title and Purpose

Mu Opioid Receptor in Addiction - The mu-opioid receptor (MOR) mediates most of the actions of morphine and other clinically relevant analgesics as well as drugs of abuse such as heroin. Recent studies have identified a number of MOR interacting proteins (MORIPs) including filamin A, protein kinase C interacting protein, and periplakin, suggesting that the MOR is organized within a supramolecular signaling complex. Through the combined proteomic and functional studies outlined in this project, we will identify and characterize a set of novel MORIPs. Identification of these MORIPs will allow us to test our hypothesis that MORIPs play important roles in regulating MOR biogenesis and MOR-mediated signal transduction, as well as providing new insight into the etiology of opioid dependence (OD).

Anticipated Duration of Project

8/9/2007 – 12/31/2010

Project Overview

The mu-opioid receptor (MOR) belongs to the superfamily of 7 TM G-protein coupled receptors (GPCRs) and mediates most of the actions of clinically relevant analgesics as well as drugs of abuse such as heroin. Recent studies have identified a number of MOR interacting proteins (MORIPs). These MORIPs have been shown to play a role in regulating MOR trafficking and signal transduction. In this project, we will identify and characterize a set of novel MORIPs. Identification of these MORIPs will allow us to test our hypothesis that MORIPs play important roles in mediating opioid dependence (OD). MORIPs also represent novel targets for the development of drugs designed to treat addictive behaviors.

Aim 1. Identification and Characterization of Mu-Opioid Receptor Interacting Proteins. Our primary goal is to identify novel MORIPs and elucidate the role these proteins play in regulating MOR-mediated signaling. We will carry out a split-ubiquitin yeast two-hybrid (Y2H) screen to identify novel MORIPs. This method is permissive for detection of interactions involving integral membrane proteins. In a complementary approach, we will perform a conventional Y2H screen to identify additional candidate MORIPs. Together, these approaches should allow us to discover many of yet unidentified components of the MOR signaling complex.

Aim 2. Validation of MOR Interacting Proteins. The major goal in Aim 2 is to validate the candidate MORIPs discovered in the Y2H screens. Several independent criteria will be used to validate protein-protein interactions including cellular colocalization, pull-down and coimmunoprecipitation. Deletion mapping will permit identification of sites within the proteins that are necessary for the interactions to occur. Validation of novel MORIPs will serve to inform the functional studies outlined in Aim 3.

Aim 3. Functional Analysis of MOR/MORIP Interactions. This aim is focused on elucidating the role that MORIPs play in regulating MOR-mediated signaling. We will examine the requirement for the MOR/MORIP interaction in regulation of MOR function including receptor trafficking, endocytosis, internalization and desensitization. To do this, we will determine whether disruption of the MOR/MORIP interaction (either by expression of a dominant negative form of the interactor, or a competing peptide against one of the protein binding domains) affects trafficking or other functional properties of the MOR. These results should provide new insight into the regulation of MOR-mediated signaling and drug dependence.

Principal Investigator

Robert Levenson, PhD
Penn State College of Medicine
Department of Pharmacology, Room C7766
500 University Drive
Hershey, PA 17033-0850

Other Participating Researchers

Jay Jin – employed by the Penn State College of Medicine

Expected Research Outcomes and Benefits

The major goal of this project is to identify a novel cohort of mu-opioid receptor (MOR) interacting proteins (MORIPs) and elucidate the functional role of MOR/MORIP interactions in regulating the multiple processes involved in MOR biogenesis and signaling. Through the identification and characterization of novel MORIPs, this project will help establish a new platform for defining cellular mechanisms of MOR signaling in the brain; as well contribute to our understanding of the underlying basis of opioid tolerance and opioid dependence (OD).

In the long term, the line of research described in this project may not simply be an approach for learning more about MOR biogenesis and signaling, but a fruitful strategy for identifying candidate risk genes for OD as well. For example, each MORIP we identify and validate will represent a candidate gene to be studied in paradigms of OD and withdrawal through OD genetic association studies that we will carry out in collaboration with Penn. MORIPs that satisfy all validation inclusion criteria may be further characterized by generating murine null mutants as a means to understand the role of novel MORIPs in opioid-related murine phenotypes.

The identification of MORIPs as modulators of MOR-mediated signaling holds the promise of opening exciting new areas relating the function of MORIPs with behavior and drug dependence. In particular, because of the well-established central role of the MOR in the rewarding actions of opioids, the identification of novel MORIPs may provide conceptual breakthroughs in our understanding of opioid tolerance and OD, as well as the development of novel therapeutic interventions. Insight into the functions of known as well as novel MORIPs should also enhance our ability to improve the efficacy of therapeutics designed for the treatment of OD.

Summary of Research Completed

Most clinically relevant opioid drugs are potent analgesics and are used for the treatment of unremitting pain. However, chronic exposure to opioid agonist drugs such as morphine and heroin, may lead to opioid dependence and addiction. The mu-opioid receptor (MOR) has been shown to be primarily responsible for mediating the analgesic and rewarding effects of opioid drugs. Elucidating the mechanisms that regulate MOR signaling is therefore critical for determining the physiological basis of opioid addiction and enhancing opioid receptor pharmacology for the treatment of pain and addiction.

MOR signaling is modulated by proteins that interact with the receptor and regulate its function. In this project, we identify and characterize novel MOR interacting proteins (MORIPs). Using a yeast two-hybrid approach, we identified GPR177 as a MORIP. GPR177 is the mammalian ortholog of *Drosophila* Wntless, a protein important for the secretion of Wnt proteins from Wnt-producing cells. Previously, we showed that opioid drugs cause a redistribution in the localization of GPR177, leading to enhanced MOR/GPR177 complex formation and the inhibition of Wnt protein secretion.

GPR177 is extremely highly conserved between vertebrate species. It therefore seems reasonable to assume that the general function of GPR177 is also likely to be conserved across species lines. However, there may be species and cell-type specific mechanisms of Wnt release. Thus, it is important to determine the specific expression profile of GPR177 in developing and adult organisms. During the present reporting period, we examined GPR177 expression during zebrafish embryogenesis and in adult mouse and rat tissues in an effort to better understand the significance of this protein's role in Wnt secretion in vertebrate organisms.

1. Development and Characterization of Anti-GPR177 Antibodies

To analyze GPR177 expression, anti-GPR177 antibodies (Abs) were raised against the C-terminal 18 amino acids of human GPR177. The specificity of the anti-GPR177 Abs was

analyzed by transfecting HEK 293 cells with either FLAG/6x His-tagged GPR177 or untagged GPR177 cDNAs. A Western blot prepared from transfected cells was probed with anti-GPR177 Abs. A band of ~46 kDa was detected in cells expressing untagged GPR177, whereas two bands of ~46 kDa and ~50 kDa were detected in cells expressing epitope-tagged GPR177. The 46 kDa band represents endogenous GPR177, while the 50 kDa band represents the epitope-tagged GPR177 polypeptide. The mobility difference corresponds to the size of the FLAG/6x His tag. When the blot was reprobed with anti-FLAG Abs, a band migrating at the position of epitope-tagged GPR177 was detected in the FLAG-tagged lane, but not in the untagged GPR177 lane. These results indicate that the anti-GPR177 Abs react specifically with GPR177.

2. Expression of GPR177 in Rodent Tissues and Brain Regions

Using the anti-GPR177 Abs, we analyzed expression of GPR177 in rat and mouse tissues. As shown in Fig. 1A, GPR177 was expressed in all rat tissues tested including skeletal muscle, heart muscle, lung, gut, liver, and kidney. GPR177 polypeptides were also detected in all mouse tissues examined (Fig. 1B). In mouse, GPR177 migrates with an apparent molecular weight of ~46 kDa in each of the five tissues tested. We next examined the distribution of GPR177 in rat and mouse brain regions. Using GPR177 Abs, we probed several rat and mouse brain regions including cortex, striatum, hippocampus (rat and mouse), ventral tegmentum, nucleus accumbens (rat), and cerebellum (mouse). As shown in Fig. 1C and D, GPR177 is expressed at similar levels in all brain regions tested (both rat and mouse) with the possible exception of hippocampus, where GPR177 is present at somewhat lower abundance. In cerebellum, expression of mouse GPR177 mRNA (Fig. 1E) and rat GPR177 protein (Fig. 1F-H) was localized predominantly within Purkinje cells.

3. Expression of the Zebrafish *gpr177* Gene During Zebrafish Embryogenesis

We analyzed expression of the single zebrafish *gpr177* gene during embryogenesis. As shown in Fig. 2J, GPR177 polypeptides were expressed at similar levels during the first ten hours of zebrafish development. At early somitogenesis (15 hpf), *gpr177* mRNA was detected in the presumptive head and tailbud, and in the head region, spinal cord, and tail bud at 18 hpf. Expression of the *gpr177* gene persisted in the spinal cord at 24 hpf, and was also detected in the midbrain, hindbrain, midbrain-hindbrain boundary, and ventricular zone (Fig. 2C). At 48 hpf, transcripts of the *gpr177* gene were predominant in the tectum, branchial arches, pectoral fin bud, hindbrain, midbrain-hindbrain boundary, ventricular zone, and ear (Fig. 2D-F). By 72 hpf, *gpr177* mRNA expression was restricted primarily to the branchial arches, midbrain-hindbrain boundary, ventricular zone, and the semicircular canals of the inner ear (Fig. 2G-I).

To analyze the function of the *gpr177* gene, we used two, non-overlapping antisense morpholinos to knock down *gpr177* mRNA translation in zebrafish. One MO was targeted to the initiating methionine (ATG-MO), while the other targeted the upstream 5'-untranslated region (UTR-MO) of *gpr177* mRNA. Injection of either MO affected brain and ear development (Fig. 3). At 24 hpf there was extensive disorganization of brain tissue and a poorly defined midbrain-hindbrain boundary. At 48 hpf, the eyes of morphants (Fig. 3G, H, J, K) were smaller compared to wild-type embryos (Fig. 3E, F), and brain tissue remained disorganized, with the absence of a clearly identifiable midbrain-hindbrain boundary (Fig. 3H, K). Morphants at 24 and 48 hpf also

exhibited abnormal ventral (Fig. 3J) and lateral (Fig. 3G) curvature of the tail. Injection of the ATG-MO produced significant cardiac edema in embryos (Fig. 3H), but was not observed with the *gpr177* UTR-MO (Fig. 3K). Knockdown of the *gpr177* gene also produced a noticeable effect on ear development. At 48 hpf, wild type otic vesicles contained two otoliths and formed the semicircular canals (Fig. 3F). In morphant embryos at 24 hpf (Fig. 3D) and 48 hpf (Fig. 3H, K), otolith formation appeared normal. At 48 hpf, however, the semicircular canals were completely absent in morphant embryos (Fig. 3H, K). These results suggest that *gpr177* gene expression is required for proper brain and ear development during zebrafish embryogenesis.

4. GPR177 Structure-Function Relationships

To determine the glycosylation state of GPR177, we treated microsomes from GPR177-transfected HEK 293 cells with *N*-glycosidase F. Microsomes from rat and mouse brain, endogenously expressing GPR177, were also treated. As shown in Fig. 4A, *N*-glycosidase F digestion of either HEK 293 cell, rat brain, or mouse brain microsomes produced a novel band migrating at ~37 (human) or ~34 kDa (rat and mouse). These results suggest that the human and rodent GPR177 polypeptides are modified by the addition of N-linked oligosaccharides. We utilized the FLAG/6x His-tagged GPR177 construct to analyze the intracellular location of the GPR177 N-terminus. HEK 293 cells were transfected with the N-terminal FLAG/6x His-tagged GPR177 construct and the distribution of the tagged protein was analyzed by immunofluorescence microscopy. The results are shown in Fig. 4. Under permeabilized conditions, HEK 293 cells transfected with an N-terminal FLAG-tagged MOR cDNA exhibited robust staining at the plasma membrane (Fig. 4B). Cells expressing the FLAG/6x His-tagged GPR177 construct showed staining in the cytoplasm as well as at the plasma membrane (Fig. 4D). In non-permeabilized cells, the tagged MOR construct was visualized at the cell surface (Fig. 4A). However, no immunostaining was detectable in non-permeabilized cells transfected with the N-terminal tagged GPR177 cDNA (Fig. 4C). These results show that the N-terminus of GPR177 is located intracellularly, and that GPR177 contains an even number of TM segments.

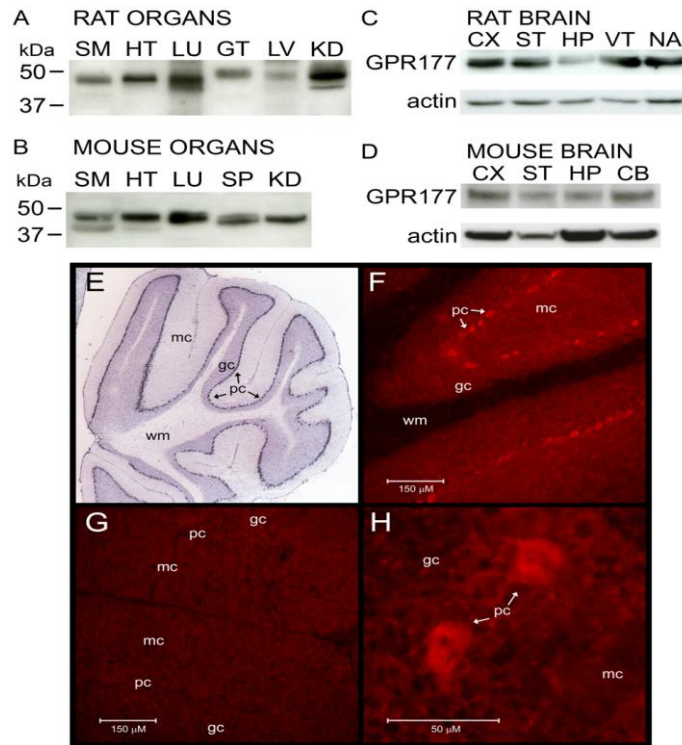


Figure 1. Expression of GPR177 in rat and mouse. Rat (A) and mouse (B) tissues. Rat (C) and mouse (D) brain regions. SM: skeletal muscle; HT: heart ; LU: lung; GT: gastrointestinal tract; LV: liver; SP: spleen; KD: kidney; CX: cortex; ST: striatum; HP: hippocampus; VT: ventral tegmentum; NA: nucleus accumbens; CB: cerebellum. (E) GPR177 mRNA in mouse cerebellum. wm: white matter; gc: granular layer; pc: purkinje layer; mc: molecular layer. Confocal images of rat cerebellum slices stained with anti-GPR177 antibodies (F, H), or no primary antibody (G). Arrows indicate Purkinje cell layer.

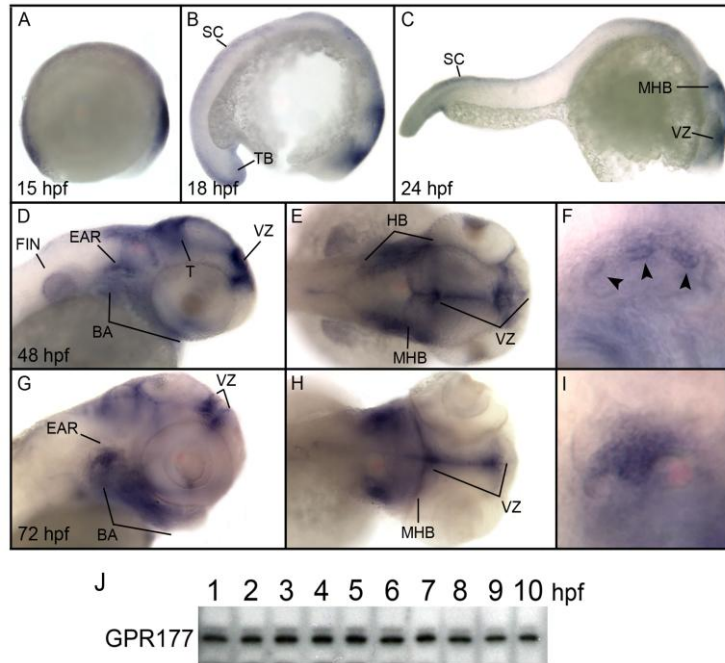


Figure 2. Expression of the *gpr177* gene in zebrafish embryos. *gpr177* mRNA analyzed by whole mount *in situ* hybridization (A-I). (A) Early somitogenesis, (B) 18 hpf, (C) 24 hpf, (D) 48 hpf, head, (E) 48 hpf, head (F) 48 hpf, ear, (G) 72 hpf, head, (H) 72 hpf, head, (I) 72 hpf, ear. Arrowheads indicate semicircular canals. BA: branchial arches; T: tectum; HB: hindbrain, MHB: midbrain-hindbrain boundary; SC: spinal cord; TB: tail bud; VZ: ventricular zone. (J) Western blot containing lysates from embryonic zebrafish probed using anti-GPR177 antibodies.

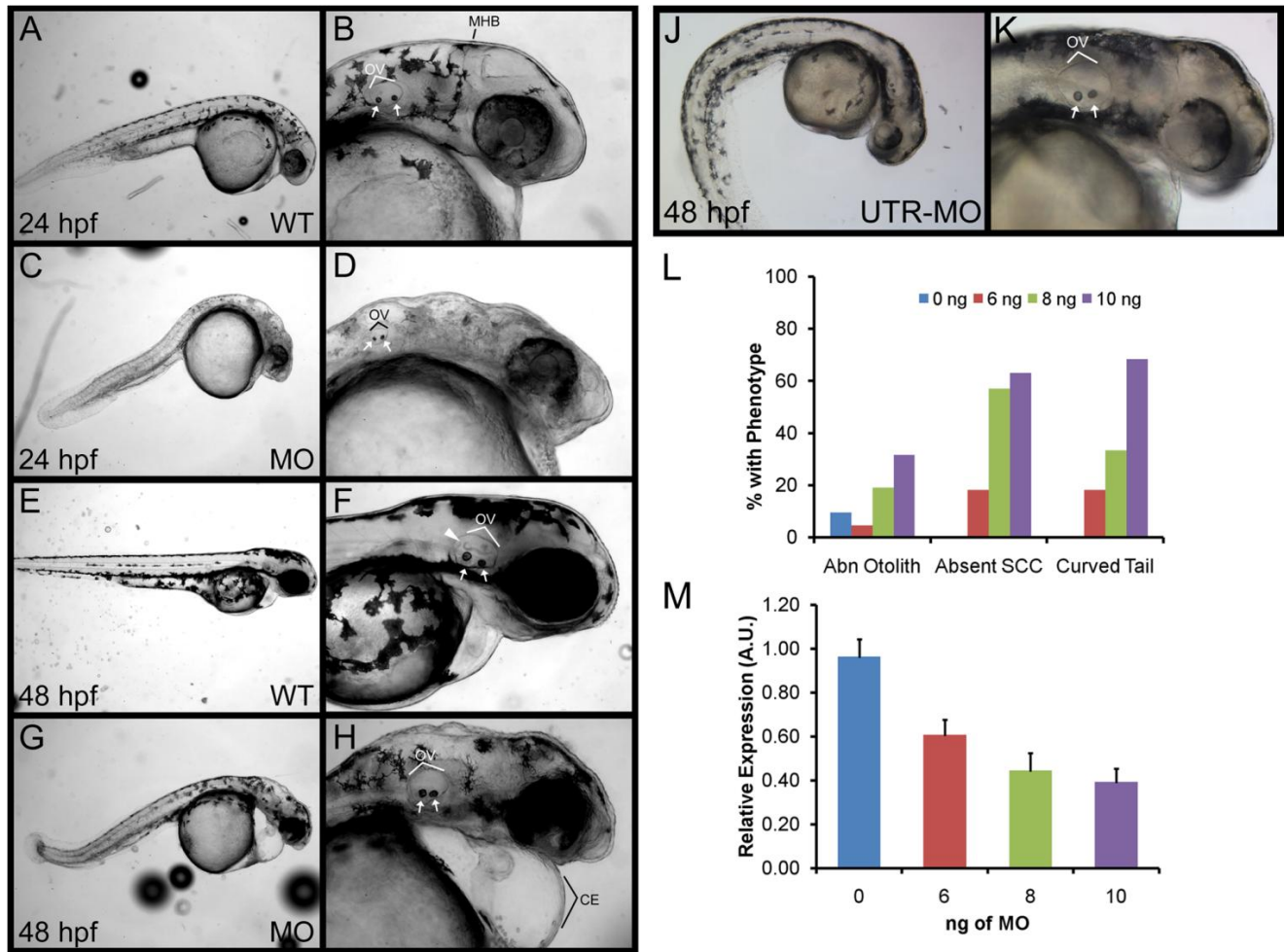


Figure 3. Knockdown of *gpr177* mRNA expression. An antisense *gpr177* MO was used to knock down *gpr177* mRNA translation. Morphants produced by the ATG-MO are in **C, D, G, H**. Morphants produced by the UTR-MO are in **J, K**. **(A)** 24 hpf wild type (WT) embryo, **(B)** 24 hpf, head of WT embryo, **(C)** 24 hpf morphant injected with 4 ng of ATG-MO, **(D)** head of 24 hpf morphant, **(E)** 48 hpf WT embryo, **(F)** head of 48 hpf embryo, **(G)** 48 hpf embryo injected with 4 ng ATG-MO, **(H)** head of 48 hpf morphant, **(J)** 48 hpf embryo injected with 6 ng of UTR-MO, **(K)** head of 48 hpf morphant. Arrows show otoliths. Arrowhead indicates semicircular canals. MHB: midbrain-hindbrain boundary; OV: otic vesicle; CE: cardiac edema. **(L)** Phenotypes of morphants injected with UTR-MO scored at 48 hpf. n=19-21 at each dose. **(M)** UTR-MO injected embryos (scored in **L**) were harvested at 48 hpf and GPR177 expression compared to that in WT embryos.

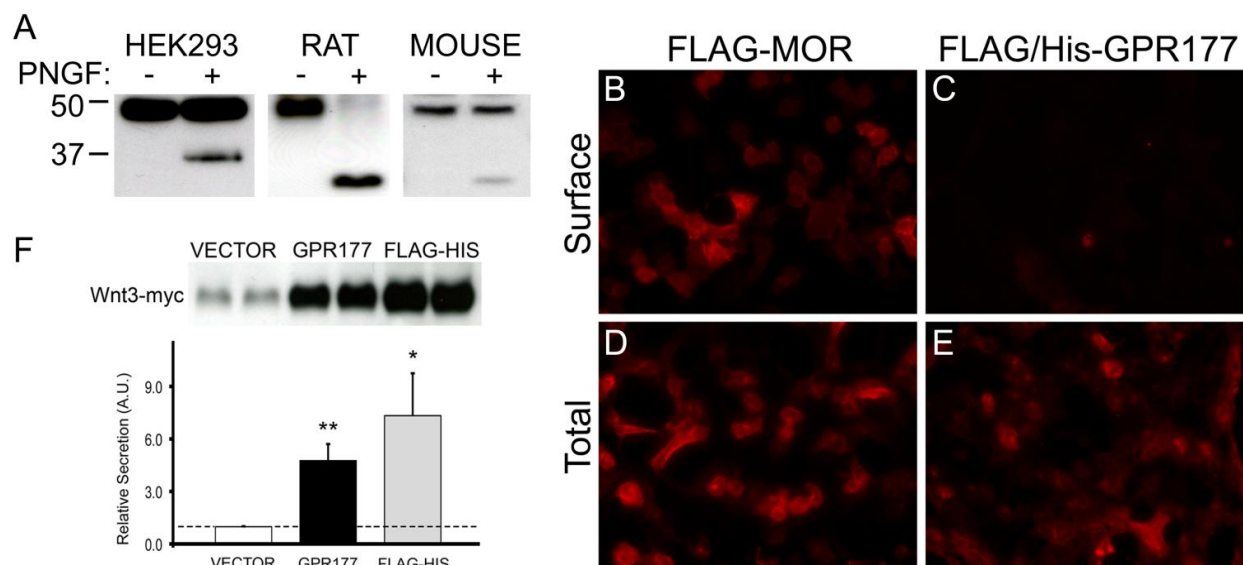


Figure 4. GPR177 structure and function. (A) Crude microsomal membrane preparations from HEK 293 cells transfected with FLAG/6x His-tagged GPR177 cDNA, rat brain, and mouse brain digested in the presence (+) or absence (-) of *N*-glycosidase F (PNGF), and probed with anti-GPR177 Abs. (B-E) HEK 293 cells transfected with FLAG-tagged MOR (FLAG-MOR) or FLAG/6x His tagged-GPR177 (FLAG/His-GPR177) cDNA and labeled with anti-FLAG Abs under permeabilized (Total) or non-permeabilized (Surface) conditions. (F) HEK 293 cells were cotransfected with myc-tagged Wnt3 cDNA and either untagged GPR177 cDNA or FLAG/6x His-tagged GPR177. Wnt3-myc secretion was assayed by Western blotting. Blots were probed with anti-myc Abs, and bands were quantitated using ImageJ software (NIH). Data was subjected to two-tailed Student's t-test. Dotted line indicates secretion obtained with empty vector control and assigned a relative value of 1.0 (n= 4-6, **p<0.01, *p<0.05).

Research Project 26: Project Title and Purpose

Role of TGFβ in Microtubule Dynamics - A major significance of the project relates to our finding that 42% of ovarian cancer patients have alterations in the motor protein subunit we discovered, termed km23, with no such alterations in normal tissues. Such a high alteration rate in ovarian cancer suggests that km23 plays an important role in this disease. The novelty of the proposed studies relates to the plan to investigate trafficking of specific TGFβ signaling components in relation to the km23 motor subunits, and to determine how these events are altered by ovarian cancer mutations. The overall goal of this project is to better understand how a critical growth regulator sends its signals to stop growth, and how these events are altered in human cancer. The results will assist with the development of novel anti-cancer agents to treat ovarian and other cancer types.

Duration of Project

8/9/2007 – 12/31/2008

Summary of Research Completed

This project ended during a prior state fiscal year. For additional information, please refer to the Commonwealth Universal Research Enhancement Annual C.U.R.E. Reports on the Department's Tobacco Settlement/Act 77 web page at <http://www.health.state.pa.us/cure>.

Research Project 27: Project Title and Purpose

Novel Therapeutic Strategies to Treat Malaria - Malaria causes 300-500 million new infections, 1-3 million deaths, and 1-4% loss of gross domestic product annually in Africa. The majority of its victims are young children and pregnant women. One child under five dies every 20 seconds of malaria and survivors frequently suffer brain damage and learning disabilities. There are few available anti-malarial drugs, no vaccines and embarrassingly few drugs in the anti-malarial drug pipeline. Thus, there is an unprecedented need to develop new drugs to treat malaria. Malaria parasites express two proteins, called 'ion channels', which are members of a large family of proteins that are essential for the survival of all living organisms. Preliminary findings indicate that targeting the malarial ion channels with drugs kills parasites *in vitro*. The purpose of this research is to develop a deeper understanding of the role ion channels play in the normal physiology of the malaria parasite and their potential as anti-malarial drug targets.

Duration of Project

8/9/2007 – 6/30/2009

Summary of Research Completed

This project ended during a prior state fiscal year. For additional information, please refer to the Commonwealth Universal Research Enhancement C.U.R.E. Annual Reports on the Department's Tobacco Settlement/Act 77 web page at <http://www.health.state.pa.us/cure>.

Research Project 28: Project Title and Purpose

Center for Functional Genomics - Our understanding of biological systems is becoming increasingly sophisticated, to the point where additional learning is being hampered by our inability to grasp the vast warehouse of knowledge. This bottleneck is being magnified exponentially as we develop increasingly more powerful means of high-throughput data collection. Moreover, teaching this complexity to students at all levels (K-12, college, and beyond) becomes increasingly more of a challenge as tech-savvy students expect more "user-friendly" learning environments. The purpose of this project is to develop a bioinformatic browser that helps students, scientists, and lay people understand the complexity of the cellular nucleus. This project will also contribute to and draw from knowledge retained in the browser.

Anticipated Duration of Project

8/9/2007 – 12/31/2010

Project Overview

The Center for Functional Genomics has three broad objectives. The first objective is to construct an internet browser that assimilates a broad range of genomic data so that relationships can be readily visualized. The browser is expected to have varying levels of sophistication such that the information would be of interest to students at all levels. Students in the primary grades would primarily use it as a “fun” way to explore. Students and laypersons at upper levels would use it to understand concepts about how cells are regulated at the molecular level. Scientists would use it to conceptualize complex relationships among gene regulatory molecules for purposes of discovery and modeling. Specific aims in this first objective include the production of a graphical user interface, and tools to retrieve, deposit, and model a variety of genomic information.

The second objective is to provide raw experimental data to upload into the browser that the information can be displayed either quantitatively or graphically through icons. Personnel associated with the project will conduct genomic experiments in a number of collaborative laboratories and upload the data sets into the browser.

The third objective is to use the browser as a discovery platform. Personnel associated with the project will use the browser to discover novel relationships among hordes of genomic information. These relationships will be formulated into a testable hypothesis that will be directly investigated in a collaborative laboratory. Funds associated with the project will be used to seed these goals, with the intent that federal support will ultimately carry the bulk of the financial needs of the project.

Specific Aims:

- 1) Develop a web-based browser to visualize genomic data.
- 2) Experimentally test the prediction that gene regulatory proteins bind to fixed locations at the beginning of genes throughout the genome of model organisms (yeast initially, then *Drosophila* and human).
- 3) Experimentally test whether regulatory proteins that co-localize to gene promoters are functionally dependent upon each other.
- 4) Use the data generated in aims 2 and 3 that has been uploaded into the browser developed in aim 1 to experimentally validate on individual genes the observed relationships.

Principal Investigator

B. Franklin Pugh, PhD
Penn State University
452 N. Frear
Department of Biochemistry and Molecular Biology
University Park, PA 16802

Other Participating Researchers

Istvan Albert, PhD, Anton Nekrutenko, PhD, Stephan C. Schuster, PhD, Ross C. Hardison, PhD, David S. Gilmour, PhD, Song Tan, PhD, Joseph C. Reese, PhD and Yanming Wang, PhD – employed by Penn State University

Expected Research Outcomes and Benefits

Specific outcomes of this project include a genome browser decorated with icons that are representative of genomic information. Such genomes include human and those of model organisms. Tracks of information include the location of nucleosomes (building blocks of chromosomes), locations of genes, locations of gene regulatory proteins and DNA regulatory sites. The browser will be navigable via one-dimensional scrolling to move along the one-dimensional string of DNA. Later versions of the browser are expected to include plug-ins that allows the genomic information to be represented as actual three-dimensional structures rather than the use of schematic icons as proxies. The plug-in will allow navigators to move around the structures in a virtual 3-D environment. A substantial portion of the data represented in the browser is expected to be generated through the project. Specific testing of hypotheses arising from the modeling will allow the hypothesis to be validated or discarded.

The benefit of this work to society is that it provides an educational tool for all people to understand the inner workings of a cell, which is critical for making informed decisions in society. Second, it provides scientists with a means of distilling a tsunami of data into simple concepts that the human brain is more adept at understanding. This will facilitate further discovery in biological systems, in particular gene regulatory systems. Understanding how genes are regulated is critical towards creating strategies to repair damaged genes or mis-regulated genes.

Summary of Research Completed

We have now completed collection of genome-wide location data of over 200 gene regulatory proteins. We have developed a genomic 3-D browser called Bioscape in which to visualize millions of data (genomic binding locations of transcriptional regulators) already generated by the project. The browser has many features, including 1) icons that represent bound proteins at specific locations in the genome, 2) dynamic displays in which icons appear and disappear in accord with measured binding levels (dwell times correlate with occupancy level over a 10 sec. cycle). Icon appearances are linked to appearance of the transcription machinery, including RNA polymerase II. RNA polymerase appears at the beginning of each gene with a frequency in accord to measured transcription rates. It then moves down the gene, producing RNA, and at the same time nucleosomes that are in the path of RNA polymerase move out of the way and return upon polymerase passage. The browser has search and navigation features, and interactive annotations. Also illustrated on the browser is the change in occupancy of gene regulators as the genome is reprogrammed. The browser is on display in a public forum at Penn State University North Frear laboratory, and is available for individuals to interact with.

To accelerate data collection, an Illumina GAIIx high throughput DNA sequencer was purchased. This instrument can measure as many as 200 million binding events in a genome in a single run. This has increased our ability to collect binding data by six orders of magnitude. In addition to creating a visualization browser and acquiring the latest technology in data collection, we have developed a novel ultra high resolution mapping strategy to determine with single base resolution the location of protein bound in the genome. This technology necessitated the acquisition of the Illumina sequencer, and will serve to benefit the 3D browser so that it may more accurately display data.

It is now becoming clear that eukaryotic genomes have a very well defined organization of chromatin (see Fig. 1, illustrating a small section of the data collected from the Illumina instrument). Chromatin utilizes nucleosomes as its basic building block. The Illumina sequencing instrument is used to continue generating complete maps of nucleosome positions in yeast under a variety of environmental conditions and when certain chromatin organizing proteins are deleted. The key to efficient mapping of proteins in the genome is tag counts (number of individually measured binding events). Other sequencing instruments (e.g. Roche 454) are inefficient because the high overall cost of this technology is used to achieve longer sequence lengths rather than higher tag counts. For mapping in yeast, 25 bp read lengths are sufficient to uniquely identify >90% of the genome (the remainder being repetitive sequences like transposable elements). For the same price, we can acquire >200 times the number of tags using the Illumina platform vs. Roche/454. This throughput capacity has allowed research to be expanded toward examination of more environmental conditions and more chromatin mutants, resulting in a more thorough understanding of the rules governing chromatin organization on a genomic scale.

We have also compared the actual mapping resolution of all three sequencing platforms (Roche, Illumina, AB) with that of Affymetrix high density tiling arrays. We have found that all three sequencing platforms provide the same resolution and that they are far superior to the tiling arrays. The higher resolution is achieved because of its single base pair mapping resolution and by the fact that MNase digestion of chromatin results in highly homogeneous and well defined nucleosome borders (which sonication does not achieve).

We have now mapped the locations of ~200 gene regulatory proteins (includes sequence-specific factors, chromatin regulators, GTFs and regulators, and elongation factors) at low resolution using our custom tiling arrays. The biggest challenge with this study has not been the generation of material or data, but moving massive numbers of large datasets through what would otherwise be a simple analysis for a few ChIP-chip datasets. We have collected approximately 8 million data points across 800 experiments. Even a simple analysis like creating a Venn diagram depicting the set of genes bound by any two factors and its statistical significance required substantial computational programming, and new ways of displaying data. For example, Figure 2 displays 40,000 hierarchically clustered Venn diagrams. The x and y axes each list 200 ChIP-chip factor datasets. For each factor we filtered the set of bound promoter regions at a 5% false discovery rate. We then determined the percentage of these significantly bound genes that are bound in common by each factor listed along the x axis in relation to each factor listed along the y axes. Each pixel in the Figure 2 heat map represents that overlap, with red being close to 100% overlap and blue being near zero overlap. This chart represents a discovery resource that

can be inspected up close. For example, if your favorite factor is Tfg1, a zoom-in on Figure 2 will tell you what other factors tend to bind the same set of genes that Tfg1 (TFIIF) binds to, and thus would be candidates for functional relationships with Tfg1 (in this case Tfa1 or TFIIE). We can further expand this type of analysis by superimposing on this heat map other properties of the genes that reside at the intersection (e.g. transcription frequency, or methylation status, or p-value of the overlap). We have also employed Cytoscape to visualize networks in our data. One is illustrated in Figure 3, where the GTFs were found connected to each other and through a sub network that includes H2A.Z/SWR1/Bdf1, which is connected to another sub network involving chromatin regulation and the mediator complex.

From these massive relationships we see many things that we expect, and many things that are novel. For example, we find that factors that tend to regulate chromatin tend to occupy the same sets of genes, yet these genes are lowly transcribed (not shown). Elongation factors also tend to occupy the same set of gene, and they are different than those occupied by chromatin regulators. Surprisingly, such genes are also moderately to lowly transcribed (not shown). Factors that regulate transcription initiation, on the other hand, tend to occur on highly transcribed genes (not surprisingly). The fundamental insight gained from these studies is that, in general, when chromatin regulators or elongation factors (FACT is an exception) are enriched at their cognate genes, their function tends to be rate-limiting in gene expression. We have also gained many other insights into the transcription process, including an identification of several novel factors bound to Pol III-transcribed tRNA genes (all of which were present in our tiling arrays).

In addition to genome-wide mapping of 200 factors under normal growth conditions, we further mapped the same 200 factors under conditions of acute heat shock (15 min. 37°C). Biological replicates were produced in all cases, and verified to be highly correlated prior to combining. Figure 4 shows a cluster plot of changes in occupancy of the 200 factors at all 6000 yeast genes in response to heat shock. We have not yet analyzed this data in detail, except to note that the changes in gene/chromatin regulatory factors occupancy is highly selective for factors and genes (despite the fact most of these factors occupy at least some promoter regions). This is important because it demonstrates that while many factors may bind genes, including heat shock response genes, not all of them are redistributed when the genome is preprogrammed.

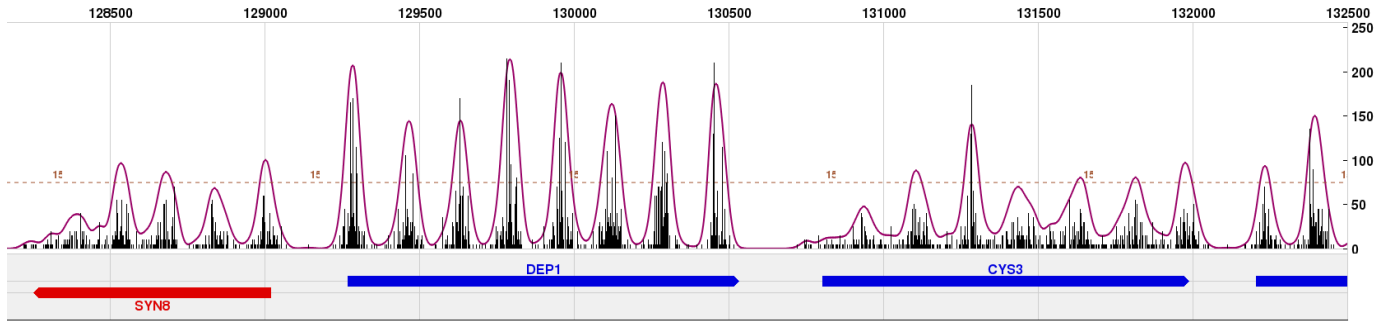


Figure 1 This figure illustrates the quality of our mapping data. Shown are a section of the yeast genome, and the Illumina-mapped reads of nucleosomes. Each peak represents the position of a nucleosome. Each black vertical bar is the tag count at that position. Note that the Y-axis indicates that a tag count at a given coordinate can be as high as 200, yet in the nucleosome-free promoters the tag count is essentially zero over 50-200 bp. This mapping display, including nucleosome calls, was developed by our bioinformatics group (Albert et al. *Bioinformatics* (2007) 24:1305-6).

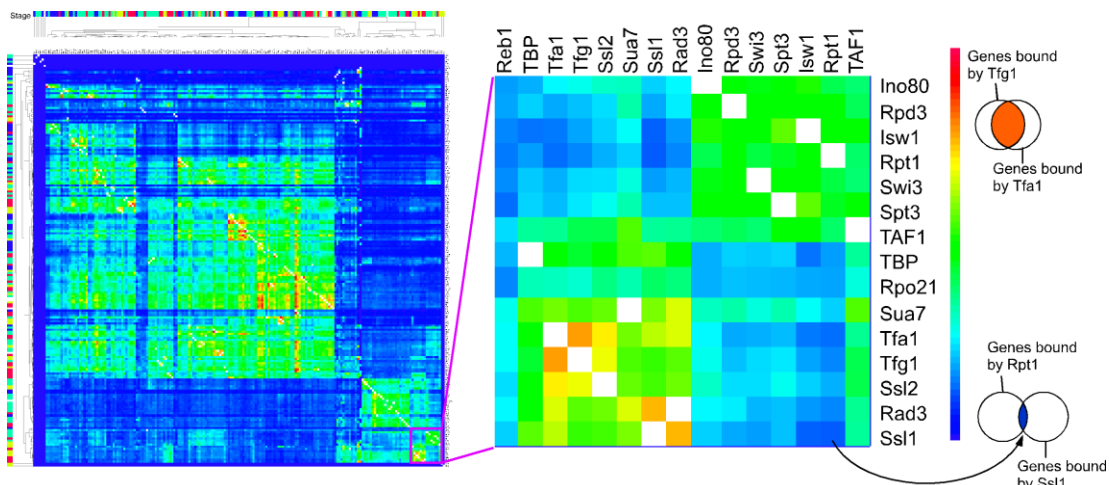


Figure 2 Heat map representing a Venn-type overlap of the set of genes bound by the factors listed across the top versus those listed vertically along the right. The “hotter” the color, the greater the percentage of significantly bound genes that bind both factors.

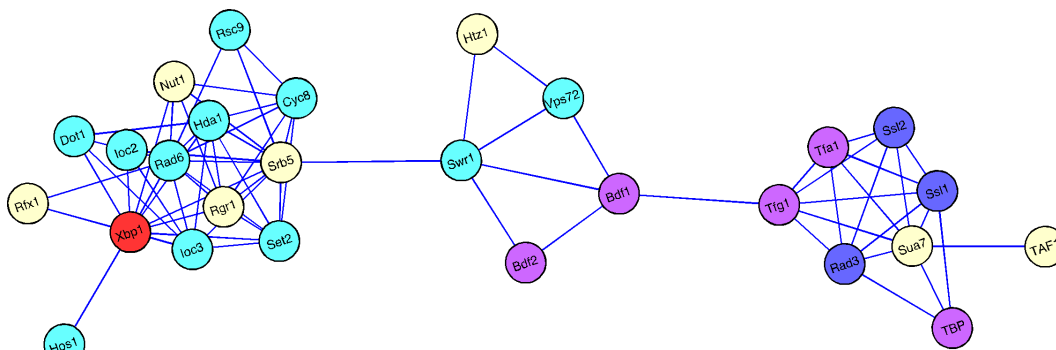


Figure 3 Cytoscape network derived from ChIP-chip datasets. Nodes are regulator proteins and the edge lengths depict the extent of overlap of genes they occupy.

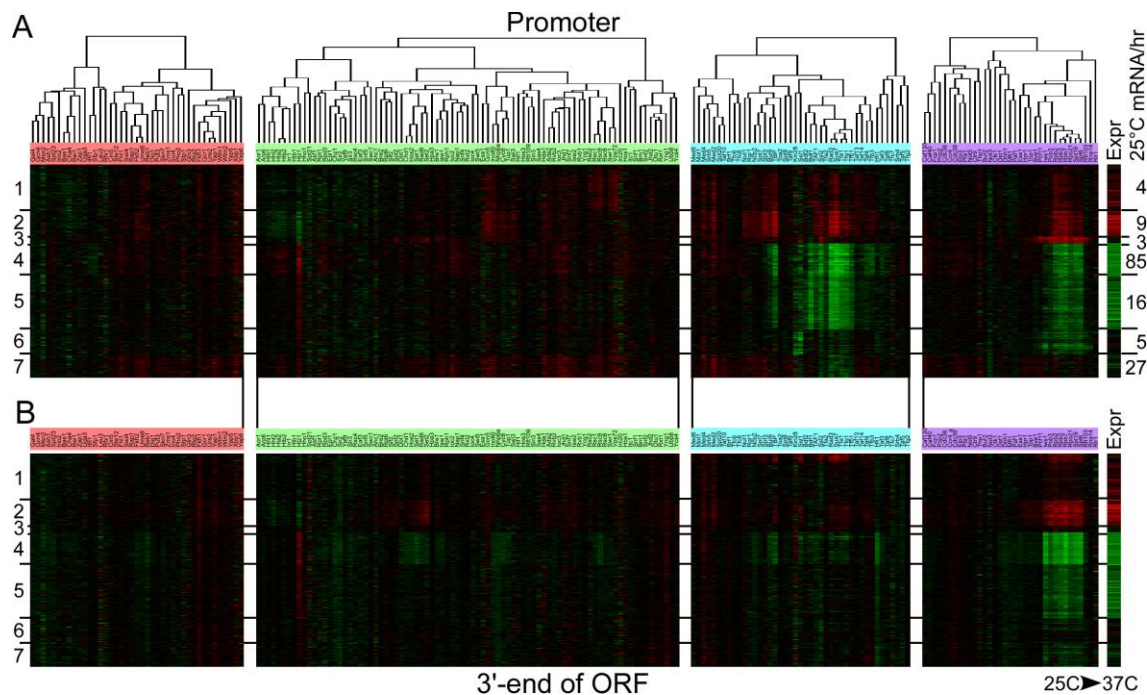


Figure 4

Research Project 29: Project Title and Purpose

Regulation of Human Sebaceous Glands by 13-cis Retinoic Acid - Severe acne can have profound psychological and physical morbidity for millions of affected patients. The overall goal of the research is to determine how isotretinoin, a potent drug for acne exerts its positive effects in the sebaceous gland by reducing sebum production and improving acne. Isotretinoin (13-*cis* retinoic acid) is the only drug effective against severe acne that targets each of the causative factors of this disease. 13-*cis* RA is also used in cancer chemotherapy. This drug however can cause birth defects. The specific goal of this project is to identify the active isomer or metabolite of 13-*cis* RA that induces apoptosis in human sebocytes. The experiments to be done with these tobacco settlement funds are critical to the overall success of a larger grant application to the NIH. This information can lead to the identification of potential therapeutic target sites that could be activated by drugs apart from 13-*cis* RA that would have an improved safety profile.

Anticipated Duration of Project

8/9/2007 – 12/31/2010

Project Overview

Lack of understanding of the mechanism of action of 13-*cis* RA in the sebaceous gland has hampered the progress to find safer alternatives in the treatment of severe acne. Our preliminary data indicate that 13-*cis* RA induces apoptosis and cell cycle arrest in sebocytes. Gene array expression analysis in sebocytes and in human skin indicates that 13-*cis* RA induces genes involved in the innate immune response, including *lipocalin 2*, that encodes a multifunctional secretory protein called neutrophil gelatinase associated lipocalin (NGAL) that is involved in the formation of the kidney, the body's defense against bacterial pathogens and in cellular apoptosis. The major goal (specific aim) of the experiments done with tobacco settlement funds is to test the hypothesis that 13-*cis* RA acts by a metabolite or metabolites to induce apoptosis in human cells. Subaims are directed at determining how 13-*cis* RA differs from all-*trans* RA in mediating apoptosis. The findings of these studies not only have the potential to advance our understanding of retinoid action in acne, but can lead to advances in the understanding of these agents in cancer biology and in innate immunity as well.

Principal Investigator

Diane M. Thiboutot, MD
Department of Dermatology HU14
Penn State University College of Medicine
500 University Drive
Hershey, PA 17033

Other Participating Researchers

Gary Clawson, MD, PhD – employed by the Penn State University College of Medicine

Expected Research Outcomes and Benefits

The desired outcome for the overall research project is the discovery of the specific means by which 13-*cis* retinoic acid exerts its beneficial effects in suppressing function of the sebaceous gland and improving acne. It is unknown as to whether the drug itself or its metabolites mediate this suppression and whether these effects are mediated by retinoic acid receptors. *The studies done with tobacco settlement funds in this project should identify the isomer or metabolites of 13-cis RA that are responsible for inducing apoptosis in human sebocytes.*

In the context of the overall grant application to the NIH, if retinoic acid receptors are not involved, then it is possible that safer classes of drugs (those that do not cause birth defects) could be used to elicit the same beneficial effects as 13-*cis* retinoic acid. If the neutrophil gelatinase associated lipocalin protein (NGAL) mediates the effects of 13-*cis* retinoic acid on apoptosis or cell cycle arrest in sebaceous cells, then an alternative treatment for severe acne might involve therapies that are aimed at increasing the expression of the NGAL protein in the skin. The data generated in the overall project can lead to the identification of new therapeutic target sites in the treatment of severe acne. As such, this project has the potential to improve health status for hundreds of thousands of patients who are being treated for severe acne with 13-

cis retinoic acid. Although this project studies the effects of 13-*cis* RA on cells from the sebaceous gland that relate to acne, the information gained from this study regarding the mechanism of action of 13-*cis* retinoic acid at a cellular level is also relevant to cancer chemotherapy since 13-*cis* retinoic acid is used to treat cancers such as neuroblastomas in children. This drug is also used in chemoprevention of cancers in patients with diseases or conditions characterized by frequent occurrence of skin cancers. As such, the data from this project including the segment funded by tobacco settlement funds has the potential to lead to advances in therapy of a common condition, acne, and serious conditions such as cancer.

Summary of Research Completed

We have successfully developed methods to detect the major isomers of 13-*cis* retinoic acid in cell culture using HPLC/MS/MS (see previous annual report). Our original hypothesis was that 13-*cis* retinoic acid was being metabolized to oxo-derivatives by cytochrome P450 hydroxylases that may be responsible for the action of this drug in inducing apoptosis in human sebaceous gland cells. In order to effectively assess the metabolites (but not required for isomers), an internal standard (pentadeuterated retinoic acid) was required. Difficulties were encountered in the chemical synthesis of pentadeuterated retinoic acid (described below). Our studies however indicated no oxo-metabolites were present and that the CYP hydroxylases required were not present in our SEB-1 sebocytes (see previous annual reports). Therefore, use of the internal standard was no longer critical to our cell culture work.

We are currently utilizing alternative techniques as outlined in Aim 1b (on page 15 of the strategic plan) to determine the importance of the different isomers in 13-*cis* retinoic acid A-induced apoptosis in sebocytes. Our previous data suggest that only 13-*cis* retinoic acid induces apoptosis in SEB-1 sebocytes; however studies in the literature support the hypothesis that 13-*cis* retinoic acid acts as a reservoir for the active isomer, ATRA. We are conducting a series of experiments involving the treatment of SEB-1 with ATRA in comparison to 13-*cis* retinoic acid, based on the hypothesis that 13-*cis* retinoic acid is serving as a “prodrug” for ATRA via spontaneous isomerization. ATRA has a shorter half-life compared to 13-*cis* retinoic acid and patients with neuroblastoma are often treated with 13-*cis* retinoic acid as it offers a more consistent level of ATRA via spontaneous isomerization. In order to test the hypothesis that ATRA may also induce apoptosis in SEB-1 sebocytes, a series of experiments were performed using different concentrations of ATRA and 13-*cis* retinoic acid, and different dosing regimens with analysis of apoptosis using fluorescence activated cell sorting (FACS) at various time points (See Figures 1-3). Both lower (1 μ M) and higher (10 μ M) doses of ATRA were used in a single dose as well as dosing every 12hr (more consistent with its half-life) to determine if ATRA induces apoptosis.

Our historical data indicated that 13-*cis* retinoic acid was the only isomer to induce apoptosis in SEB-1 sebocytes, most notable at 72 hours. These studies indicate that apoptosis is in fact also induced by ATRA beginning at 24 hours in multiple dosing regimens and at 48 hours in single dosing experiments. In fact, in multiple dosing regimens, ATRA precedes 13-*cis* retinoic acid in its ability to induce apoptosis favoring the hypothesis that ATRA is the active isomer in the induction of apoptosis as 13-*cis* retinoic acid is gradually isomerized to ATRA as shown in previous experiments. Both ATRA and 13-*cis* retinoic acid have been shown to induce

expression of the neutrophil gelatinase associated lipocalin (NGAL) protein that mediates apoptosis in SEB-1 and other cell lines. The increased extent of apoptosis at the 72 hour time point likely results from accumulation of NGAL in the cell culture medium. These experiments suggest that 13-*cis* retinoic acid, as in the case of neuroblastoma, is exerting its apoptotic effect in acting as a reservoir of ATRA.

We now have developed the methodologies using these funds, to assess the relative levels of 13cRA, ATRA and 9-*cis* retinoic acid (9cisRA) in the serum of patients with acne that are undergoing treatment with 13-*cis* retinoic acid. A protocol has been approved by the IRB and serum samples have been collected at baseline, one week, 4, 8 and 20 weeks. To date, 12 patients have completed their 8 week samples and we are prepared to correlate their serum isomer levels with the levels of NGAL protein on the skin surface and with the patient's rate of secretion of sebum (skin oil).

Details on efforts to synthesize pentadeuterated retinoic acid:

The first phase of production of the pentadeuterated retinoic acid standard (shown in Figure 4. Scheme 1) involved the synthesis of the phosphonium salt of ethyl 3,7-dimethyl-8-oxo-2,4,6-octatrienoate. The key intermediate in the synthesis is the chloro ester, which was prepared from isoprene. Isoprene, purchased from Aldrich chemical company (Milwaukee, WI), was reacted with *tert*-butyl hypochlorite in acetic acid and further reacted with copper sulfate in sulfuric acid to produce the desired compound, chloro acetate derivative, in 61% yield. (E)-4-chloro-3-methyl-2-buten-1-ol acetate was then hydrolyzed with sodium carbonate to give the corresponding alcohol that was oxidized with pyridinium chlorochromate in methylene chloride for an overall yield of 65% over two steps of aldehyde as E/Z stereo isomers. Phosphonium salt prepared from ethyl 4-bromo-3-methyl-2-buten-1-olate was reacted with Sodium bis(trimethylsilyl)amide to generate the anion. The orange colored anion was reacted with aldehyde followed by acidic workup and further purification by column chromatography to produce the key intermediate ester in 55% yield. Phosphonium salt of ethyl 3,7-dimethyl-8-oxo-2,4,6-octatrienoate was prepared by fusion of triethoxyphosphate with corresponding chloro compound by heating the material at 130°C.

The final phase of production (shown in Figure 4. Scheme 2) is the synthesis of deuterated ethyl (E)-retinoate. The above synthesized phosphonium salt of ethyl 3,7-dimethyl-8-oxo-2,4,6-octatrienoate is converted to an anion and reacted with deuterated β -cyclocitral by using Horner-Emmons reaction at room temperature, and also at -20°C, -78°C. After several attempts, the desired anion could not be generated. However, the deuterated β -cyclocitral was reacted with the compound generated with sodiumbis(trimethylsilyl)amide and phosphonium salt followed by isolation of the major product by column chromatography. The desired standard, deuterated ethyl (E)-retinoate, was not able to be isolated.

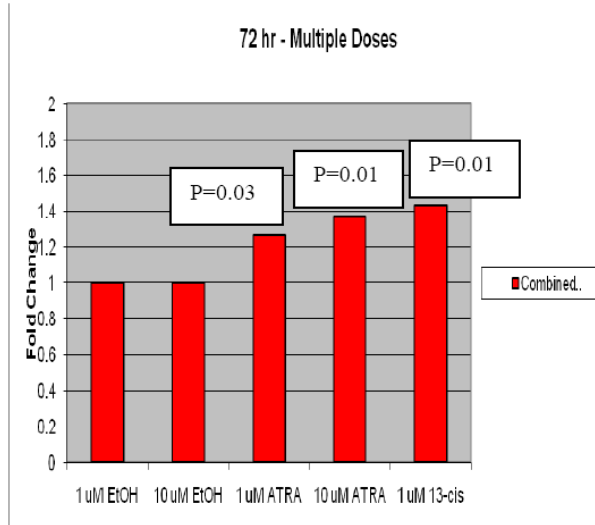
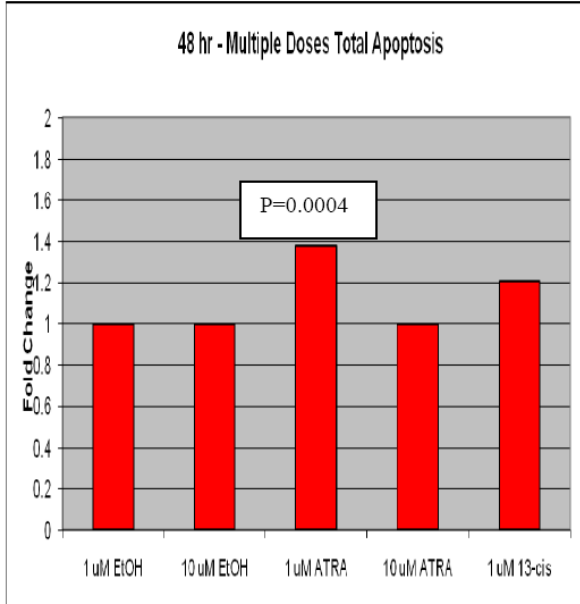
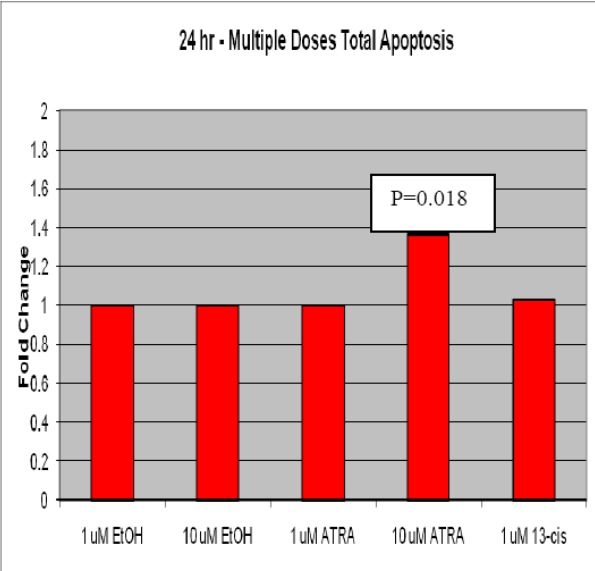


Figure 1. Fold change in apoptosis (vs. vehicle) for SEB-1 treated with ATRA or 13cRA multiple dosing.
 SEB-1 cells were treated every 12 hours by adding additional ATRA or 13cis-RA to the culture medium and FACS analysis was performed at 24, 48 and 72 hours assessing the % cells in early and late apoptosis. The % cells in early and late apoptosis were combined and compared as a fold change compared to the % cells in early and late apoptosis in the vehicle (EtOH) group. Each sample was run in triplicate and each experiment was repeated for a total of 3 times. Data were analyzed using 2-factor ANOVA.

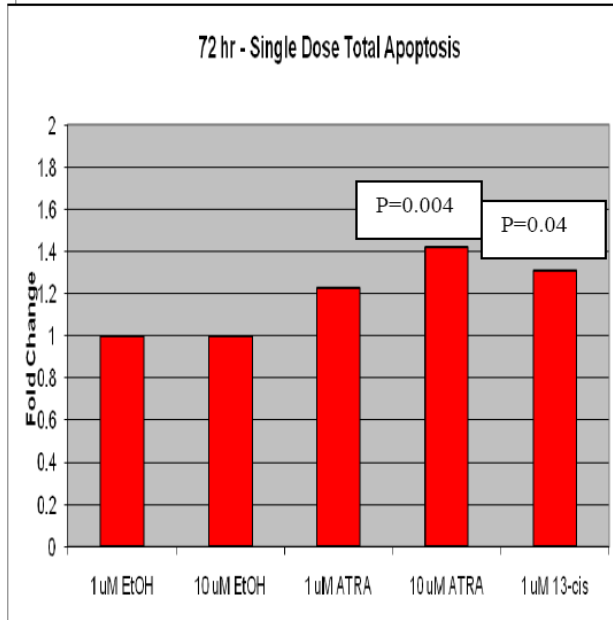
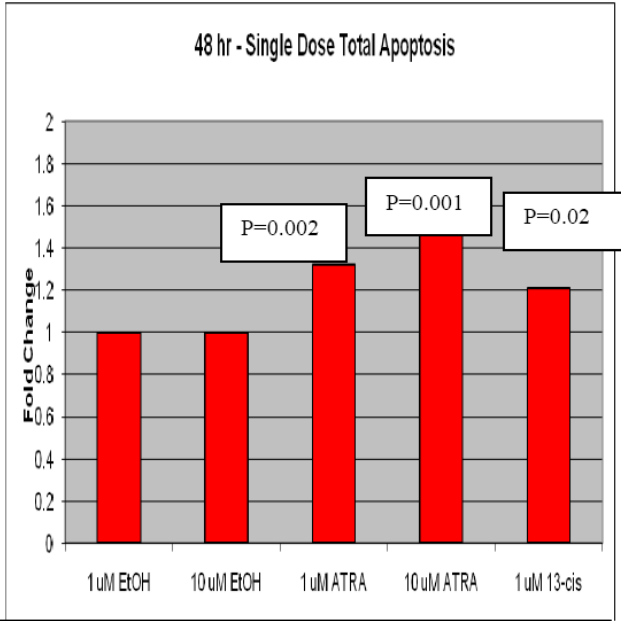


Figure 2. Fold change in apoptosis (vs. vehicle) for SEB-1 treated with ATRA or 13cis-RA as a single dose. SEB-1 cells were treated once by adding ATRA or 13cRA to the culture medium and FACS analysis was performed at 24, 48 and 72 hours assessing the % cells in early and late apoptosis. The % cells in early and late apoptosis were combined and compared as a fold change compared to the % cells in early and late apoptosis in the vehicle (EtOH) group. Each sample was run in triplicate and each experiment was repeated for a total of 3 times. Data were analyzed using 2-factor ANOVA. Data are shown for 48 and 72 hours. No significant differences were noted at 24 hours (data not shown).

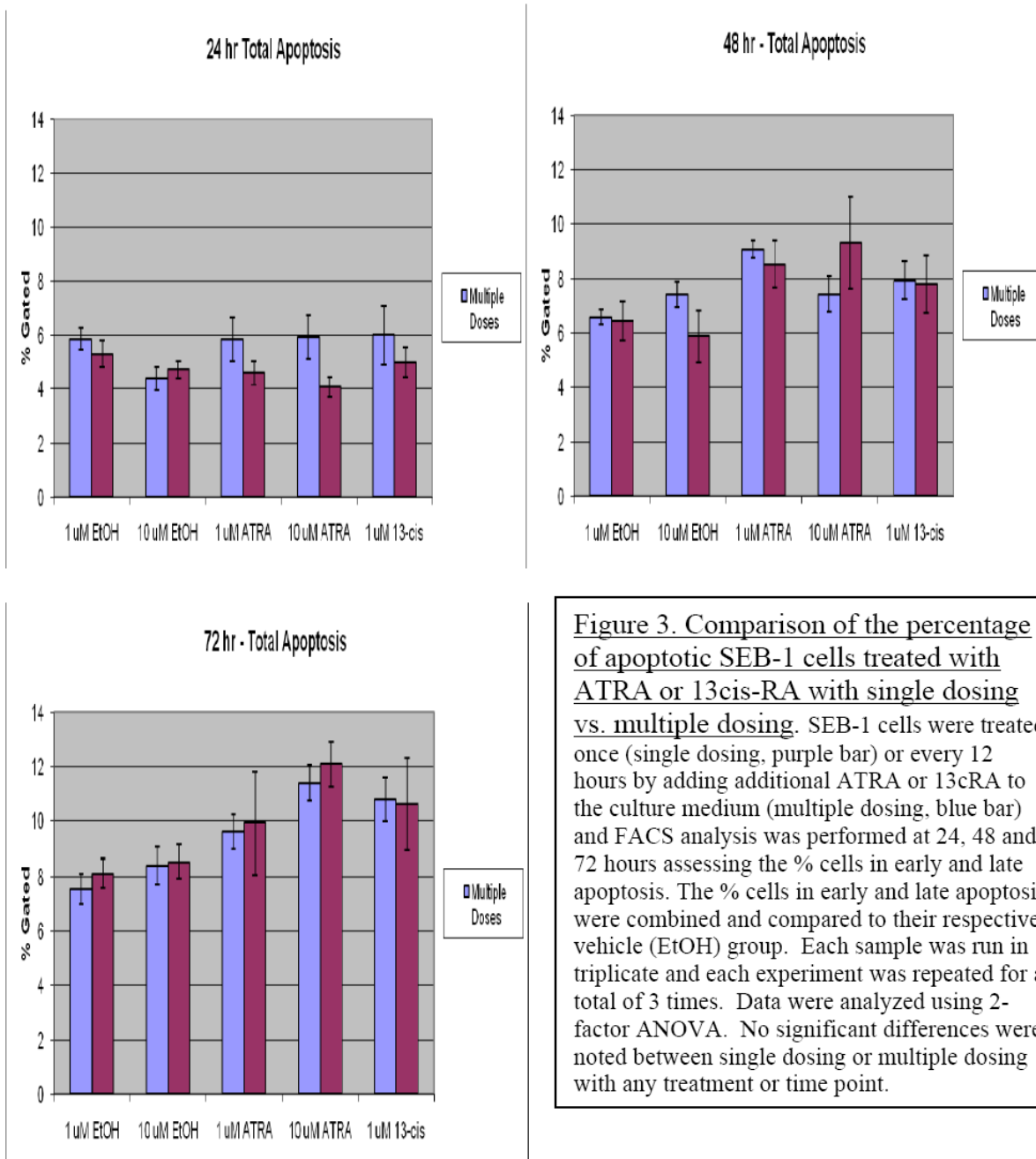
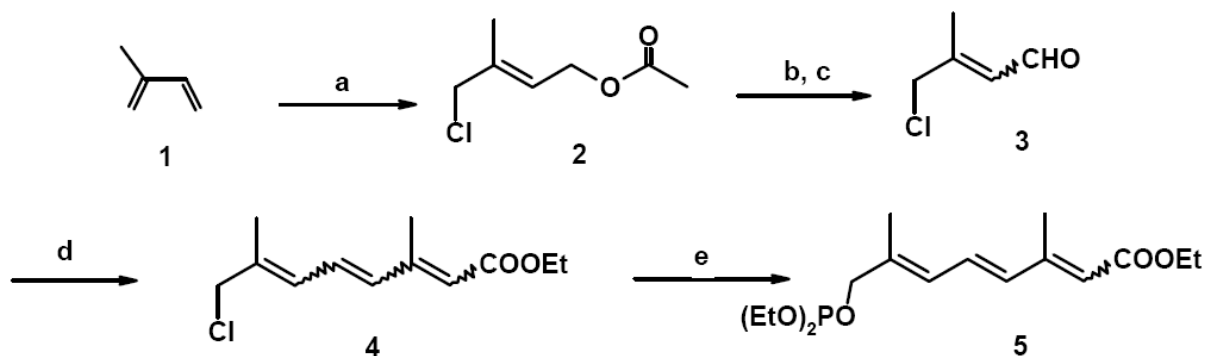


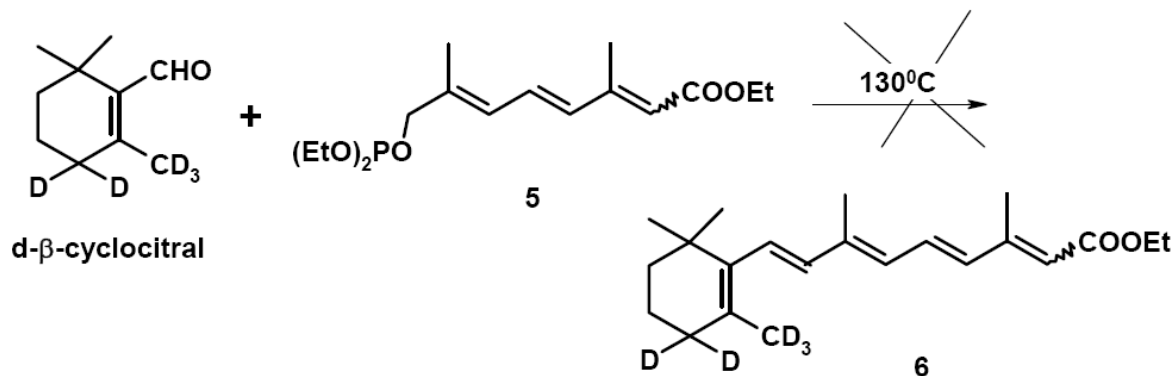
Figure 3. Comparison of the percentage of apoptotic SEB-1 cells treated with ATRA or 13cis-RA with single dosing vs. multiple dosing. SEB-1 cells were treated once (single dosing, purple bar) or every 12 hours by adding additional ATRA or 13cRA to the culture medium (multiple dosing, blue bar) and FACS analysis was performed at 24, 48 and 72 hours assessing the % cells in early and late apoptosis. The % cells in early and late apoptosis were combined and compared to their respective vehicle (EtOH) group. Each sample was run in triplicate and each experiment was repeated for a total of 3 times. Data were analyzed using 2-factor ANOVA. No significant differences were noted between single dosing or multiple dosing with any treatment or time point.

Figure 4. Synthesis of deuterium labeled standard for mass spec (MS) analysis. Scheme 1 shows the steps involved in the production of diethoxyphosphonate salt intermediate while Scheme 2 shows the last reaction, involving the use of the diethoxyphosphate salt intermediate in the attempted production of the final product, deuterated ethyl (E)-retinoate.



a) $t\text{BuOCl}$, AcOH then CuSO_4 , H_2SO_4 ; b) Na_2CO_3 , $\text{MeOH}/\text{H}_2\text{O}$; c) PCC , CH_2Cl_2 ;
 d) $\text{Ph}_2\text{P}=\text{CHC}(\text{CH}_3)=\text{CHCOOEt}$ then I_2 ; e) $(\text{EtO})_3\text{P}$, $130\text{ }^\circ\text{C}$

Scheme 1: Synthesis of Diethoxyphosphonate salt (5)



Scheme 2: Synthesis of deuterated ethyl (E)-retinoate (6)

Research Project 30: Project Title and Purpose

Center for Computational Proteomics - The purpose of this grant is to establish a Center for Computational Proteomics. The initial goals of this center are (i) to establish the infrastructure for the cutting edge computational tools we are developing which are capable of simultaneous measures of protein structure, function, and evolutionary information and (ii) to unify a core of researchers committed to utilizing this infrastructure towards answering important scientific questions related to human health and disease. Through the further development of these technologies, we hope to make large steps towards problems facing the health communities including rational drug design, drug delivery, and bioengineering. These tools will be available to the Penn State community at large and hopefully, in the future, to the entire scientific community.

Anticipated Duration of Project

8/9/2007 – 12/31/2010

Project Overview

The protein problem has remained unsolved despite decades of heroic efforts. In principle, one expects that protein sequence ought to determine structure, function, and evolutionary (SF&E) characteristics; while in reality, there still is no reliable method for predicting the native state structure of a protein or its function given only its primary amino acid sequence either experimentally or theoretically. In addition, evolutionary measurements are stymied when homologous proteins are highly divergent from one another. It is also well known that the number of putative protein sequences of any given length is enormous yet only a very few of these can be classified as proteins which fold rapidly and reproducibly and have useful function. Despite this fact, there seems to be an astonishing simplicity to the protein problem because the number of distinct native state folds is extremely limited.

In general, the protein problem occurs due to the inability of current algorithms to identify homology between highly divergent protein sequences with statistical confidence. Moreover, sequence alignment is generally unreliable for matching two sequences when the pairwise identity is less than a threshold figure of about 25%, and alignments with lower identity (i.e. in the “twilight zone”) are usually treated as random events. However, a small number of conserved residues (~8% identity) can coordinate the 3D fold and/or function of proteins, with large portions of these proteins comprising heteromorphic pairs (i.e. protein sequences that form different folds depending on their sequence environment). This is likely because the key amino acids responsible for coordinating the fold (“signal”) are preserved in evolutionarily related sequences, while less evolutionarily taxing amino acid substitutions (“noise”) result in dilution of the identity signal below the threshold required by search algorithms to detect homology between sequences.

The recent explosion in the availability of knowledge-bases and computational techniques for the analysis of complex data has created an unprecedented opportunity for teasing out invaluable information from protein sequences. Starting with a basic premise that protein sequence encodes

information about SF&E, we developed a unified framework for inferring SF&E from sequence information using a knowledge-based approach in which we measure the similarity between a query sequence and a set of biologically relevant profiles in an unbiased manner. Results from this Gestalt Domain Detection Algorithm-Basic Local Alignment Tool (GDDA-BLAST) provide phylogenetic profiles that have the capacity to model SF&E relationships of various proteins. We propose that sequence information present within the “twilight zone” of sequence similarity can provide key insight into SF&E relationships among distantly related and/or rapidly evolving proteins. We expect that the tools and resources generated from this project will be accessible and user-friendly to the bench scientist, thereby speeding the discovery process of other clinically-relevant research endeavors. This specific aims of this project are to evaluate and optimize the performance of GDDA-BLAST on the detection of structural, functional, and evolutionary homology.

Principal Investigator

Damian B. van Rossum, PhD
Penn State University
506 Wartik Lab
The Huck Institutes of the Life Sciences
University Park, PA 16802

Other Participating Researchers

Steve Benkovic, PhD, Mary Poss, PhD, Eddie Holmes, PhD, Jayanth Banavar, PhD, Hong Ma, PhD, Wendy Hanna-Rose, PhD, Aimin Liu, PhD, Randen Patterson, PhD, Michael Teng PhD, Biao He PhD, Reka Albert PhD and Song Tan, PhD, Kouacou Konan, PhD – employed by Penn State University

Expected Research Outcomes and Benefits

Just as physicists strive to develop a TOE (theory of everything) which explains and unifies the physical laws of the universe, the life-scientist wishes to uncover the TOE as it relates to cellular systems. This can only be achieved with a quantitative platform that can deduce and relate protein structure, functional, and evolution in a comparative fashion. Were this perfected, proper analyses would start to uncover the underlying physical laws governing the emergent behavior of biological systems. These ideas are far-reaching; however, progress is not possible without the attempt.

The long-term implication of this project is the development of a unified framework for *high-resolution and simultaneous measurements of structure, function, and evolution*. Should this be possible: (i) functional and evolutionary measurements could quantitatively inform structural modeling to derive accurate atomic resolution protein structures, (ii) structural and functional measurements could inform evolutionary histories to derive accurate evolutionary rates, deep-branch relationships, and homologous spaces within each protein, and (iii) structural and evolutionary measures would inform as to the location of functionalities contained within any protein and the regulatory elements which control these functions. Armed with this

information, speeds at which diseases could be understood and pharmacophores/therapies developed to combat them would likely increase dramatically.

It is our intent that the project presented here will help to pave the way for future work aimed at decoding the proteomes of disease causing organisms such as Influenza H1N1, *P. falciparum* (malaria), and antibiotic-resistant bacteria. We envision that in the future the GDDA-BLAST could be used to create proteomic libraries, which contain structural, functional, and evolutionary information. This innovation will likely provide unprecedented predictive power for a broad range of important questions such as those related to rational drug development, protein structure determination, cell biology, epidemiology, and bio-engineering.

Summary of Research Completed

In the last year we have made significant advances in completing the aims of the project. Since the last update, we have conducted extensive evolutionary analyses on simulated datasets and structural modeling analyses on benchmark datasets. These experiments have enabled us to better understand the underlying mechanisms of our algorithm thus optimizing and refining our approach. Indeed, we have actualized improvements in speed, sensitivity, and specificity. These upgrades make it possible for us to compete in the structural modeling competition CASP09, which is currently ongoing. With respect to the two experimental structures released so far, we are competitive with the top-5 algorithms from CASP08 and our models are highly similar. In addition, our evolutionary simulations demonstrate unprecedented resolution in relating highly divergent sequences. Taken together we feel confident in the efficacy of our approach and its utility in biomedical science.

Published Manuscripts supported by CURE project grant (06/2009-06/2010)

1. Hong Y, Kang J, Lee D, Patterson RL, van Rossum DB. Adaptive BLASTing through the Sequence Dataspace: Theories on Protein Sequence Embedding. Physics Archives. (2009) Quantitative Methods (q-bio.QM) [arXiv:0911.0650v1](https://arxiv.org/abs/0911.0650v1)
2. Ko KD, Hong Y, Bhardwaj G, Killick TM, van Rossum DB*, Patterson RL*. (*co-corresponding author). Brainstorming through the Sequence Universe: Theories on the Protein Problem. Physics Archives. (2009) Quantitative Methods (q-bio.QM) [arXiv:0911.0652v1](https://arxiv.org/abs/0911.0652v1)
3. Bhardwaj G, Wells CP, Albert R, van Rossum DB*, Patterson RL*. (*co-corresponding author). Mapping Complex Networks: Exploring Boolean Modeling of Signal Transduction Pathways. Physics Archives. (2009) Molecular Networks (q-bio.MN) [arXiv:0911.0656v1](https://arxiv.org/abs/0911.0656v1)
4. Kiselyov K, van Rossum DB, Patterson RL. TRPC Channels in Pheromone Sensing. 2010. Review (in Press). Text book

Phylogenetic Reconstruction (PHYRN)

Accurate measurement of protein evolution allows for deep inferences of structure/function relationships. However, reliable methods for measuring evolution in the “twilight zone” of sequence similarity are currently lacking. Our recent advance in measuring evolutionary relationships with phylogenetic profiles has allowed us to make advances in measuring

fundamental protein lineages that have evaded measurement due to either high divergence or rapid evolution.

This is exemplified by our performance on simulated phylogenetic trees. Since there is no protein family in the “twilight-zone” that has a known evolutionary history, we artificially generated protein sequences using the ROSE and SeqGen simulation packages to test the performance of our approach. In both sets of simulations, sequences are created from a common ancestor to produce a data set of known size, divergence, and history. In this *in silico* evolutionary process, an accurate phylogenetic history is recorded since the multiple sequence alignment is created simultaneously, and this allows us to test the reliability of PHYRN at different levels of sequence divergence. A key difference between SeqGen and ROSE is that the former does not include indels while generating these simulated protein families.

Figure 1 provides the results from PHYRN compared to the MSA program MUSCLE, using 67 sequences simulated for 17% identity by ROSE. On this data set MUSCLE recaptures only 72% of true evolutionary history and 53% of the deep nodes, (Figure 1b). Conversely, PHYRN recaptures 93% of the true evolutionary history and 94% of the deep nodes (Figure 1a). In a second simulation, we maintained a similar level of divergence while increasing the size of the simulated data set to 584 sequences. In this simulation, MUSCLE performance decreases significantly (no deep-nodes are correctly obtained), while PHYRN performance is still robust; PHYRN recaptures 76% of the true evolutionary history at the deepest 64 nodes.

We also generated multiple replicates ($n = 25$) of simulated protein families using SeqGen at 7 different ranges of divergence (40%-7% identity, Figure 1c). At lower levels of divergence, PHYRN marginally outperforms MUSCLE at recapitulating deep nodes; however, at higher divergences, PHYRN performs significantly better. Even at extreme divergence range of p-distance ~ 0.93 (7% identity, SeqGen scaling factor = 1), PHYRN recapitulates 51.7% of deep nodes correctly. In the same data sets, MUSCLE recovers only 24.3% of deep nodes correctly and Dialign fails to generate trees at all. Within 4 different ROSE data sets ($n=25$) including indels, PHYRN performs significantly better than MUSCLE at recapitulating deep nodes in divergent data sets (Figure 2d). For data sets generated using ROSE at an average distance of 600 PAM* (p-distance ~ 0.92 , 8% identity), PHYRN recapitulates 95% of deep nodes correctly, while MUSCLE is only able to recapitulate 33% of deep nodes. We could not test PHYRN’s performance at $<7\%$ identity and $<17\%$ similarity as both ROSE and SeqGen as these variables become saturated. We reason that the Gap Weight variable in our scoring scheme improves PHYRN’s performance within sequences containing indels. This works only to a point as at higher PAM scores, gaps become the predominant variable increasing divergence. Indeed, at severe gap rates (PAM950, 4.2 gaps per amino acid), our performance is significantly degraded as would be expected. Overall, the 325 total simulations assessed here provide confidence that PHYRN reliably measures branching orders in highly divergent or rapidly evolving sequences.

Functional Genomics

One of the major challenges in the genomic era is annotating function to the vast quantities of sequence information now available. We have been successful in identifying fundamental protein interactions (e.g. protein-nucleic acid, protein-lipid, protein-protein, protein-small molecule).

Indeed, we have been successful in our study of RNA-binding domains. RNAs in a cell generally have many functions such as (i) a carrier of genetic information, (ii) a catalyst of biochemical reactions, (iii) an adapter molecule in protein synthesis, and (iv) a regulator of RNA splicing and maintenance of the telomeres or chromosome ends. Often, changes in transcription and translation occur during oncogenic processes. If we are to identify all the functions of any specific RNA, we can then understand the functions of their binding proteins as they can control post-transcriptional processes such as pre-mRNA processing, splicing, and translation, and likely regulate RNA-enzymatic activity (e.g. dicer). Obviously, this type of information could be directly applied for the identification of therapeutic sites, as well as pharmacophore design.

However, since RNA structures are various, the structures of proteins to interact with the RNAs can be very diverse. Indeed, RNA binding proteins are currently classified into six families on the basis of their basic binding motifs; however, the proteins in the same family do not necessarily share common structures. This highlights the underlying difficulties in identifying RNA-binding domains. To overcome these hurdles, we employed phylogenetic profiles to derive a quantitative measure of RNA-binding.

We were pleasantly surprised with the results. Our method can also separate two functions which are notoriously difficult to discriminate due to their high structural homology (e.g. double-stranded RNA binding vs. double-stranded DNA binding domains). As shown in Table 1, our performance is quite promising. Further, SVM methods, Interproscan, nor other algorithms known to us can accurately classify these benchmark proteins accurately.

Structural Genomics

In the last year we have initiated multiple lines of research to identify structural homology using benchmark structural datasets such SABmark, Balibase, and SCOP. As shown in Figure 2, phylogenetic profiles are capable of identifying homologous folds in sequences containing less than 25% identity better than all known methods. We measured the performance of our method using only statistically significant alignments from rps-BLAST (e-value = 0.01, no coverage threshold). We observed a significant left-shifting of our results, with a maximum sensitivity of ~ 58% at a 0.01 false positive rate (Fig. 2a). Intriguingly, the alignments obtained from this filtering strategy still reside in the “twilight zone” (Fig. 2a inset). Moreover, when these results are averaged with those obtained at e-value = 10^{10} , we obtain ~70% sensitivity at a 0.05 false positive rate (Fig. 2a).

Figure 2b quantifies the independence between predictions of *structural sequence profiles*, FFAS03, and prof_sim for true-positives, false-positives, and false-negatives. The diagrams indicate that *structural sequence profiles* obtain more unique true positive pairs and false-negative pairs while predicting fewer false-positive pairs. The most dramatic increase occurs between true positives whereby *structural sequence profiles* obtain 4.20 fold increase over FFAS03 and a 6.41 fold increase over prof_sim. Surprisingly, when we made the same comparison between our own datasets at e-value 0.01 and 10^{10} , we also observe a significant number of unique true-positive pairs (Fig. 3d). This suggests that comparative measurements are likely to be useful for the identification of true-positive pairs. We have also started performing 3D modeling experimentation on ion-channels and transporters/exchangers. The initial results have been exciting. We have generated a model for the *C.elegans* TRP channel OSM-9 (Figure

3). This model is being vigorously evaluated biochemically by Dr. Liedke's group at Duke University.

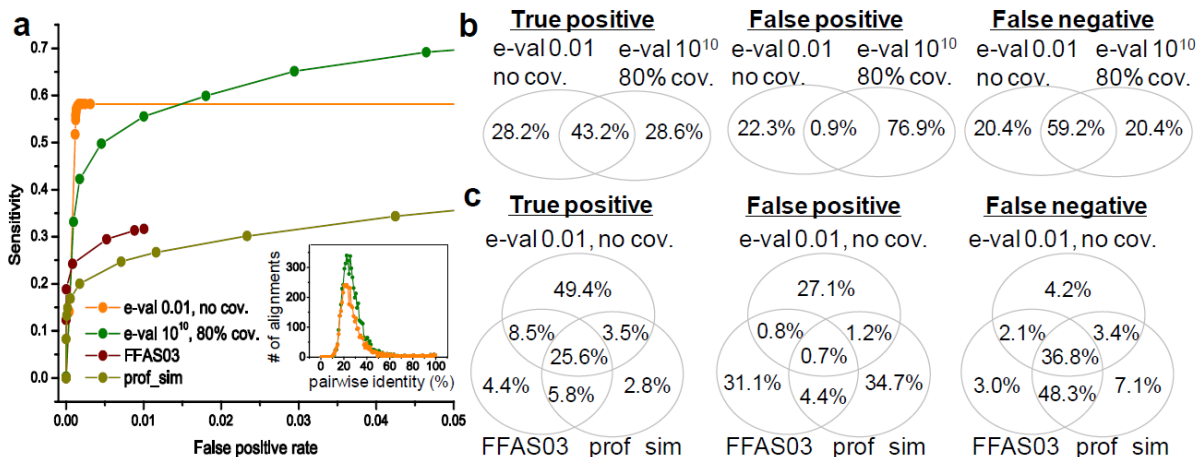


Figure 2. Fold Recognition Performance and Comparative Statistics. (a) Comparison of ROC curves of *structural sequence profiles* with two different settings, FFAS03 and prof_sim. Pairwise identities of the alignments between queries and the PSSMs from their true fold-specific library, which were collected with different e-value and coverage thresholds, are shown (*inset*). (b) Comparison of true-positive, false-positive, and false-negative pairs in top-9 result (sequences returned with the highest 9 structural similarity scores or the lowest 9 e-value/p-value for each of TZ-SABmark queries) of *structural sequence profiles* of e-value 0.01 and 10¹⁰. The numbers of true-positive, false-positive, and false-negative pairs predicted by *structural sequence profiles* of e-value 0.01 are 2645, 2161, and 4211, respectively. (c) Comparison of true-positive, false-positive and false-negative pairs in top-9 result of *structural sequence profiles* (e-value 0.01, no coverage), FFAS03, and prof_sim. The numbers of true-positive pairs predicted by *structural sequence profiles*, FFAS03, and prof_sim are 2666, 2030, and 1731, respectively. The numbers of false positive pairs are 613, 2776, 3075, while the numbers of true negative pairs are 4176, 4826, and 5125 (*structural sequence profiles*, FFAS03, and prof_sim respectively).

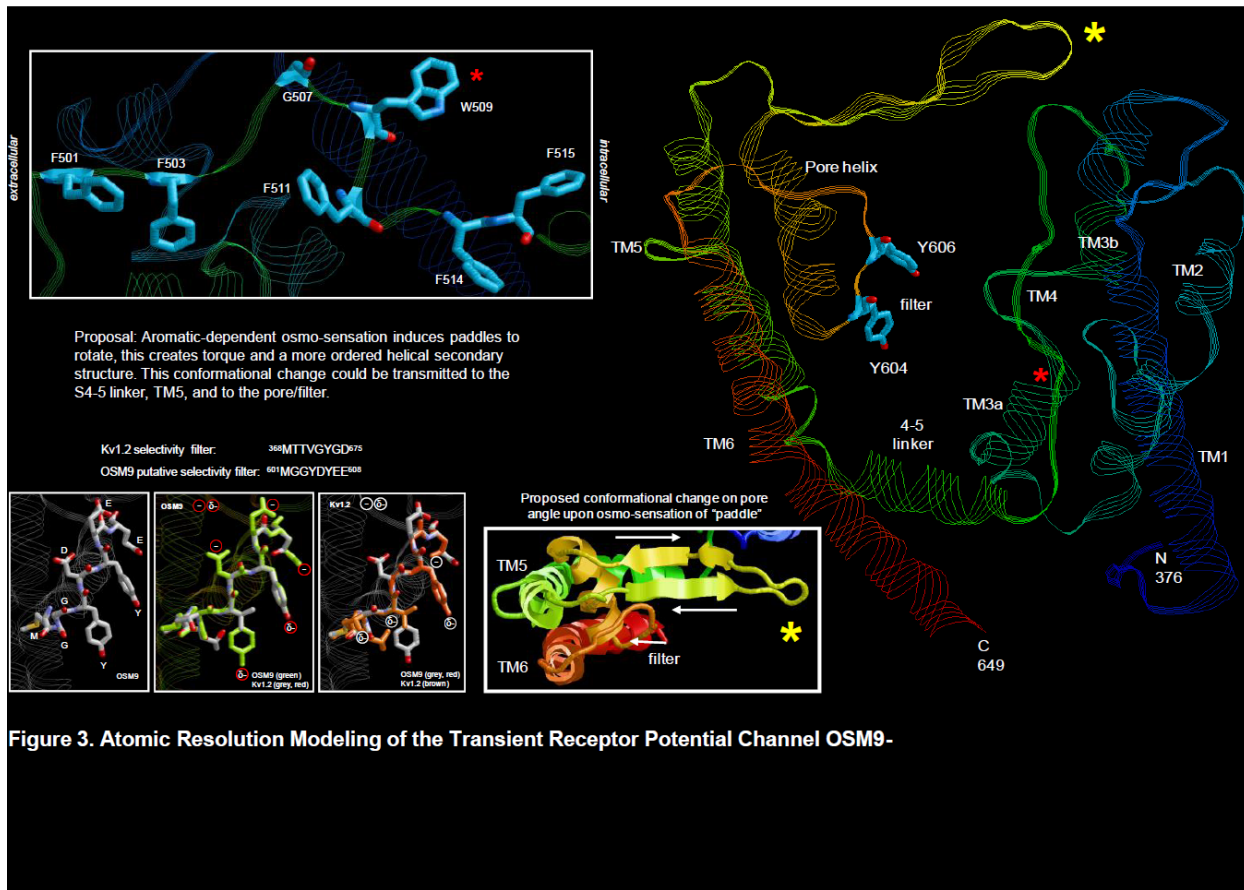


Figure 3. Atomic Resolution Modeling of the Transient Receptor Potential Channel OSM9-

Research Project 31: Project Title and Purpose

Structures of Protein in a DNA Replisome - The crystal structures of key proteins, the primase and the clamp loader protein will be sought. Although the structures of several individual protein components are known, structures for several key proteins are not available. Since it is highly improbable that the crystal structure of an intact replisome will be solved, the structures of individual proteins are required to construct and infer the structure of the replisome. Our understanding of the function of the replisome is incomplete without its structure. In addition, the tobacco funds will partially match a recently approved NIH-NCRR grant of \$500,000 for procuring a Rigaku Micromax 007 X-ray generator and Varimax optics, CCD detector and Xstream 2000 cooling system for the X-ray crystallography facility.

Duration of Project

8/9/2007 – 6/30/2009

Summary of Research Completed

This project ended during a prior state fiscal year. For additional information, please refer to the Commonwealth Universal Research Enhancement Annual C.U.R.E. Reports on the Department's Tobacco Settlement/Act 77 web page at <http://www.health.state.pa.us/cure>.

Research Project 32: Project Title and Purpose

Galaxy Workbench for Analysis of Biomedical Data: Application to Overlapping Coding Regions - Biomedical research is rapidly becoming extremely data intensive. High throughput experimental techniques are putting biology on par with the physical sciences in terms of raw data generating capacity. In this project we aim to capitalize on these developments. *First*, we propose to build on our success to date and develop novel algorithms for the two most rapidly evolving areas of biomedical research: (a) human variation analysis and (b) processing of data generated by next generation sequencing technology. *Next*, we will use the developed methodology for empirical and theoretical investigation of human genes with overlapping coding regions. This study will include *Ink4a* gene – a tumor suppressor locus implicated in ~50% of human cancers. Understanding the molecular dynamics of these genes will widen our understanding of human genome organization.

Anticipated Duration of Project

7/1/2008 – 12/31/2010

Project Overview

The broad objectives of this project are two-fold. The *First Aim* details a research project focused on development of novel computational algorithms enabling analysis of the latest types of biomedical data. This Aim also lays out the technological foundation for the research described in the second aim of this project – the use of the state-of-the-art experimental

techniques for investigation of the molecular dynamics of human genes with overlapping coding regions. The *Second Aim* will broaden our understanding of the human genome in general and provide new insight into function of loci implicated in key disorders such as cancer.

Aim 1. Maintaining Penn State's dominance as the National Leader in biomedical computation.

The translation from large volumes of experimental data to clinically relevant insights relies on sophisticated computational analysis algorithms that can handle the enormous high-throughput sequence, polymorphism, and functional datasets. We have developed a system – GALAXY – that makes substantial progress toward solving this problem and positions Penn State as the leader in the field of genomic data analysis. Specifically, it bridges a critically important gap between data resources, computational algorithms and users. Here we propose to develop novel features specifically designed for biomedical translational research. We will develop a statistical genetics toolkit allowing clinicians to manipulate and interpret human variation data on any scale. Next, we will implement novel algorithms for the analysis of next generation sequencing data. These tools will be used to process data from the ABI SOLiD sequencer that will be acquired jointly with this proposal and to conduct research within the framework of Aim 2.

Aim 2. Analysis of overlapping genes in human genomes. How “an average” gene is structured, expressed, and regulated is reasonably well understood. Yet, *nulla regula sine exceptione* – no rule without exception. This project deals with one of the most unexpected, controversial, and fascinating exceptions – the ability of eukaryotic genes to code multiple proteins via the use of overlapping coding regions. This phenomenon, previously attributed almost exclusively to viruses, finds an unexpected place in eukaryotes, where it may provide a unique means for tight coupling between gene regulation and protein expression. Here we will use a combination of computational and experimental methodologies (such as the next-generation sequencing) to understand the dynamics of change within overlapping genes and their potential link to human disease.

Principal Investigator

Anton Nekrutenko, PhD
505 Wartik Laboratory
Penn State University
University Park, PA 16802

Other Participating Researchers

Gregory Von Kuster, MA, Benjamin Dickins, PhD, Deb Grove, PhD – employed by the Pennsylvania State University
Ross Lazarus, MB, BS, MPH – employed by Harvard University, Cambridge, MA

Expected Research Outcomes and Benefits

Outcome 1

The sheer size of modern biomedical datasets (billions of data points) represents a substantial technical challenge for most potential users, who currently lack ready access to effective

methodologies that can scale to the size of these valuable translational resources. More importantly, the data must be secured to prevent unauthorized access by each recipient (e.g., human subject protection). A considerable amount of research needs to be performed to address these issues. One deliverable for this project is the development of new algorithms allowing experimental biologists and clinicians to gain a novel insight into genetic causes of human disorders. At present there are no integrated methods for quality control, filtering, aligning, and interpreting short read data generated by the next-generation sequencers. Here we propose to design such algorithms and to make them freely available to the community. Once this goal is achieved, a researcher will be able to manipulate, sequence, and base quality scores, survey and filter the data, align reads against appropriate databases, interpret these alignments, and visualize the results.

Outcome 2

A textbook human gene encodes a protein using a single reading frame. Alternative splicing brings some variation to that picture, but the notion of a single reading frame remains. Although this is true for most of our genes, there are exceptions. Like viral counterparts, some eukaryotic genes produce structurally unrelated proteins from overlapping reading frames. The examples are spectacular (G-protein alpha subunit [Gnas1] or INK4a tumor suppressor) and are implicated in a large number of human disorders. Because these genes are so unique, we currently do not understand the molecular details of their function. The proposed research will change this situation by documenting the fine scale process of molecular change within overlapping coding regions and applying gained knowledge to model proliferation trajectories of human disease-linked loci.

Summary of Research Completed

Handling NGS sequencing data at the Penn State Genomics Facility

During the reporting period we were able to build and deliver a comprehensive system for management of next generation sequencing data at the Penn State Genomics Facility.

SOLiD and 454 sequencing instruments. Functionality of the system is described in detail at this URL: <http://main.g2.bx.psu.edu/u/rc/p/sts>. Briefly, a user submits request for sequencing, which is received by the genomics facility. The facility approves the request and sends the user a set of barcoded tubes to be used for samples. The user places samples in the tubes and sends them back to the facility. The facility scans the tubes with Galaxy-aware barcode readers and initiates the run. Barcoding associates the samples with the user. Once the run is completed, sequences corresponding to the initial samples are automatically deposited into the user's data library as shown in Figure 1.

While the Penn State facility is our primary customer, the system we built is generic and is now being used at multiple core facilities throughout the United States. Thus the funds allowed us to build functionality that helps Penn State achieve its local needs and promote tools engineered at the University across the Nation. Below we briefly describe features that have been developed.

Instrument-specific plug-ins for data acquisition

We added to the Galaxy framework support for pluggable modules that communicate with different types of sequencing instruments operated at the Penn State Genomics facility (SOLiD and 454 sequencing instruments). Because of the wide variety of sequencing machines available now or in the future, and because the mechanisms for communicating with each machine are still evolving these plug-ins are engineered to be flexible enough to accommodate varied communication mechanisms. This flexibility is achieved with the same strategy that has been used for other interfaces between Galaxy and external systems (such as the interface to cluster management systems or to security information providers). Specifically we 1) designed a layered plug-in interface, which is simple to implement at a high level, but allows for deep customization if necessary, and 2) provided reusable components that can be used and extended in constructing instrument plug-ins. We built two generic communication interfaces. First, an instrument triggered protocol where the instrument can notify via a simple HTTP message that data is ready and where to fetch it. Second, a polling protocol where the instrument deposits data somewhere (e.g. a instrument-local or network-shared filesystem), and the Galaxy instance regularly checks for new data and processes it when available.

Depositing instrument generated datasets directly to Galaxy libraries

Data acquired from a sequencing instrument, along with metadata if provided by the instrument, is now deposited as one or more datasets in a Galaxy library (see Figure 1). By default, sequence data is deposited in a library specific to the user whose data is being sequenced. However a user is able to specify a different library either for all their sequencing or for specific samples. A critical aspect of automatic data acquisition was to automate as much as possible the mapping of samples and sequencing runs to Galaxy users, so that data can be automatically deposited in the correct library with the correct identifying information. We implemented two solutions to this problem. If the instrument is capable of providing metadata that identifies the user or sample, Galaxy is able to use this to automatically match data to users. On the other hand, if all that is available is an instrument specific identifier (which is the case at the Penn State facility), Galaxy provides a simple interface for associating these identifiers with users and sample metadata when the sequencing run is initiated.

Tools for analysis of NGS data

Tools for mapping of short reads and metagenomic analyses have been added to Galaxy's main public site at <http://usegalaxy.org>. These include tools for manipulation and quality control of sequencing reads produced by 454, Illumina, and SOLiD technologies. At the time of writing two short read mappers were accessible from the public site (Bowtie and BWA) with the third (lastz) being tested at the developer's site (<http://test.g2.bx.psu.edu>). In addition, we work on tools for post-processing of mapping results including SAM-tools (Figure 2) and our own in-house toolset for metagenomic applications.

As we expect that the demand for analysis of NGS datasets will grow exponentially in the near future we are working on making Galaxy framework "Cloud-aware". In particular we have 32- and 64-bit Machine Images for Amazon cloud environment (AMIs) that can be instantiated (provided the user has an active Amazon account) as described at this URL: <http://bitbucket.org/galaxy/galaxy-central/wiki/cloud>.

Estimation of sequencing accuracy with next-generation sequencing technologies

In addition to developing Galaxy we continue our project aimed at understanding the dynamics of overlapping coding regions. Specifically, we conducted a pilot study to confirm accuracy of sequence variants identified with the NGS technologies. Recent papers (including our own) have exploited this to analyze changing patterns of polymorphism in evolving populations of microorganisms. This application is very exciting, but accurate polymorphism estimation is difficult because we do not understand the nature and impact of sequencing errors. One rational approach, adopted in these studies, is to estimate errors for a given set of presumably polymorphic samples by sequencing DNA that is minimally processed or clonal from the same genome. But the illusion of predictability can prevail if experimenters attend to particular genomic sites after the fact or because estimation procedures, leveraging real data, make assumptions about error profiles. To address this we have formalized an empirical approach by Illumina sequencing a small plasmid genome and cross validating the results with dideoxy sequencing of multiple subclones. We were surprised to discover that some sites exhibited high levels of apparent polymorphism at prodigious coverage, but were invariant in subclones. We sought explanations for these rare events and, crucially, tested their tendency to recur by repeating the entire procedure. We believe our results and our approach have important implications for polymorphism detection, a major application of next-generation sequencing.

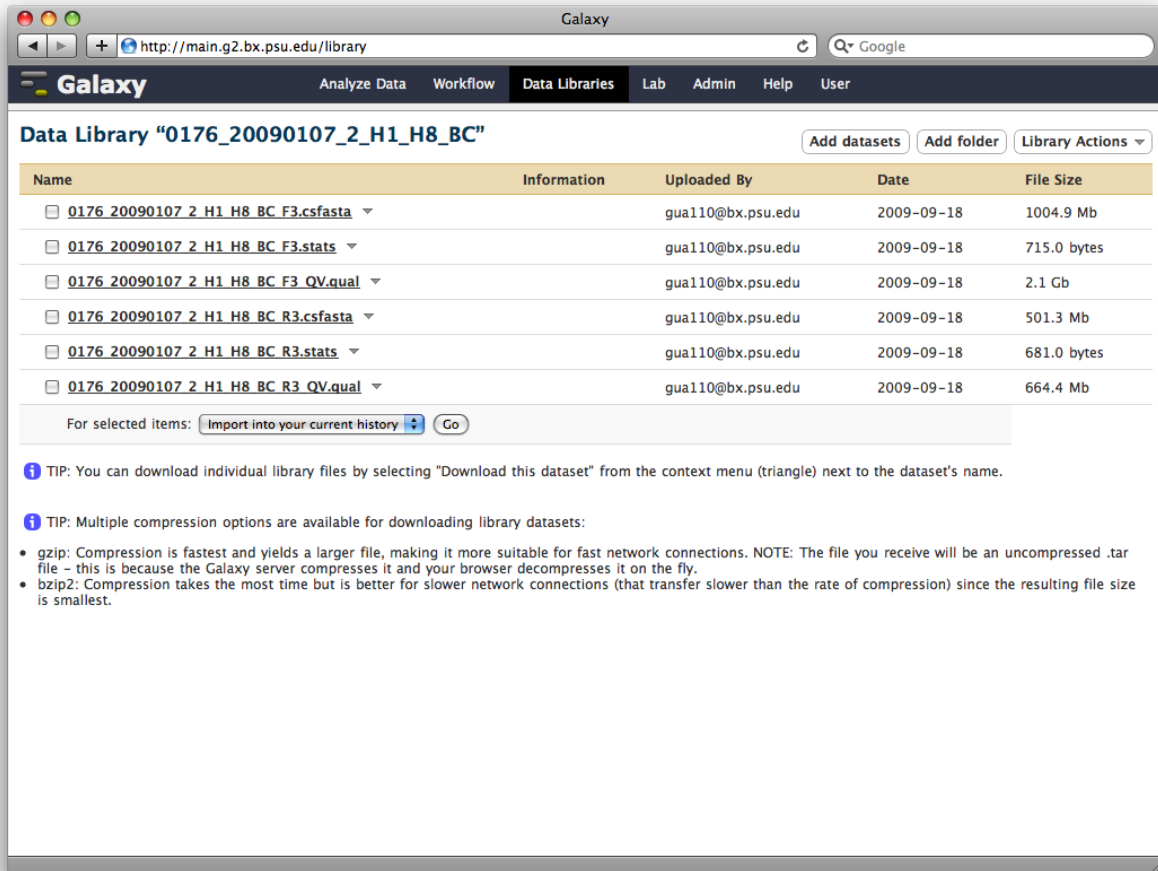


Figure 1. Result of SOLiD run deposited into Galaxy Data Library. From here users can download the data or analyze it using a variety of tool including those listed in Figure 2 below.

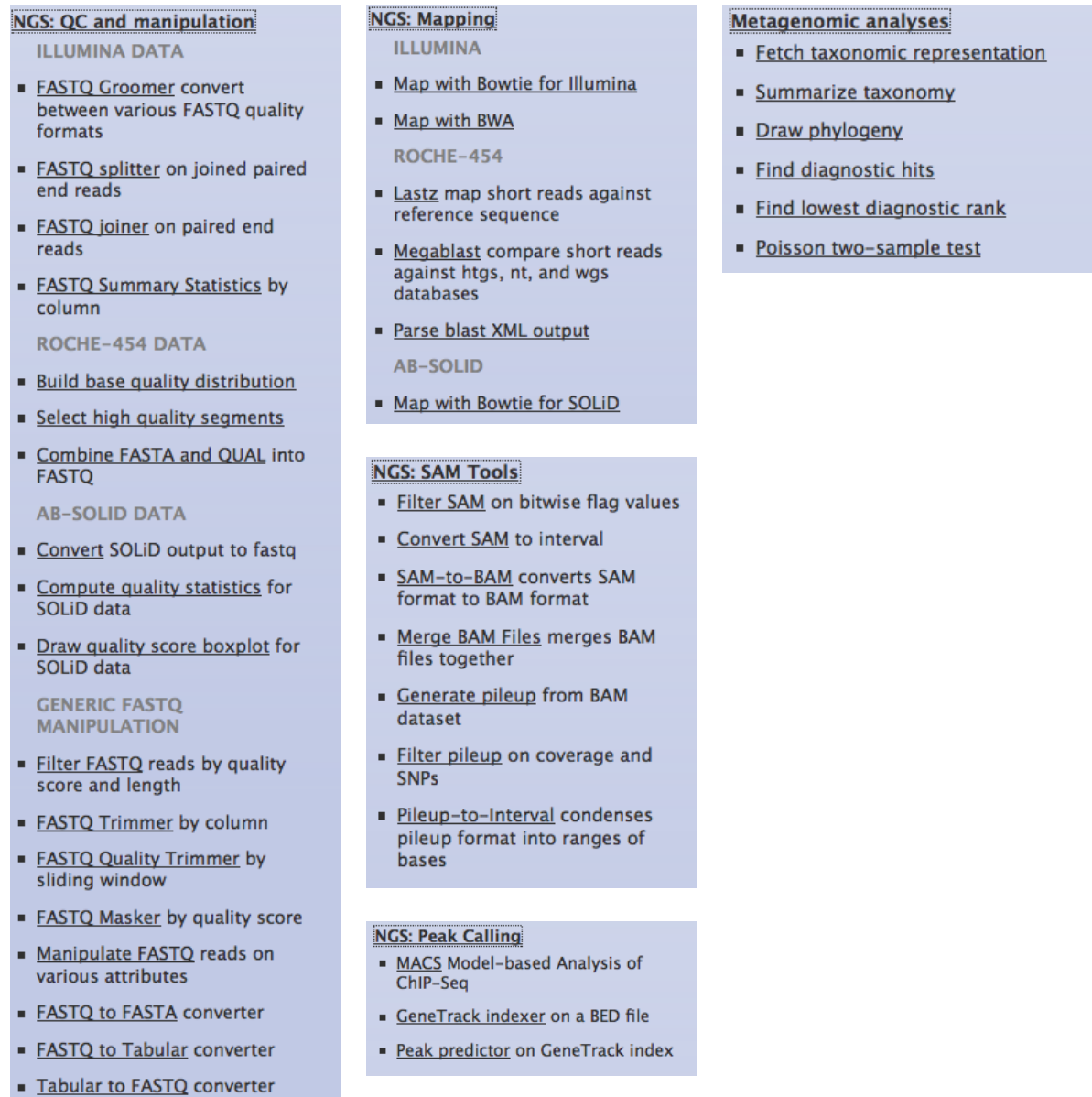


Figure 2. Categories of tools for the Analysis of Next-Generation Sequencing data available for Galaxy users at Penn State and across the World

Research Project 33: Project Title and Purpose

Using a Highmark-Medicare-Registry Merged File to Study Care, Outcomes, and Costs for Cancer - The overall purpose of this project is to demonstrate how we can use existing linked cancer insurance claims and cancer registry databases to develop much more powerful and specific research regarding cancer care. This will allow us to link patient information (stage at diagnosis, age, co-morbidities, gender, etc.) with treatment information (surgery, radiation, chemotherapy, hormones, etc.) for a large population that will include both insured people under 65 years old and cancer patients who are Medicare recipients 65 years old and over. Such a strategy will allow us to investigate the factors that contribute to better quality cancer care.

Anticipated Duration of Project

7/1/2008 – 12/31/2010

Project Overview

A data set linking Highmark insurance claims data with PA cancer registry data will be used to examine treatment patterns, outcomes, and costs for breast and colorectal cancers in Pennsylvania. We expect to include 50,000-100,000 patients with breast cancer or colon cancer insured by either Highmark commercial or the Medicare Advantage products in Pennsylvania in 1998-2006. The proposed method of looking at cancer data eventually can be applied to other cancer sites. There are two specific aims: (1) To develop an innovative and detailed method of linking cancer data from claims and registry data. Highmark has administrative claim data from both commercial and Medicare Advantage members. The new (combined) data set will be constructed by linking patient records from the Highmark claims data, their Medicare claims data, and the cancer registry data sets, to create an analytical file. It is important to note that this file will be stripped of all patient identifiers; and (2) To use this linked data set to study the relationship between various patient characteristics and treatment patterns for breast and colorectal cancer, the relationship between various treatment patterns for these cancers and costs and outcomes, the relationship between evidence-based research/recommendations from professional groups and actual practice patterns for these types of cancer, the effect of type of insurance on treatment patterns, and the effect of rural vs. urban patient locations on stage at diagnosis on treatment choices for these types of cancers.

Principal Investigator

Li Wang, PhD
Penn State University College of Medicine
Department of Public Health Sciences, A210
600 Centerview Drive
Hershey, PA 17033

Other Participating Researchers

Susan DesHarnais, PhD – employed by Thomas Jefferson University

Tareq (Fabian) Camacho, MS, MA – employed by the Pennsylvania State University

Patricia Gladowski, RN – employed by Highmark, Harrisburg, Pennsylvania

Expected Research Outcomes and Benefits

Because it is very expensive to gather detailed clinical data on the cancer care received by individual patients, it is important to develop innovative and valid methods to make use of existing claims and registry databases. Claims/registry databases can be used to discover relationships between various processes of cancer treatment, subsequent outcomes of care, and the costs of different treatment options. While clinical trials give us information about the effectiveness of specific treatments for a very limited population of cancer patients (only those who agree and qualify for specific clinical trials), we must depend on other data to learn about process/outcome correlations for the various types of cancer patients who are actually treated, rather than those who are typically studied in clinical trials. We will use a linked data set to examine treatment patterns, outcomes, and costs for breast and colorectal cancers over a five year time period. We expect to include approximately 125,000 breast cancer patients and 55,000 colon cancer patients insured by either Highmark commercial or the Medicare Advantage products in Pennsylvania. The proposed method of looking at cancer data eventually can be applied to other cancer sites. This project includes both cancer control and health services research components. First, it is relevant to cancer control research because it investigates how information can be efficiently and effectively applied at the community level. Second, the project is applicable to health services research in that it examines the interface of the health care system with patients, and aims to improve outcomes and quality of care.

Summary of Research Completed

Data linkage: The first linkage data had some problems, so Highmark and the PA cancer registry jointly conducted a 2nd linkage this year. The current data linkage was based on matching patient's name, date of birth, gender and last four digits of social security number using a probabilistic matching algorithm. The linked database referred to below and used in our analysis is based on the 2nd linkage. The linked database that Penn State received was de-identified.

Linked database: One goal of this study was to create the Highmark-cancer registry linked database as a valuable database potentially suitable for many cancer care studies. Compared to the widely used SEER-Medicare data by National Cancer Institute (NCI), our database contains predominantly younger patients (60.5% patients younger than 65 years) and predominately white patients (95.9%). This linked dataset contains a total of 33,673 cancer patients diagnosed in 1998-2006, with 21,881 breast cancer patients and 11,792 colon cancer patients. Of those patients, 21% were from rural areas. This database is one of the largest and most recent claims-registry linked databases, containing rich information on cancer diagnosis, patient characteristics, cancer treatment details, outcome measures and costs.

Studies using the linked dataset: Based on our team's research interests, we have focused on the following three studies.

Study 1: Treatment choice and costs of breast conserving surgery and mastectomy for regional stage breast cancer patients

Breast conserving surgery (BCS) and mastectomy are shown to have similar survival outcomes for early stage cancer. Little is known about what affects patients' treatment choice, and how costs differ between these two options. Using the linked dataset, we identified 1842 patients with first primary breast cancer at regional stage, who had breast surgery, and were enrolled in the Highmark insurance one month prior to diagnosis plus 6 continuous months after diagnosis. Of these patients, 949 had BCS and 893 had a mastectomy. The mean age for patients with BCS was 53.5 (std = 12.0) and was 53.3 (std = 13.0) for patients with a mastectomy. For patients living in rural areas, 49.0% had BCS while 52.3% of those in urban areas had BCS. 52.7% married patients got BCS and 48.9% single patients got BCS. In a multivariate analysis, no explored factors (marital status, race/ethnicity, membership in Medicare Advantage Program, Rural/Urban status, age, Charlson comorbidity index, or year of diagnosis) were found to be associated with higher likelihood of receiving BCS.

The cancer-related costs in the initial phase (one month prior to diagnosis plus 6 months after diagnosis) consisted of costs of claims with cancer ICD-9 codes ranging from 140.xx to 208.xx, and the costs were expressed in 2006 year dollar value using the medical care component of Consumer Price Index to adjust for inflation. The cancer-related costs were \$28,174 (std = \$18,545) for BCS and \$28,057 (std = \$20,773) for mastectomy.

Study 2: Obstacles to receiving radiation therapy after breast conserving surgery

It is recommended that patients who have BCS receive radiation to prevent recurrence and make the surgery more effective. However, in practice, many patients fail to receive radiation after BCS. In our database, 5034 patients were identified as having received BCS, but only 81% of those patients were given adjuvant radiation therapy and 90% received any radiation therapy. For patients with BCS younger than 65, 92.8% got radiation; and for patients aged 65 and above, 85.9% got radiation. Among patients living in rural areas, 90.4% got radiation. Among married patients, 92.2% got radiation; and among single patients, 87.4% got radiation. Using a multivariate logistic regression, marital status (single patients less likely than married to receive radiation, OR = 0.678, 95 % CI: 0.55-0.83) age category (65+ less likely than 45-64 to receive radiation, OR = 0.41, 95% CI: 0.30-0.56), Charlson comorbidity index (one unit increase of comorbidity index decreased the likelihood of radiation, OR = 0.89, 95% CI: 0.83-0.96), and membership in Medicare Advantage plan (non-Medicare Advantage patients less likely to receive radiation, OR = 0.68, 95% CI: 0.49-0.94) were statistically significant factors that affected the receipt of radiation. Race, rural location, and year of diagnosis were not significant.

Study 3: Hospital size and rectal surgery outcomes for rectal cancer

This study aims to explore the relationship between hospital size and rectal surgery outcomes. It is hypothesized that patients in larger hospitals where surgeons had higher surgery volume should have better outcomes for rectal cancer surgery after controlling for other variables. This study is still underway and no results are ready to be reported at this time.

Research Project 34: Project Title and Purpose

Structural Determinants of Closed State Inactivation of N-type Calcium Channels - The enhancement of inactivation is an excellent mechanism to reduce calcium channel activity that is utilized by a class of antihypertensives called dihydropyridines (e.g. Norvasc®). The recent FDA approval of Prialt® for the treatment of neuropathic pain demonstrated the utility of blocking N-type calcium channels as a treatment for this debilitating human disease. However, the poor side effect profile of Prialt has limited its usefulness. Drawing from lessons learned from dihydropyridines, we are investigating drugs that enhance inactivation of these pain-mediating calcium channels. To facilitate this effort, we will use ion channel mutagenesis to determine structures within the N-type calcium channel that regulate inactivation. These structures would then be targeted for drug development to obtain lead compounds for further testing as pain treatments.

Anticipated Duration of Project

7/1/2008 – 12/31/2010

Project Overview

N-type calcium channels are primarily expressed in neurons where they, along with other calcium channels called P/Q-channels, are involved in providing the Ca^{2+} that triggers neurotransmitter release. However, the N-channel appears to be primarily responsible for mediating neurotransmitter release from primary nociceptors (pain sensing neurons), and blocking these channels relieves neuropathic pain in both animal models and humans. Prialt® is currently the only N-channel blocking drug that is approved to treat neuropathic pain, but the poor pharmacokinetics result in an extremely poor side-effect profile. Thus, new N-channel targeted drugs are required. Ion channels have three functions (permeation, activation and inactivation) that are generally affected by clinically relevant drugs. Prialt is a permeation blocker, which contributes to its poor side-effect profile since it blocks all N-channels regardless of activity level. Drugs affecting activation suffer from the same problem, but enhancement of inactivation is a method to selectively block hyperactive channels. Injured nociceptive neurons have high action potential activity relative to uninjured neurons, which would make channels in these neurons highly susceptible to drugs that enhance inactivation. The goal of this project is to better understand N-channel structures that regulate inactivation. Such structures could then be the focus for the development of drugs that specifically enhance inactivation to block pain signaling in the nervous system. This will be accomplished by mutating specific structures that have been shown to play a role in sodium channel inactivation, but have yet to be tested for calcium channels. Specifically, we will investigate the role of the N-channel voltage sensors in regulating inactivation. The movement of the four voltage sensors regulates both activation and inactivation, but based on sodium channel work the impact of each sensor is not equal. By the end of this study we will learn which voltage sensors most strongly affect inactivation and will begin determining if drugs that specifically affect N-channel inactivation do so by targeting these structures. Through this work and future studies we will understand the mechanism by which voltage regulates inactivation and will identify drugs that can enhance this process.

Principal Investigator

Blaise Z. Peterson, PhD
Penn State College of Medicine
Department of Cellular and Molecular Physiology
Penn State College of Medicine
500 University Drive
Hershey, PA 17033

Other Participating Researchers

Keith S. Elmslie, PhD – employed by the Pennsylvania State University at time work was done.
Viktor Yarotsky, PhD – employed by the Pennsylvania State University at time work was done.

Expected Research Outcomes and Benefits

It has been estimated that 1/3 of all adults suffer from chronic pain, which reaches a sufficient level of suffering in some individuals to compel them to seek treatment. According to NIH, 50 million patients/year seek treatment for chronic pain, which has negative economic impact of ~\$100 billion in associated healthcare costs and lost productivity. Much of this economic impact results from poorly controlled pain that prevents patients from returning to a normal lifestyle. Advances in the treatment of chronic pain syndromes are desperately needed. A blocker of N-type calcium channels, Prial[®], was recently approved as a treatment for neuropathic pain illustrating that the N-channel is a crucial therapeutic target that is just beginning to be exploited. To further these efforts, we have undertaken a line of research to understand the channel structures involved in generating the unique N-channel gating properties. Through these experiments we will gain an understanding of how N-channel blockers affect gating and establish novel targets for the generation of drugs that reduce N-channel activity.

Summary of Research Completed

Previously, we demonstrated that roscovitine can affect voltage-dependent ion channels at clinically relevant concentrations (10–50 μ M). We found that (*R*)-roscovitine differentially affects voltage-dependent calcium channels. (*R*)-Roscovitine has two effects on Ca_v2 channels (N-type, P/Q-type, and R-type), which are a rapid onset agonist effect and a more slowly developing antagonist effect. We have demonstrated that the agonist effect results from (*R*)-roscovitine specifically binding to activated Ca_v2 channels to slow channel closing, which results in a significant enhancement of action potential induced calcium influx. The antagonist effect appears to result from (*R*)-roscovitine preferentially enhancing occupancy of a “resting” inactivated state to inhibit channel activity. Interestingly, the racemic variant (*S*)-roscovitine has been found to exhibit only an antagonist effect on N-channels, which is one result supporting unique binding sites for the agonist *versus* antagonist effects.

During this reporting period (7/1/2009-6/30/2010), we found that L-type channels are also inhibited by (*R*)-roscovitine. The inhibitory mechanism is unique relative to N-channels. L-channel inhibition results from slowed activation and enhanced open state voltage-dependent

inactivation (VDI), but the resting inactivated state is not affected. These two effects were characterized by approximately equal EC_{50} values ($\sim 30 \mu\text{M}$), which suggested a single binding site. However, the Hill coefficient for (*R*)-roscovitine-induced slowed activation was ~ 1 , whereas that for enhanced inactivation was >2 , which could result from multiple binding sites. Intracellularly applied (*R*)-roscovitine failed to affect L-channel activity, which supported an extracellularly exposed binding site(s) mediating both effects.

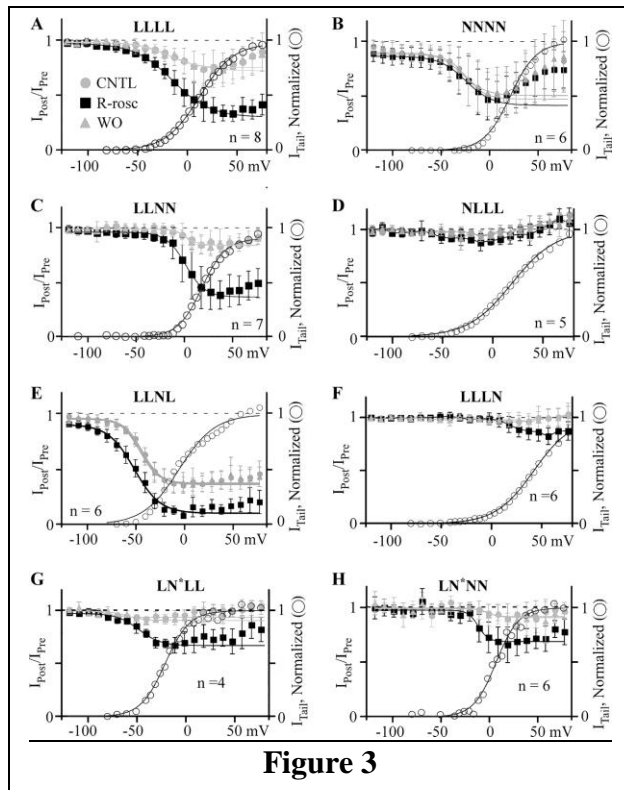
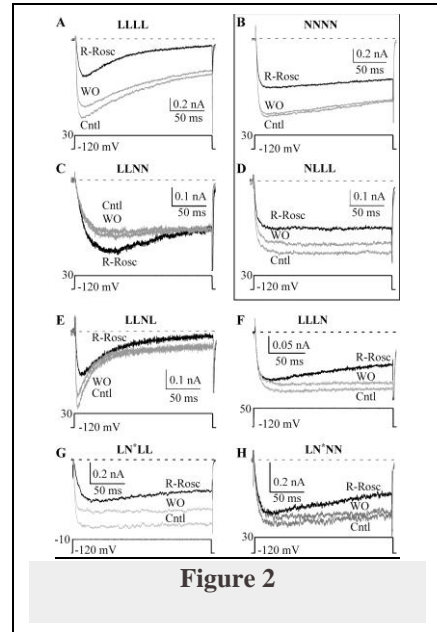
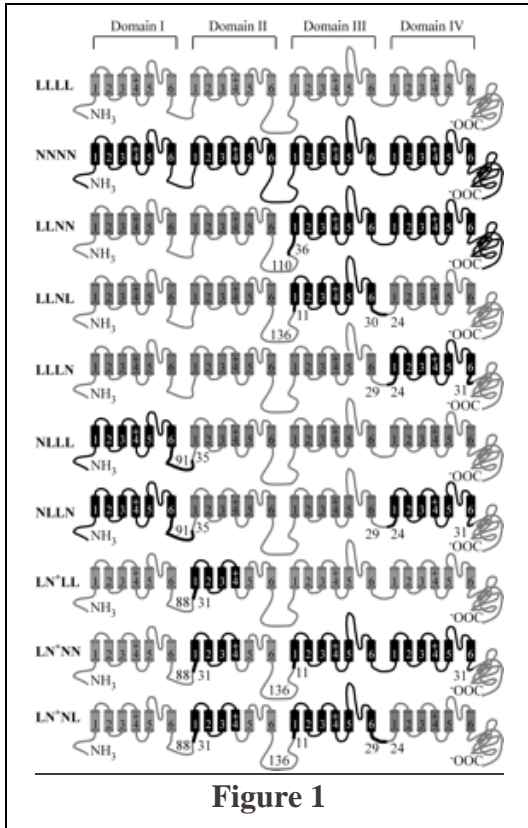
Chimeric calcium channel constructs. We have used a chimeric approach to investigate the differential effect of (*R*)-roscovitine on N-type *versus* L-type channels. This approach provides an opportunity to localize the L-channel binding site(s) and to better understand the mechanisms that underlie the modulation of L-type and N-type channels by roscovitine. In Figure 1, Domains I–IV are shown with each domain represented as a set of six transmembrane segments, 1–6. Loops between the segments and domains are shown as *lines*. N-channel structures are shown in *black*, whereas those from the L-channel are in *gray*. The *numbers* at the connections between N-type and L-type domains show the number of amino acid residues within that intracellular loop contributed by a given channel type. To highlight the connection, the N-channel section is shown as a *thicker line*. For LN*LL, LN*NN, and LN*NL chimeras, *N** refers to an engineered N-DII, which is composed of N-type transmembrane segments 1–4 and L-type transmembrane segments 5 and 6. The loop between segments 4 and 5 is from the L-channel.

(*R*)-roscovitine enhances inactivation of channels containing the L-channel domain I. In Figure 2, currents were evoked by 200-ms steps to the indicated voltage for LLLL (A), NNNN (B), LLNN (C), NLLL (D), LLNL (E), LLLN (F), LN*LL (G), and LN*NN (H) channels were used to evaluate the effect of $100 \mu\text{M}$ (*R*)-roscovitine (*black traces*). (*R*)-Roscovitine enhanced inactivation of WT L- (LLLL), LLNL, LLLN, LN*LL, and LN*NN channels but failed to alter inactivation of WT N- (NNNN) and NLLL channels. These results indicate that (*R*)-roscovitine does not enhance U-type inactivation of N-type calcium channels expressed in HEK293 cells and that N-L chimeric channels can be used to localize L-channel domain(s) transducing the roscovitine effects.

(*R*)-Roscovitine enhances VDI of channels containing L-DI. Inactivation was measured as the $I_{\text{Post}}/I_{\text{Pre}}$ ratio using the three-pulse protocol. Control (*CNTL*, *gray circles*), $100 \mu\text{M}$ (*R*)-roscovitine (*R-Rosc*, *black squares*), and washout (*WO*, *gray triangles*) data from -120 to peak inactivation were fitted using a single Boltzmann equation (*smooth lines*) to yield $V_{1/2}$ and slope. The activation-voltage relationship in control (*right axis*, *open circles*) is superimposed here for comparison with the voltage dependence of inactivation. (*R*)-Roscovitine enhanced VDI of LLLL (A), LLNN (C), LLNL (E), LLLN (F), LN*LL (G), and LN*NN (H) channels but did not affect NNNN (B) and NLLL (D) channels. For LLLL channels (A), the Boltzmann parameters for inactivation were $V_{1/2} = -19.6, -15.3, \text{ and } -16.4$; slope = $-13.6, -19.1, \text{ and } -18.7$; maximum inactivation = $0.23, 0.67, \text{ and } 0.27$ for control, (*R*)-roscovitine, and washout, respectively, whereas those parameters for activation were $V_{1/2} = 15.0$ and slope = 15.6 . For NNNN channels (B), the Boltzmann parameters for inactivation were $V_{1/2} = -24.1, -24.7, \text{ and } -28.6$; slope = $-13.9, -14.5, \text{ and } -15.6$; maximum inactivation = $0.48, 0.47, \text{ and } 0.45$ for control, (*R*)-roscovitine, and washout, respectively, whereas those for activation were $V_{1/2} = 21.0$ and slope = 12.6 . For LLNN channels (C), the Boltzmann parameters for inactivation were $V_{1/2} = 1.4, 0.8, \text{ and } 0.6 \text{ mV}$; slope = $-6.8, -10.0, \text{ and } -5.0$; maximum inactivation = $0.15, 0.6, \text{ and } 0.15$ for

control, (*R*)-roscovitine, and washout, respectively, whereas those parameters for activation were $V_{1/2} = -17.7$ mV and slope = 9.6. It was not possible to accurately describe the inactivation data from the NLLL chimera (*D*) using the Boltzmann equation, but for activation, the Boltzmann parameters were $V_{1/2} = 18.7$ and slope = 21.7. For LLNL channels (*E*), the Boltzmann parameters for inactivation were $V_{1/2} = -43.5, -51.8,$ and -45.8 mV; slope = $-9.8, -13.3,$ and -9.5 ; maximum inactivation = 0.6, 0.81, and 0.58 for control, (*R*)-roscovitine, and washout, respectively, whereas those for activation were $V_{1/2} = -9.2$ mV and slope = 18.1. For LLLN channels (*F*), inactivation in control was too small to allow for Boltzmann fitting. However, the Boltzmann parameters for activation were $V_{1/2} = 41.7$ mV and slope = 19. For LN*LL channels (*G*), the Boltzmann parameters for inactivation were $V_{1/2} = -79.1, -48.5,$ and -60.8 mV; slope = $-9.1, -11.2,$ and -9.0 ; maximum inactivation = 0.07, 0.30, and 0.09 for control, (*R*)-roscovitine, and washout, respectively, whereas those parameters for activation were $V_{1/2} = -21.7$ mV and slope = 12.5. For LN*NN channels (*H*), the Boltzmann parameters for inactivation were $V_{1/2} = -2.4, -12.1,$ and -2.5 mV; slope = $-4.9, -5.2,$ and -7.1 ; maximum inactivation = 0.07, 0.29, and 0.09 for control, (*R*)-roscovitine, and washout, respectively, whereas those parameters for activation were $V_{1/2} = 6.5$ mV and slope = 11.6.

These results demonstrate that the (*R*)-roscovitine-induced effects on N-type and L-type channels are unique. We utilized N-L chimeras to determine the domains containing the roscovitine binding sites. The chimeras were generated by “domain swapping” in an attempt to localize the binding sites using relatively few manipulations, and the technique was successful. The LLNN chimera demonstrates that RR_{EI} is localized to L-DI and/or L-DII. The strong (*R*)-roscovitine-induced slowed activation of the LLNL chimera along with the loss of that effect with the LLLN chimera supported L-DIV for RR_{SA} . The RR_{SA} site appears to span two L-channel domains; we conclude that RR_{EI} is contained within L-DI. (*R*)-Roscovitine-enhanced VDI was observed in all chimeric channels containing L-DI, including LLNN, LLNL, LLLN, and LN*LL. The two critical tests of the L-DI hypothesis were the absence of enhanced inactivation of the NLLL chimera and the transfer of (*R*)-roscovitine-enhanced VDI to the N-channel by inserting L-DI to generate the LN*NN chimera. The dose-response for (*R*)-roscovitine-induced enhanced VDI was almost identical between LN*NN and WT L-channels, which strongly suggests that RR_{EI} is transferred to the N-channel by the insertion of L-DI. Thus, our results are consistent with the localization of RR_{EI} to L-DI and support the hypothesis that the two (*R*)-roscovitine-induced effects are mediated by physically distinct structures.



Research Project 35: Project Title and Purpose

The Exaggerated Exercise Pressor Reflex in Rats with Heart Failure - The project will attempt to determine the role played by mechanoreceptors and metaboreceptors in evoking the exaggerated sympathoexcitation seen both at rest and during exercise in patients with heart failure. These sympathoexcitatory responses are important because they affect blood flow in peripheral circulation resulting in altered (poor) muscle perfusion. In addition, these responses may be in part responsible for the exercise intolerance associated with heart failure. Resolving the exact mechanisms of exaggerated sympathoexcitation is imperative in developing adequate treatments to improve physiological changes and the general quality of life for heart failure patients.

Duration of Project

7/1/2008 – 6/30/2009

Summary of Research Completed

This project ended during a prior state fiscal year. For additional information, please refer to the Commonwealth Universal Research Enhancement Annual C.U.R.E. Reports on the Department's Tobacco Settlement/Act 77 web page at <http://www.health.state.pa.us/cure>.

Research Project 36: Project Title and Purpose

Epigenetic Chromatin Factors Involved in Cardiomyocyte Hypertrophy - The purpose of this project is to understand the role of epigenetic heterochromatin factors in cardiac hypertrophy, a heart muscle disorder leading to heart failure and increased mortality. Several epigenetic heterochromatin factors: histone methyltransferase Suv39H1, histone H3(K9) methylation, and histone H2A.Z have been previously shown to control muscle cell differentiation and/or cardiac hypertrophy. Here we propose to examine chromatin organization in primary control and hypertrophic rat cardiomyocytes in parallel with cardiac myoblast cell culture and thus test the validity of primary cardiomyocytes and cultured cardiac H9C2 myoblast cell line as models for heterochromatin transitions. We also plan to conduct proteomic experiments with chromatin isolated from hypertrophic cardiomyocytes to reveal hypertrophy-associated changes of yet unknown epigenetic chromatin factors.

Duration of Project

7/1/2008 – 6/30/2010

Project Overview

The broad objective of this project is to understand the role of chromatin structure transitions and chromatin epigenetic factors in cardiac hypertrophy, a condition associated with increased risk of heart failure and mortality. At present, nothing is known about whether or not chromatin structure and epigenetic state of heterochromatin are changed or impaired in the process of

cardiomyocyte hypertrophy, but several key chromatin proteins that are known to change chromatin structure: histone H2A.Z, histone deacetylases, and HMGA1 have been shown to be associated with cardiomyocyte hypertrophy. Our laboratory has extensively studied epigenetic chromatin transitions during terminal differentiation and we will now focus our research on heterochromatin in hypertrophic muscle cells. In this project we will pursue two specific aims:

Specific aim 1: Chromatin transitions in hypertrophic cultured and primary cardiomyocytes. In these experiments we will examine chromatin structure and the expression of key heterochromatin epigenetic factors in hypertrophic cultured rat cardiac myocytes from the H9C2 cell line and primary rat cardiac myocytes. Myocyte hypertrophy will be induced by commercial reagent angiotensin II (Sigma) using already existing experimental protocols for H9C2 cells and primary cardiomyocytes. Heterochromatin morphology, expression, and localization of key chromatin epigenetic factors in control and hypertrophic cells will be analyzed by immunofluorescence and western blotting as we previously did with several differentiated cell systems.

Specific aim 2: Proteomic analysis of nuclear proteins associated with cardiomyocyte hypertrophy. To identify other heterochromatin proteins that participate in myocyte hypertrophy, we will conduct proteomic analysis of chromatin protein from control and hypertrophic cells using iTRAQ, a multiplexed mass-spectroscopic analysis of proteins labeled by “8plex” isobaric peptide tags provided by Applied Biosystems (see www.appliedbiosystems.com). Peptides isolated from control and hypertrophic H9C2 cells and control and hypertrophic primary cardiomyocytes each will be labeled with one of eight available tags. After labeling, the peptides will be mixed and simultaneously analyzed by MS/MS spectrometry. Proteins showing significant changes (over two fold) will be validated with Western blotting or 2D electrophoresis if antibodies for this protein are not available. The Penn State COM core facility successfully uses the iTRAQ technique in many applications and provides detailed protocols.

Principal Investigator

Sergei A. Grigoryev, PhD
Penn State University
College of Medicine
Department of Biochemistry and Molecular Biology H171
500 University Drive
Hershey, PA 17033

Other Participating Researchers

Michael Gomberg, BS – employed by the Pennsylvania State University

Expected Research Outcomes and Benefits

Heart muscle cells (cardiomyocytes) cannot proliferate but can grow in response to mechanical stress, hypertension, or special cell growth-stimulating signals in a process called cardiomyocyte hypertrophy. Extensive cardiomyocyte hypertrophy is associated with increased risk of heart

failure and mortality. Heterochromatin, a complex of condensed and repressed genetic material with a special set of modified histones, is a dynamic structure that spreads from pericentromeric chromosomal loci in the processes of cell differentiation and senescence to inhibit genes required for cell proliferation. Heterochromatin factors may also repress genes necessary for tissue-specific differentiation pathways and cause epigenetic changes leading to tissue developmental disorders. Several heterochromatin regulating architectural factors such as H2A.Z, HMGA1, and histone deacetylases are directly involved in cardiac myocyte hypertrophy, thus illuminating the biomedical importance of heterochromatin regulation for myocardial development and the events leading to heart failure. An expected research outcome is that our studies should reveal which chromatin factor(s) are associated with heterochromatin structural transitions in myocyte cell cultures and primary cardiomyocytes so that heterochromatin regulation in heart tissue could be subsequently studied using *in vivo* model systems. Since some of the heterochromatin-regulating epigenetic factors, in particular histone deacetylases, are targeted by cell-penetrating drugs approved for treatment of other diseases, understanding their role in heterochromatin transitions in cardiomyocyte hypertrophy may lead either to the development of new chromatin-targeting therapeutics promoting normal myocardial development or a better understanding of the adverse effect(s) of these drugs on the cardiovascular system.

Summary of Research Completed

Extended work period and animal research protocol: One year no-cost extension of the projected work period (initially planned to be finished on June 30, 2009) was granted. Animal research protocol for cardiomyocyte isolation (2008-062) was extended by IACUC through July 2010.

Work on Specific aim 1: “chromatin transitions in hypertrophic cultured and primary cardiomyocytes.” In the previous year, we analyzed chromatin structure and heterochromatin factors in rat cardiac myoblast cell line H9C2 where hypertrophy was induced by incubating with 100 nM angiotensin II (AgtII). In these experiments, imaging of heterochromatin morphology and chromatin epigenetic factors did not detect any significant changes in heterochromatin markers between normal and hypertrophic cells. To examine, if the observed changes were not observed because of insufficiency of AgtII to induce hypertrophic changes sufficient enough to induce strong chromatin changes, we conducted experiments with two alternative hypertrophy inducers, Endothelin-1 (ET-1) and Phenylephrine (PE) that have been shown before to be more efficient hypertrophy inducer than AgtII (Majumdar et al. Mol Cell Biochem (2008) 312:47–60).

Nuclear protein samples were obtained from cells incubated with and without fetal bovine serum and with 100 nM AgtII, 50 mM PE, and 10 nM ET-1. These protein samples were analyzed by polyacrylamide gel SDS-electrophoresis and Western blotting with antibodies against the key heterochromatin factor H3K9me2 using ECL West Pico detection system (Pierce). Consistent with our previous analysis, Western blotting showed no significant alterations of H3K9me2 in AgtII-treated samples, but a notable increase in PE-treated cells (Fig. 1, lanes 9, 10). With ET-1, like with AgtII we did not observe any significant changes (Fig. 1, lanes 11-13). We concluded that PE-induced hypertrophy was associated with most prominent changes in heterochromatin.

We therefore asked if PE was also capable of inducing stronger hypertrophic phenotype. To access the hypertrophic state we grew the cells in the absence of serum (control) and with angiotensin II and PE. We then stained the cells with TRITC-conjugated fluorescent Phalloidin and Hoechst 33258, imaged the cells under fluorescent microscope (Fig. 2 A-C) and measured the areas of each cell in the image using Nikon NIS-elements software. The results of the measurement show a significant larger increase of cell area in PE-treated cells than in AgtII-treated cells (Fig. 2 D). We tested cells grown in the presence of 50, 100, and 200 mM PE. We concluded that at 50-100 mM, PE was the strongest hypertrophy inducer in our system and thus the strong increase in H3K9me2 could be attributed to this stronger cardiomyocyte hypertrophy induced by PE.

Being encouraged by the stronger hypertrophy induced by PE, we conducted a comparative fluorescence imaging of heterochromatin morphology and chromatin epigenetic factors in control, AgtII-treated and PE-treated H9C2 cells detected with antibodies against the key heterochromatin markers, histone H3 dimethylated (H3K9me2) and trimethylated (H3K9me3) at Lysine 9. However, immunofluorescence analysis did not detect any significant changes in heterochromatin morphology or distribution of these two markers between normal and hypertrophic cells (Fig. 3).

In the next set of experiments, we conducted immunofluorescence of control and hypertrophic cells with antibodies against a number of candidate architectural proteins proposed known to induce large-scale heterochromatin transitions associated with myogenic differentiation and cardiac hypertrophy: MeCP2, DNMT1, and SirT1. Immunofluorescence analysis (Fig. 3) did not detect any significant changes in heterochromatin markers between normal and hypertrophic cells. Thus, our studies confirmed previously our reported conclusion that the observed changes in nuclear chromatin organization resulting from cardiomyocyte hypertrophy are not likely to result from heterochromatin structures associated with the architectural chromatin proteins. The altered shape of the nuclei suggests that such changes are more likely to result from some alterations in the nuclear envelope.

Finally, we analyzed heterochromatin in primary cardiomyocytes with hypertrophy induced by ET-1 and PE (experiments with AgtII were conducted in the previous year). Primary cardiomyocytes were isolated and cultured from hearts of 1-day old Sprague-Dawley rat pups and cultured in DMEM supplemented with 10% FBS. After 24 hours, in some samples DMEM-fetal bovine serum was exchanged for DMEM without serum and hypertrophy was induced by incubating with ET-1 or PE. Immunofluorescence imaging was conducted with antibodies against H2A.Z, HMGA1, and H4K12ac. As with myoblasts treated with AgtII, there was no significant change in these heterochromatin markers between normal and ET-1 or PE-treated hypertrophic cells (Fig. 4).

Work on specific aim 2: Proteomic analysis of nuclear proteins associated with cardiomyocyte hypertrophy. To identify other heterochromatin proteins that might participate in myocyte hypertrophy, we conducted proteomic analysis of chromatin protein from control and hypertrophic cells using iTRAQ, a multiplexed mass-spectroscopic analysis of proteins labeled by “8plex” isobaric peptide tags provided by Applied Biosystems (see www.appliedbiosystems.com). Nuclei were isolated from the following cell samples - 1-3:

primary cardiomyocytes from hearts of 1-day old Sprague-Dawley rat pups cultured in DMEM supplemented with 10% FBS (1). After 24 hours, DMEM-fetal bovine serum was exchanged for DMEM without serum and incubated for 48 hr either without (2) or with 100 mM PE (3) to induce hypertrophy. 4-8: H9C2 cells were cultured in DMEM with 10% FBS (4). After 24 hours, DMEM-fetal bovine serum was exchanged for DMEM without serum and incubated for 48 hr either without (5, 7) or with 100 mM PE (6, 8) to induce hypertrophy.

The isolated nuclei were extracted 2M NaCl to elute histones and maximum of nonhistone nuclear proteins and the residual DNA was separated by ultracentrifugation. 100 mg of protein from each sample were completely digested with Trypsin. Peptides isolated from control and hypertrophic primary cardiomyocytes and control and hypertrophic H9C2 cells each were labeled with one of eight available tags in the following order: 1 – 113; 2 – 114; 3 – 115; 4 – 116; 5 – 117; 6 – 118; 7 – 119; and 8 – 121. After labeling, the peptides were mixed and simultaneously analyzed by MS/MS spectrometry at the Penn State COM Macromolecular Core Facility using Biosystems 4800 Proteomics Analyzer (MALDI TOF-TOF).

In total, peptides from 1674 different proteins were identified by homology with the rat genome and the data was analyzed using Protein Pilot (Proteus LIMS) software. Chromatin proteins were identified by their accession number and function assigned by the NCBI databank. Figs. 5 and 6 show a list of chromatin-associated proteins with at least 1 peptide identified at > 95% confidence. For H9C9 cells we did not find a single chromatin-associated protein with expression level changed more than 2-fold (Fig. 5). For primary cardiomyocytes, we found several proteins whose expression level was <2-fold lower in hypertrophic cells than in control cells (highlighted by red color on Fig. 6). The most prominent changes involved core histones H3.1, germinal histone H4, and nuclear lamina-binding protein L2BP1. None of the detected differences involved known epigenetic factors or architectural components of heterochromatin. Thus the results of the proteomic study are consistent with no significant changes in epigenetic heterochromatin factors associated with nuclear hypertrophy. However, the proteomic data point to some changes in core histone composition indicating that the down regulated histones could be replaced by histone variants specific for non-dividing cells.

Conclusions: Based on our previous findings, we hypothesized that in hypertrophic cells, the heterochromatin organization is substantially changed and, specifically, the tertiary chromatin structure is inhibited due to de-regulation or mislocalization of a number of candidate heterochromatin factors. In the experiments that we have completed in the last year, we confirmed our previous finding that there no significant changes in any architectural heterochromatin factor or the internal organization of nuclear heterochromatin during cardiomyocyte hypertrophy. The observed global chromatin changes associated with cardiomyocyte hypertrophy are more likely to reflect changes resulting from an altered histone composition and/or chromatin-lamina interactions than in chromatin higher-order (tertiary) structure. This finding is further supported by our proteomic study that resulted in identifying changes in expression levels of a number of core histones and nuclear envelope components – lamin A and L2BP1 but not heterochromatin-regulating proteins. Thus, our study indicates that nuclear envelope and not the internal heterochromatin organization plays an important role in reorganization of nuclear chromatin during cardiomyocyte hypertrophy.

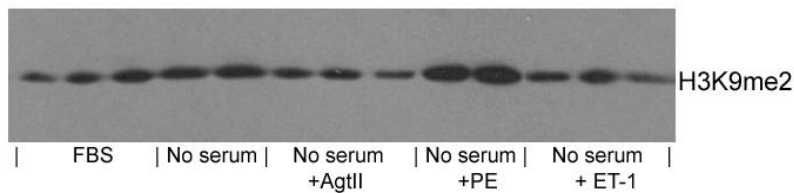


Fig. 1. Western blotting of heterochromatin marker H3K9me2 in hypertrophic and control H9C2 myoblasts. Protein samples from the nuclei of H9C2 cells either proliferating in the presence of fetal bovine serum or induced to hypertrophy by serum withdrawal and treatment with angiotensin II, PE, and ET-1 as indicated were separated by SDS-PAGE and transferred to a nylon membrane. Western blots were probed with antibodies against histone H3 dimethylated at lysine 9 (H3K9me2).

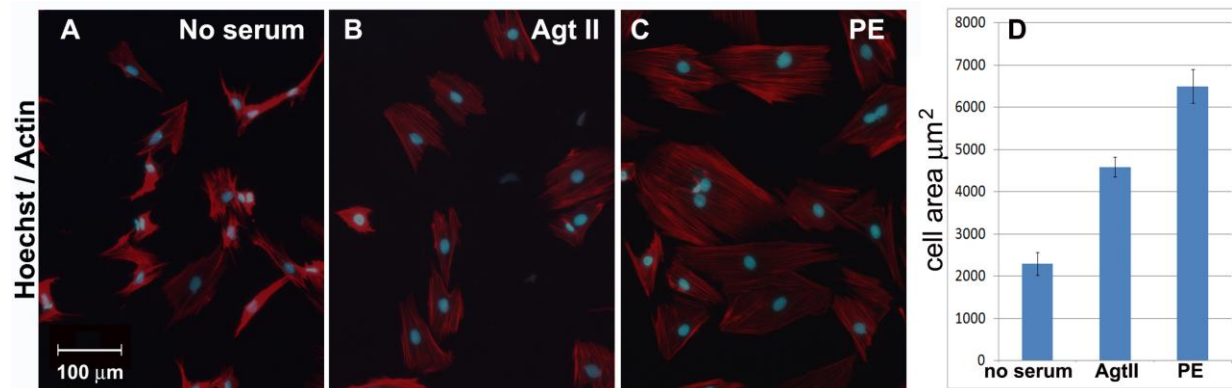


Fig. 2. Cell morphology and surface area in control and hypertrophic H9C2 cells.

Rat cardiac myoblasts H9C2 were incubated in DMEM without serum (A) and additionally treated with AgtII (B) and PE (D) to induce hypertrophy. Cells were grown on microscopy cover glasses, fixed with 2.7 % paraformaldehyde, stained with Hoechst 33258 fluorescence for nuclear DNA (blue) and Phalloidin-TRITC for cytoplasmic actin (red), and imaged by fluorescence microscopy. D: Surface areas were determined by the image scanning using Nikon NIS elements software.

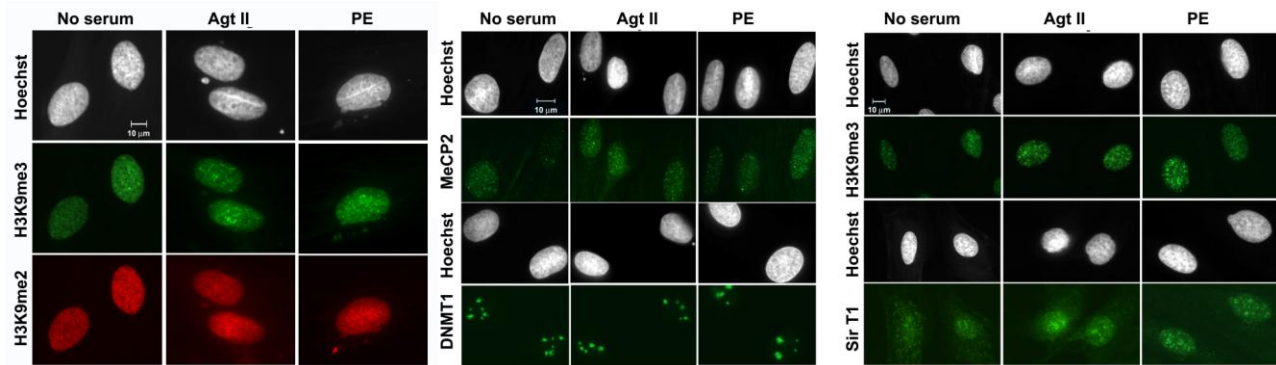


Fig. 3 Immunofluorescence analysis of histone H3K9 methylation in H9C2 cells.

Rat cardiac myoblasts H9C2 were incubated in DMEM without serum and additionally treated with AgtII and PE to induce hypertrophy as indicated on top of each vertical row. Cells were grown on microscopy cover glasses, fixed with 2.7 % paraformaldehyde, stained with Hoechst 33258 fluorescence, and immunostained with antibodies against histone H3 trimethylated at lysine 9 (H3K9me3), histone H3 dimethylated at lysine 9 (H3K9me2), MeCP2, DNMT1, and SirT1 as indicated at the left of each horizontal row and visualized by fluorescence microscopy.

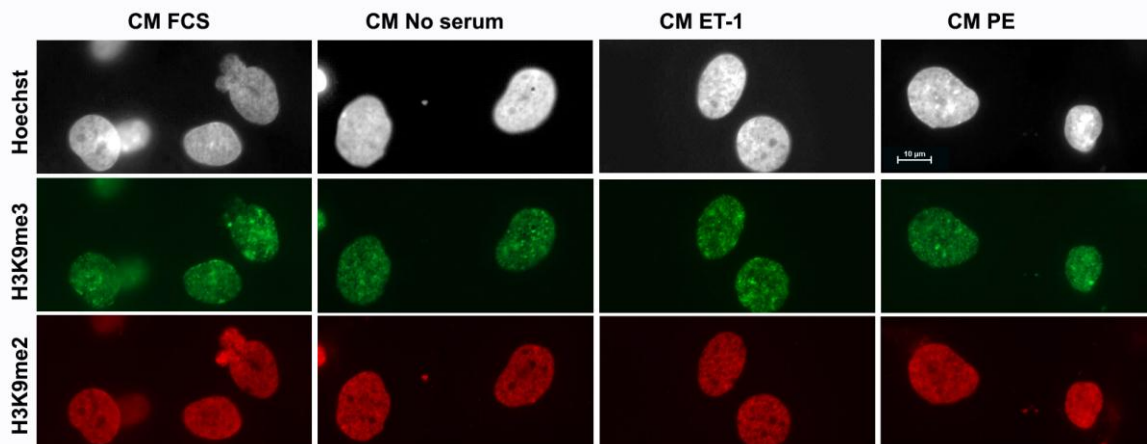


Fig. 4 Immunofluorescence analysis of histone H3K9 methylation in primary rat cardiomyocytes.

Primary cardiomyocytes were dissociated from the minced heart tissue of 1-day old Sprague-Dawley rat pups by trypsin and collagenase treatment using Neonatal Cardiomyocyte Isolation System (Worthington, Lakewood, NJ) and cultured in DMEM supplemented with 10% FBS (left column). After 24 hours, in some samples DMEM-fetal bovine serum was exchanged for DMEM-horse serum (second column from the left) and hypertrophy was induced by incubating with 10 nM ET-1 (third from the left) and 50 μ M PE (right column). Cells were grown on microscopy cover glasses, fixed with 2.7 % paraformaldehyde, stained with Hoechst 33258 fluorescence, and immunostained with antibodies against histone H3 trimethylated at lysine 9 (H3K9me2) and histone H3 dimethylated at lysine 9 (H3K9me3) as indicated and visualized by fluorescence microscopy.

| N | Accession Name | Species | Peptide | -PE | +PE | -PE | +PE |
|-----|---|------------|---------|---------|---------|---------|---------|
| | | | | 117:116 | 118:116 | 119:116 | 121:116 |
| 10 | gi 149048 lamin A, isoform CRA_b [Rattus norvegicus] | Rattus nor | 55 | 1.4859 | 1.5704 | 1.4588 | 1.4997 |
| 44 | gi 276864 PREDICTED: similar to Histone H2B 291B [Rattus norvegicus] | Rattus nor | 52 | 1.0864 | 0.8091 | 1.3428 | 0.9204 |
| 36 | gi 109504 PREDICTED: similar to germinal histone H4 gene [Rattus norvegicus] | Rattus nor | 36 | 0.492 | 0.4487 | 0.6427 | 0.6486 |
| 28 | gi 109505 PREDICTED: similar to Histone H1.2 (H1 VAR.1) (H1c) [Rattus norvegicus] | Rattus nor | 26 | 0.7727 | 0.6855 | 0.6918 | 0.8017 |
| 290 | gi 444788 histone H1d | | 21 | 0.871 | 0.912 | 0.912 | 0.9908 |
| 234 | gi 901014 RecName: Full=Histone H2A type 1 | RAT | 19 | 1.6749 | 1.2706 | 1.5996 | 1.2474 |
| 60 | gi 818841 RecName: Full=Histone H2A type 1-F | RAT | 18 | 1 | 0.9727 | 1.0375 | 0.863 |
| 65 | gi 724216 nucleophosmin (nucleolar phosphoprotein B23, numatrin) [Rattus norvegicus] | Rattus nor | 17 | 1.7539 | 2.0137 | 1.8707 | 1.9953 |
| 273 | gi 157817 H2A histone family, member X [Rattus norvegicus] | Rattus nor | 15 | 1.0375 | 0.955 | 1.0186 | 0.9376 |
| 82 | gi 157821 histone cluster 1, H1b [Rattus norvegicus] | Rattus nor | 13 | 0.9908 | 0.6546 | 0.879 | 0.7447 |
| 79 | gi 818638 RecName: Full=Histone H3.1 | RAT | 9 | 0.7798 | 0.7244 | 0.863 | 0.6918 |
| 118 | gi 818853 RecName: Full=Heterochromatin protein 1-binding protein 3 | RAT | 9 | 2.4889 | 3.5975 | 3.4041 | 2.9376 |
| 77 | gi 513165 RecName: Full=DNA topoisomerase 1; AltName: Full=DNA topoisomerase I | RAT | 8 | 1.0864 | 1.1482 | 1.0471 | 0.8954 |
| 163 | gi 698100 H1 histone family, member 0 [Rattus norvegicus] | Rattus nor | 7 | 1.0666 | 0.8954 | 1.1803 | 1.0666 |
| 142 | gi 819117 RecName: Full=Histone-binding protein RBBP7; AltName: Full=Retinoblastoma | RAT | 6 | 1.5704 | 1.1169 | 0.8551 | 0.9376 |
| 146 | gi 281427 apoptotic chromatin condensation inducer 1 [Rattus norvegicus] | Rattus nor | 6 | 1.0568 | 1.0666 | 1.0568 | 0.955 |
| 172 | gi 901100 RecName: Full=Core histone macro-H2A.1; Short=Histone macroH2A1; Short= | RAT | 6 | 0.929 | 1.3804 | 1.3552 | 1.0471 |
| 194 | gi 832884 RecName: Full=Histone H2A.z; Short=H2A/z | RAT | 6 | 1.0471 | 0.9908 | 1.0471 | 0.9817 |
| 170 | gi 625121 RecName: Full=NHP2-like protein 1; AltName: Full=High mobility group-like r | RAT | 5 | 1.5996 | 2.0701 | 2.0137 | 1.8197 |
| 412 | gi 197246 Rbbp4 protein [Rattus norvegicus] | Rattus nor | 5 | 2.0701 | 3.5645 | 3.6983 | 0.0223 |
| 186 | gi 215490 Sin3A-associated protein, 18kDa [Rattus norvegicus] | Rattus nor | 3 | 0.929 | 0.9817 | 0.9817 | 0.879 |
| 228 | gi 570806 L2BP1 [Rattus norvegicus] | Rattus nor | 3 | 0.1644 | 0.182 | 0.863 | 0.6668 |
| 230 | gi 157817 SWI/SNF related, matrix associated, actin dependent regulator of chromatin, | Rattus nor | 2 | 0.6194 | 0.7112 | 0.7379 | 0.7798 |
| 342 | gi 515562 DNA (cytosine-5-)-methyltransferase 3 alpha isoform 1 [Rattus norvegicus] | Rattus nor | 2 | 4.3652 | 4.6132 | 6.1376 | 3.4041 |
| 369 | gi 109481 PREDICTED: similar to Lamin-B2 [Rattus norvegicus] | Rattus nor | 2 | 0.8318 | 1.0864 | 1 | 1.0375 |
| 341 | gi 833058 RecName: Full=FACT complex subunit SSRP1; AltName: Full=Facilitates chrom | RAT | 1 | 1.1482 | 1.5276 | 1.1695 | 1.3677 |
| 357 | gi 413841 SMC-protein [Rattus norvegicus] | Rattus nor | 1 | 0.9638 | 0.9817 | 1.0568 | 1.0471 |
| 380 | gi 149024 regulator of chromosome condensation 2 (predicted), isoform CRA_b [Rattus | Rattus nor | 1 | 1.0093 | 1.0666 | 0.955 | 1.0375 |
| 385 | gi 567994 chromobox homolog 3 [Rattus norvegicus] | Rattus nor | 1 | 0.8872 | 0.9462 | 0.955 | 0.9817 |
| 430 | gi 208022 histone deacetylase 2 [Rattus norvegicus] | Rattus nor | 1 | 0.871 | 0.8954 | 0.8954 | 0.955 |
| 534 | gi 216678 HMGA1b [Rattus norvegicus] | Rattus nor | 1 | 0.6486 | 0.787 | 0.7244 | 0.6668 |
| 536 | gi 197245 Chromobox homolog 5 (HP1 alpha homolog, Drosophila) [Rattus norvegicus] | Rattus nor | 1 | 1.0965 | 1 | 0.9727 | 1.0093 |
| 556 | gi 189491 regulator of chromosome condensation 1 [Rattus norvegicus] | Rattus nor | 1 | 0.9817 | 0.8472 | 0.8395 | 0.7727 |
| 579 | gi 832882 RecName: Full=High mobility group protein HMG-I/HMG-Y; Short=HMG-I(Y); A | RAT | 1 | 0.7727 | 1.0965 | 0.8166 | 0.8472 |
| 598 | gi 681634 SWI/SNF related, matrix associated, actin dependent regulator of chromatin, | Rattus nor | 1 | 1.0093 | 0.9727 | 0.9204 | 1 |

Fig. 5. Relative expression levels of nuclear proteins detected in H9C2 cells by iTRAQ mass-spec analysis.

Cell nuclei were isolated from Rat cardiac myoblasts H9C2 incubated in DMEM with FBS serum, no serum without PE (-PE) and with PE (+PE) to induce hypertrophy. Nuclear proteins were extracted with 2M NaCl. 100 µg of protein from each sample were completely digested with Trypsin and the peptides were labeled with iTRAQ mass tags 116 (FBS), 117 (-PE); 118 (+PE); 119 (-PE); and 121 (+PE). The last four samples represent two independently repeated experiments. After labeling, the peptides were mixed and simultaneously analyzed by MS/MS spectrometry. Protein expression levels calculated using Protein Pilot (Proteus LIMS) software are show in relation to the protein levels in the FBS (116) sample.

| N | Accession # | Name | Species | -PE +PE | | |
|-----|--------------|--|------------|---------------|---------|---------|
| | | | | Peptides(95%) | 114:113 | 115:113 |
| 117 | gi 462286 | RecName: Full=Non-histone chromosomal protein HMG-17; AltName: Full=High-mobility group nucleos | RAT | 7 | 9.0365 | 8.7096 |
| 142 | gi 81911796 | RecName: Full=Histone-binding protein RBBP7; AltName: Full=Retinoblastoma-binding protein 7; Short | RAT | 6 | 2.6792 | 3.281 |
| 44 | gi 27686409 | PREDICTED: similar to Histone H2B 291B [Rattus norvegicus] | Rattus nor | 52 | 6.2517 | 3.2509 |
| 118 | gi 81885307 | RecName: Full=Heterochromatin protein 1-binding protein 3 | RAT | 9 | 4.0551 | 2.4434 |
| 18 | gi 224493240 | Heterogeneous nuclear ribonucleoproteins A2/B1; Short=hnRNP A2 / hnRNP B1 | RAT | 48 | 2.0512 | 1.9231 |
| 28 | gi 109505801 | PREDICTED: similar to Histone H1.2 (H1 VAR.1) (H1c) [Rattus norvegicus] | Rattus nor | 26 | 1.8535 | 1.6749 |
| 163 | gi 6981004 | H1 histone family, member 0 [Rattus norvegicus] | Rattus nor | 7 | 1.5704 | 1.6144 |
| 79 | gi 81863898 | RecName: Full=Histone H3.1 | RAT | 9 | 3.8726 | 1.5996 |
| 556 | gi 189491881 | regulator of chromosome condensation 1 [Rattus norvegicus] | Rattus nor | 1 | 1.5417 | 1.4723 |
| 579 | gi 83288238 | RecName: Full=High mobility group protein HMG-1/HMG-Y; Short=HMG-1(Y); AltName: Full=High mobil | RAT | 1 | 1.1376 | 1.4322 |
| 385 | gi 56799436 | chromobox homolog 3 [Rattus norvegicus] | Rattus nor | 1 | 1.2359 | 1.3552 |
| 337 | gi 109480098 | PREDICTED: similar to SWI/SNF-related matrix-associated actin-dependent regulator of chromatin c2 | Rattus nor | 2 | 1.1169 | 1.3183 |
| 462 | gi 81908653 | RecName: Full=RNA polymerase II-associated factor 1 homolog | RAT | 1 | 1.1482 | 1.2706 |
| 569 | gi 109473131 | PREDICTED: similar to high mobility group nucleosomal binding domain 1 (predicted) [Rattus norveg | Rattus nor | 1 | 1.1912 | 1.1376 |
| 534 | gi 21667872 | HMG1b [Rattus norvegicus] | Rattus nor | 1 | 1.5417 | 1.1272 |
| 536 | gi 197245751 | Chromobox homolog 5 (HP1 alpha homolog, Drosophila) [Rattus norvegicus] | Rattus nor | 1 | 1.1272 | 1.1272 |
| 34 | gi 51980308 | Heterogeneous nuclear ribonucleoprotein A3 [Rattus norvegicus] | Rattus nor | 30 | 1.0765 | 1.0666 |
| 146 | gi 281427182 | apoptotic chromatin condensation inducer 1 [Rattus norvegicus] | Rattus nor | 6 | 0.9727 | 1.0186 |
| 369 | gi 109481544 | PREDICTED: similar to Lamin-B2 [Rattus norvegicus] | Rattus nor | 2 | 0.9036 | 1.0093 |
| 430 | gi 208022663 | histone deacetylase 2 [Rattus norvegicus] | Rattus nor | 1 | 1.0471 | 1 |
| 194 | gi 83288410 | RecName: Full=Histone H2A.Z; Short=H2A/z | RAT | 6 | 0.955 | 0.9817 |
| 65 | gi 7242160 | nucleophosmin (nucleolar phosphoprotein B23, numatrin) [Rattus norvegicus] | Rattus nor | 17 | 0.5546 | 0.955 |
| 598 | gi 68163423 | SWI/SNF related, matrix associated, actin dependent regulator of chromatin, subfamily e, member 1 [R | Rattus nor | 1 | 0.871 | 0.9462 |
| 273 | gi 157817664 | H2A histone family, member X [Rattus norvegicus] | Rattus nor | 15 | 1.0666 | 0.9376 |
| 290 | gi 444788 | histone H1d | | 21 | 1.1169 | 0.912 |
| 82 | gi 157821427 | histone cluster 1, H1b [Rattus norvegicus] | Rattus nor | 13 | 1.1588 | 0.912 |
| 230 | gi 157817975 | SWI/SNF related, matrix associated, actin dependent regulator of chromatin, subfamily a, member 5 [R | Rattus nor | 2 | 0.863 | 0.879 |
| 380 | gi 149024445 | regulator of chromosome condensation 2 (predicted), isoform CRA_b [Rattus norvegicus] | Rattus nor | 1 | 0.7178 | 0.879 |
| 591 | gi 52138631 | TOX high mobility group box family member 4 [Rattus norvegicus] | Rattus nor | 1 | 0.8395 | 0.8091 |
| 21 | gi 55250726 | Nucleolin [Rattus norvegicus] | Rattus nor | 28 | 0.9727 | 0.8017 |
| 226 | gi 109502181 | PREDICTED: similar to topoisomerase (DNA) II beta [Rattus norvegicus] | Rattus nor | 3 | 0.8395 | 0.7047 |
| 40 | gi 4378711 | nucleic acid binding factor pRM10 [Rattus norvegicus] | Rattus nor | 16 | 1.2359 | 0.6546 |
| 10 | gi 149048132 | lamin A, isoform CRA_b [Rattus norvegicus] | Rattus nor | 55 | 1.1272 | 0.6427 |
| 35 | gi 109463555 | PREDICTED: similar to AHNK nucleoprotein isoform 1 isoform 4 [Rattus norvegicus] | Rattus nor | 16 | 0.5248 | 0.6427 |
| 170 | gi 62512125 | RecName: Full=NHP2-like protein 1; AltName: Full=High mobility group-like nuclear protein 2 homolog | RAT | 5 | 0.413 | 0.6252 |
| 36 | gi 109504921 | PREDICTED: similar to germinal histone H4 gene [Rattus norvegicus] | Rattus nor | 36 | 1.556 | 0.5546 |
| 234 | gi 90101451 | RecName: Full=Histone H2A type 1 | RAT | 19 | 1.2359 | 0.5445 |
| 519 | gi 3298564 | non-histone chromosomal architectural protein HMGI-C [Rattus norvegicus] | Rattus nor | 1 | 0.8551 | 0.5445 |
| 228 | gi 5708069 | L2BP1 [Rattus norvegicus] | Rattus nor | 3 | 2.5586 | 0.5405 |
| 94 | gi 81907772 | RecName: Full=PDZ and LIM domain protein 7; AltName: Full=LIM mineralization protein; Short=LMP; Al | RAT | 7 | 0.4571 | 0.3192 |
| 60 | gi 81884124 | RecName: Full=Histone H2A type 1-F | RAT | 18 | 0.4018 | 0.2312 |
| 172 | gi 90110024 | RecName: Full=Core histone macro-H2A.1; Short=Histone macroH2A1; Short=mH2A1; AltName: Full=H2i | RAT | 6 | 0.4406 | 0.2312 |

Fig. 6. Relative expression levels of nuclear proteins detected in primary cardiomyocytes by iTRAQ mass-spec analysis.

Cell nuclei were isolated from primary cardiomyocytes isolated from 1-day old Sprague-Dawley rat pups and incubated in DMEM with FBS serum, no serum without PE (-PE) and with PE (+PE) to induce hypertrophy. Nuclear proteins were extracted with 2M NaCl. 100 µg of protein from each sample were completely digested with Trypsin and the peptides were labeled with iTRAQ mass tags 113 (FBS), 114 (-PE); and 115 (+PE). After labeling, the peptides were mixed and simultaneously analyzed by MS/MS spectrometry. Protein expression levels calculated using Protein Pilot (Proteus LIMS) software are show in relation to the protein levels in the FBS (113) sample. Changes in protein expression > 2-fold are highlighted by red color.

Research Project 37: Project Title and Purpose

Blood-Brain Barrier Nutrient Transport - The primary focus of this project is to determine the mechanism by which glucose in the circulation traverses the endothelial cells that make up the blood-brain barrier and thus gains access to the brain. Specifically we will investigate the regulation of the glucose transporter(s) in the luminal (blood facing) and abluminal (brain facing) membranes of the endothelial cells that facilitate the transport of glucose across the respective membranes.

Duration of Project

7/1/2008 – 6/30/2009

Summary of Research Completed

This project ended during a prior state fiscal year. For additional information, please refer to the Commonwealth Universal Research Enhancement Annual C.U.R.E. Reports on the Department's Tobacco Settlement/Act 77 web page at <http://www.health.state.pa.us/cure>.

Research Project 38: Project Title and Purpose

Interaction between Survivin and Aurora B in Primary T Lymphocytes - The major goal of this study is to determine the relationship of survivin and aurora B in primary T cells from survivin transgenic mice. We will define proliferation, expansion, cell cycle progression, cytokine production, survival, and memory development of T cells from survivin transgenic mice. Since survivin and aurora B have been suggested to promote T-cell proliferation and expansion, and sustain survival, we hypothesize that T cells from survivin transgenic mice will proliferate/expand strongly, and survive longer than T cells from normal background C57BL/6 mice.

Duration of Project

7/1/2008 – 6/30/2010

Project Overview

Aim 1. To define the profiles of T cells from survivin transgenic mice

We hypothesize that T cells from survivin transgenic mice will proliferate/expand strongly and have enhanced survival advantage. In this specific aim, we will isolate naïve CD4⁺ or CD8⁺ T cells from survivin transgenic mice and stimulate *in vitro* to determine their functions for proliferation, expansion, cell cycle progression, cytokine production, long-term T cell survival, and memory development.

Aim 2. To determine the relationship of survivin and aurora B in T cells from survivin transgenic mice

We will carry out experiments on immunoprecipitation to identify new members in the complex from primary T cells. The mTOR and downstream molecules 4E-BP1, S6K1, raptor, and INCENP will be tested. Naive T cells from survivin transgenic mice will be stimulated with plate-bound anti-CD3 antibody (4 µg/ml, 2C11) and soluble anti-CD28 antibody (4 µg/ml) at different time points (0hr, 4hr, 8hr, 16hr, 24hr, 36hr, 48hr, 72hr), cellular lysates from live T cells will be performed for analysis of protein interaction of survivin and aurora B as well as mTOR, 4E-BP1, S6K1, raptor and INCENP, and *in vitro* kinase assay. Furthermore, we will also determine whether in the presence of mTOR specific inhibitor Rapamycin or other chemical inhibitors (e.g., Wortmannin, LY 294002, Rotterlin) would affect biological functions of survivin, aurora B.

Principal Investigator

Jianxun Song, PhD

Penn State University
College of Medicine
Department of Microbiology and Immunology H107
500 University Drive
Hershey, PA 17033

Other Participating Researchers

Rizwanul Haque, PhD – employed by the Pennsylvania State University

Expected Research Outcomes and Benefits

We will obtain evidence that survivin transgenic mice, which over-express survivin protein in lymphocytes and other types of cells, have higher CD4⁺ and CD8⁺ T cell responses as compared to same background non-transgenic mice both *in vitro* and *in vivo*

The mechanisms by which T cell costimulation sustains T cell activation and full function still need to be unraveled. Identifying the molecular targets that are involved in costimulation will help us to understand the mechanisms by which costimulatory signals contribute to T cell activation. More importantly, because some of these targets are common and appear to sustain T cell response, the development of immunotherapeutic strategies that are based on such molecules can augment T cell immunity.

Summary of Research Completed

Interaction between Survivin and Aurora B in Primary T Lymphocytes - The major goal of this study is to determine the relationship of survivin and aurora B in primary T cells from survivin transgenic mice. We defined proliferation, expansion, cell cycle progression, cytokine production, survival, and memory development of T cells from survivin transgenic mice.

Aim 2. To determine the relationship of survivin and aurora B in T cells from survivin transgenic mice

In this specific aim, we performed experiments on immunoprecipitation to identify new members in the complex from primary T cells. The mTOR and downstream molecules 4E-BP1, S6K1, raptor, and INCENP have been tested. Naive T cells from survivin transgenic mice were stimulated with plate-bound anti-CD3 antibody (4 µg/ml, 2C11) and soluble anti-CD28 antibody (4 µg/ml) at different time points (0hr, 4hr, 8hr, 16hr, 24hr, 36hr, 48hr, 72hr), cellular lysates from live T cells were performed for analyses of protein interaction of survivin and aurora B as well as mTOR, 4E-BP1, S6K1, raptor and INCENP, and *in vitro* kinase assay. Furthermore, we have determined in the presence of mTOR specific inhibitor Rapamycin or other chemical inhibitors (e.g., Wortmannin, LY 294002, Rotterlin) affected the biological functions of survivin, aurora B. Collectively, we delineate that survivin and aurora B can form a complex, which cooperatively promotes T cell activity as we described in Figs.1 and 2.

